THE DEVELOPMENT OF ELECTROCHEMICAL SENSORS

A Thesis submitted

for the

Degree of Doctor of Philosophy

by

Barry Gerald Denis Haggett

Imperial College of Science and Technology

London

September 1984

ABSTRACT

Development work on amperometric nitrate and dissolved oxygen sensors is described.

(a) Nitrate measurement is based on reduction at a copper cathode in aqueous perchloric acid. The limiting current at the copper surface was found to decrease with time - the change is described by a poisoning process whose kinetics are first-order with respect to the number of active sites. Electrode regeneration could be brought about by (i) mechanical polishing or (ii) maintenance of the electrode potential in the hydrogen evolution region or (iii) stripping of copper ions from the copper surface.

A packed bed wall-jet electrode is being developed. This provides a renewable surface for nitrate measurement by plating on to the working electrode copper stripped from the upstream packed bed of copper chips.

(b) Sensors for dissolved oxygen based on the Clark electrode principle could be improved by operating in a transient rather than steady state current mode. Transient currents, however, are not entirely due to faradaic oxygen reduction and this complicates extraction of concentration information.

Several analytical models are described which allow faradaic currents to be calculated for potential step transients. These transients may be described by a two parameter model but the analysis is greatly simplified by designing the electrode and tailoring the operating conditions so as to allow the use of a much simpler model.

The sensitivity of this type of transient measurement is limited by the magnitude of background currents which are more significant than in the steady state.

To

My Parents

ACKNOWLEDGEMENTS

I would like to express my appreciation to all of the following:

Professor John Albery for his help and remarkable tolerance.

Huvin Thompson and Malcolm Riley at EIL, Kent Industrial Measurements Ltd. for their support.

All members of Professor Albery's extended research group - especially Peter Barron, Phil Bartlett, Rob Bird, Humphrey Drummond, Nick Goddard, Rob Hillman, John Hooper, Chris P. Jones, Nani Mendes-Neto, Mike Pritchard, Gougang Pu and Rob Svanberg.

Mary, Paddy and Johnny.

My family.

Paul Begley for bullying me.

Sue Frazer for her expert typing.

The Science and Engineering Research Council.

CONTENTS

Contents

List of diagrams

List of tables

Chapter 1. The development of electrochemical sensors. 1

1.0 Introduction 1

1.1 Applications of nitrate and dissolved oxygen sensors 2

1.1.1 Natural waters 2

1.1.2 Waste water treatment 3

1.1.3 Boiler feed waters 4

1.1.4 Agriculture 4

1.2 Methods of analysis 6

1.2.1 Voltammetric reduction of nitrate 6

1.2.2 Voltammetric reduction of dissolved oxygen 9

1.3 Membrane-covered amperometric sensors 10

1.3.1 Oxygen flux across the membrane 10

1.3.2 Steady-state current 12

1.3.3 The membrane 16

1.3.4 Improved Clark cells 17

1.4 Summary 19

Chapter 2. Experimental details. 20

2.0 Introduction 20

2.1 Disc electrodes 20

2.1.1 Materials 20

2.1.2 Dimensions 22

2.1.3 Preparation 22

2.1.4 Rotation of the electrodes 24

2.2 Membrane-covered electrodes 24

2.2.1 General purpose electrodes 25

2.2.2 Microelectrodes 25

2.2.3 Silver/silver chloride reference electrodes 30

2.2.4 Nickel hydroxide counter electrodes 30

2.2.5 Other electrodes 31

2.3 The electrochemical cell 34

2.4 Gas mixtures 34

2.4.1 Flowmeters 34

2.4.2 Gas blenders 36

2.5 Chemicals 41

2.5.1 Purified water 41

2.5.2 Chemicals and solutions 45

2.6 Analogue electronics 45

2.6.1 Decoupling 46

2.6.2 Modules 46

2.6.3 The Oxford box 48

2.7 Chemistry Microprocessr Unit Interface System 49

2.7.1 Function Boards 49

2.7.2 Combination of digital and analogue electronics 51

2.7.3 Software for the CMUIS 51

2.8 Commercial Instrumentation 53

Chapter 3. Development of a voltammetric nitrate sensor. 55

3.0 Introduction 55

3.1 Copper foil electrodes 55

3.1.1 Cyclic voltammetry at foil electrodes 55

3.1.2 Linear sweep voltammetry at foil electrodes 56

3.1.3 Mixed perchlorate electrolyte 62

3.2 The Stationary copper disc electrode 62

3.2.1 Linear sweep voltammetry 62

3.2.2 Concentration dependence of the peak current 67

3.2.3 Nitrite reduction 69

3.2.4 Effect of chloride on the nitrate reduction peak 71

3.3 The rotating copper disc electrode(RCuDE) 73

3.3.1 Sweep rate dependence of the reduction current 75

3.3.2 Concentration dependence of the reduction current 75

3.3.3 Rotation speed dependence of the reducton current 75

3.3.4 Poisoning of the electrode surface 82

3.3.5 Electrode poisoning at constant potential 86

3.3.6 First-order model for electrode poisoning 90

3.3.7 Potential step transients 99

3.3.8 Concentration dependence of the potential step transients 99

3.3.9 Rotation speed dependence of the potential step transients 102

3.3.10 Summary of potential step analysis on the RCuDE 106

3.3.11 Copper plating on an 'inert' substrate 107

3.4 Wall-jet electrodes 107

3.4.1 Packed bed wall-jet electrode(PBWJE) 109

3.5 Summary 109

Chapter 4. Development of a dissolved oxygen sensor. 112

4.0 Introduction 112

4.0.1 Transient current measurements 112

4.1 Equilibrium oxygen concentration 114

4.2 Diffusion layer thickness 114

4.3 Switch from open-circuit 117

4.4 Potential step into the diffusion limited region 117

4.4.1 Double layer charging 118

4.4.2 Electrode time constant 120

4.4.3 Uncompensated resistance 121

4.4.4 Membrane electrode simulation 122

4.5 Background current 122

4.6 Linear addition model 126

4.6.1 Determination of the time constant 128

4.6.2 Implementation of the $it^{1/2}$ analysis 130

4.7 Induced charging model 136

4.7.1 Faradaic current 138

4.7.2 Analysis of the induced charging model 142

4.7.3 Faradaic current and concentration polarisation 145

4.8 Case 1. Bounded faradaic current 147

4.8.1 Surface and bulk concentrations 149

4.8.2 Sand equation 152

4.8.3 Surface reactions 156

4.8.4 Silver migration 156

4.8.5 Step size and the electron transfer coefficient 159

4.8.6 Summary 162

4.9 Case 2. Unbounded faradaic current 162

4.9.1 Concentration dependence 163

4.9.2 Simplification of transient analysis 163

4.10 Summary 166

References 168

FIGURES

1.1 Diagrammatic representation of Clark electrode 11

1.2 Steady state concentration profile across Clark cell 13

2.1 Projection of section through typical disc electrode 21

2.2 General purpose membrane-covered sensor 26

2.3 Construction of membrane cell with micro-sized gold working electrode 27

2.4 Construction of double-reference membrane electrode with micro-size gold working electrode 28

2.5 Cyclic voltammogram showing nickel hydroxide peaks 32

2.6 Construction of gold microelectrode 33

2.7 Double-walled glass cell for electrochemical studies 35

2.8 Calibration of flowmeter 336859/03 37

2.9 Calibration of flowmeter 336861/E 38

2.10 Calibration of flowmeter 454129/H-J 39

2.11 Decoupling of operation amplifiers 46

3.1 Nitrate reduction on a stationary,pretreated copper foil eletrode 57

3.2 Effect of potential sweep rate on the nitrate reduction current using a stationary copper foil electrode 59

3.3 (a) i_p vs $v^{1/2}$, (b) $\ln(i_p)$ vs E_p for nitrate reduction on a copper foil electrode 60

3.4 Effect of potential sweep rate on nitrate reduction current using a stationary copper disc electrode 63

3.5 Plot of peak current vs square root of sweep rate 64

3.6 Plot of $\ln(i_p)$ vs E_p 65

3.7 Concentration dependence of nitrate reduction

peak on a stationary CuDE 68

3.8 Nitrite reduction on a stationary CuDE 70

3.9 Effect of chloride on peak potential 72

3.10 Effect of potential sweep rate on nitrate reduction voltammogram 76

3.11 Nitrate reduction on a RCuDE 77

3.12 Effect of sweep rate on magnitude of nitrate limiting reduction current on a RCuDE 78

3.13 Voltammograms showing effect of rotation speed on nitrate reduction wave using a copper electrode 79

3.14 (a) Levich and (b) Koutecky-Levich plots for nitrate reduction on the RCuDE 81

3.15 Decay of nitrate reduction wave on RCuDE 83

3.16 Tafel plot for nitrate reduction on RCuDE 85

3.17 Effect of rotation speed during different stages of nitrate reduction current decay at RCuDE 87

3.18 (a) Levich and (b) Koutecky-Levich plots for nitrate reduction on freshly polished RCuDE with fixed potential 88

3.19 Rotation speed dependence during later stages of nitrate reduction on RCuDE 89

3.20 Plots describing first-order decay of nitrate reduction limiting current on RCuDE 95,6

3.21 Sampled current response to nitrate concentration after four days of applying a potential pulse sequence to a RCuDE 100

3.22 Sampled current response to nitrate concentration after 24hours of a double pulse sequence on a RCuDE 101

3.23 Double pulse sequence showing resulting current transients 103

3.24 Sampled current response to nitrate on fresh double-pulsed RCuDE 104

3.25 Detail from double potetial pulse sequence on CuDE showing the effect of rotation speed on nitrate reduction current transient 105

3.27 Reduction of Cu^{2+} on a PtRDE 108

3.28 Packed bed wall-jet electrode(PBWJE) 110

4.1 Simulated voltammogram 113

4.2 Changes in concentration profile: switch on to steady state 115

4.3 Single point sample response from a pulsed membrane-covered electrode 119

4.4 Resistor-capacitor analogue of a non-faradaic system 118

4.5 Single point sample response from a pulsed gold disc electrode 123

4.6 Time course of background current transient currents on a gold disc electrode 124

4.7 Simulated transient (linear addition model) 127

4.8 $it^{1/2}$ plot of simulated transient 129

4.9 Potential step transient on general purpose membrane-covered electrode 131

4.10 $it^{1/2}$ plot of transient in Fig.4.9 132

4.11 Potential step transient on microdisc membrane-covered electrode 134

4.12 $it^{1/2}$ plot of transient in Fig.4.11 135

4.13 Concentration dependence of $it^{1/2}$ plots 137

4.14 Resistor-capacitor analogue of simple faradaic system 136

4.15 Potential step transients analysed according to Perone 140

4.16 Collected data from Perone-type analyses 141

4.17 Simulated potential step transient (case 1) 150

4.18 Potential step transient showing current pause 151

4.19 Simulated effect of increasing concentration 153

4.20 Effect of uncompensated resistance on potential step transients 154

4.21 Potential step transients, 0-25% O_2 155

4.22 Background current in sodium hydroxide 157

4.23 Effect of surface reactions on potential step transients 158

4.24 Voltammogram showing result of silver migration 160

4.25 Effect of step size and electron transfer coefficient on the shape of the current pause transient 161

4.26 Simulated potential step transient (case 2) 164

4.27 Simulated effect of decreasing concentration 165

4.28 $it^{1/2}$ plot of simulated transient (case 2) 167

TABLES

2.1 Disc and ring-disc electrode specifications 23

2.2 Square-root density ratios 41

2.3 Calibration of Signal blender 852P6S No.1951 42

2.4 Calibration of Signal blender 853V1S No.3039 43

2.5 Calibration of Signal blender 853V1B No.3038 44

2.6 Typical operational amplifier specifications 47

3.1 Reduction transfer coefficient as a function of scan number 84

3.2 Measured values of $k^{`}$, k_p and k_R 97

CHAPTER 1

THE DEVELOPMENT OF ELECTROCHEMICAL SENSORS

1.0 Introduction

This thesis contains theoretical and experimental results which form the basis for the continuing development of an amperometric nitrate sensor and a dissolved oxygen monitor.

The nitrate sensor is based on the direct, amperometric reduction of nitrate ions at an active copper electrode and for this purpose a packed bed, wall-jet cell is being developed in order to provide a renewable copper surface on an otherwise inert substrate. This will enable quantitative nitrate reduction to be carried out under optimum conditions.

The development work for the dissolved oxygen monitor is based on a Clark-type, membrane-covered electrode. This type of sensor is widely used, but there are a number of problems associated with membrane fouling, flow rate dependence, etc.. Thus, it was desired to develop a technique for carrying out the measurements in such a way as to reduce or circumvent these problems. To this purpose a number of potential step techniques were used and much of the work is concerned with the interpretation of the date thus obtained.

A few of the areas of application will be described in this first chapter, as well as some other techniques used, by other workers, for carrying out the measurements. It will conclude by going on to describe, in a little more detail, the particular techniques chosen for development in this thesis.

1.1 Applications of nitrate and dissolved oxygen sensors

This work forms, in part, a contribution to a much larger project to provide a library of sensors for measurement and control of nutrients in the water used to grow crops by a hydroponic technique whereby plants are grown with their roots in circulating water rather than in soil[1].

The scope for use of these sensors is, however, much wider than the field of hydroponics. Sometimes they are used in conjunction with each other, whilst in many cases one may be used without the other. An indication of a few of the areas where existing sensors are already applied is given below.

1.1.1 Natural Waters

Dissolved oxygen is essential to aquatic life and its concentration is closely related to the amount of nitrogen in the water. Most nitrogen is utilised in the form of ammonium salts. Fish, however, can be adversely affected by even small concentrations of ammonia, which originates from the degradation of organic molecules such as proteins, etc.. Ammonia is removed in sufficiently aerated water by nitrification[2];

$$2NH_3 + 3O_2 \xrightarrow{\text{nitrosomonas}} 2NO_2^- + 2H^+ + 2H_2O \quad (1.1)$$

$$2NO_2^- + O_2 + 2H^+ \xrightarrow{\text{nitrobacter}} 2NO_3^- + 2H^+ \quad (1.2)$$

Both nitrates and nitrites may accumulate if nitrification activity is high and this is undesirable, particularly in drinking-water supplies since it causes the disease methaemoglobinaemia in young children.

The delicate balance between biochemical oxygen depletion and reoxygenation, by aeration and photosynthetic activity, may be seriously disrupted by pollution from, for example, waste discharge or the run-off from fertilisers. In this case the dissolved oxygen concentration may fall below the level to support aerobic activity. Anaerobic processes, including denitrification to form N_2 and/or N_2O may occur and the water will stagnate[2,3].

It can be seen from the above that it is very important, for those concerned with water quality, to be able to measure and record both nitrate and dissolved oxygen levels.

1.1.2 Waste Water Treatment[2,4,5]

Sewage treatment systems are generally designed to reduce to an acceptable level the biological oxygen demand (BOD) and the concentration of suspended solids. Breakdown of sewage is brought about by bacterial attack, but in the absence of sufficient oxygen there is an increase in the activity of anaerobic, sulphate reducing bacteria with a consequent production of hydrogen sulphide which may lead to serious corrosion problems. Aeration, however, is expensive, thus it is usual to try and attempt to maintain the level of dissolved oxygen between predetermined upper and lower set limits.

The concentration of nitrogen, in all its forms, is becoming of increasing concern and the subject of statutory control. It is necessary to remove dissolved ammonia because of its harmful effect on fish, whilst high concentrations of nitrate are also to be avoided. Thus, where nitrogen control criteria are important, the usual

treatment scheme is biological nitrification-denitrification, i.e. oxidation of ammonia to nitrate and nitrite, in aerobic conditions, followed by anaerobic reduction to nitrogen or nitrous oxide, both of which are lost from solution.

In order to give the best possible treatment, for the least possible cost, it is essential to be able to monitor and control both nitrate and dissolved oxygen levels at every stage of the process.

1.1.3 Boiler Feed Waters

Electrical power generation frequently involves the use of thousands of tons of very high temperature pressurised water in order to raise steam for driving turbines. It is necessary to use ultrapure water because of the aggressive environment. It these circumstances even a few ppb of dissolved oxygen can give rise to serious corrosion which may lead to expensive plant failure. Boiler feed waters are thus deoxygenated and the levels are closely monitored at several points in the steam-water circuit[6,7].

1.1.4 Agriculture

From extensive studies of classical agriculture, using soil based techniques, it has long been known that plant respiration occurs above and below ground. Soil aeration affects the uptake of minerals through the roots and without sufficient oxygen the plant may become diseased.

Using the hydroponic technique, crops such as tomatoes, cucumbers and lettuce may be grown with

their roots in circulating water rather than in soil[8,9]. The problems of root aeration are similar, however, and it is essential to maintain an adequate supply of dissolved oxygen which tends to be severely depleted in the thick root mats.

An important difference between growing crops in soil and in solution is that soil tends to have a much greater buffer capacity of nutrients such as nitrogen, phosphorous and potassium. In hydroponics the concentrations of these nutrients may fluctuate wildly, unless preventive measures are taken. For complete control a whole array of sensors, including nitrate and dissolved oxygen, is important both for the increased understanding of the processes occurring in hydroponic systems and for the maintenance of optimum growing conditions.

Nitrate is also very important in other areas of agriculture. Modern farming techniques often entail the use of not only manufactured fertilisers but also animal slurries and these constitute a significant threat of pollution to both surface waters, via run-off, and to underground waters via leeching of the soil[3]. Nitrogen entering surface waters can cause excessive organic growth followed by stagnation, while contamination of underground reservoirs, which may be used for drinking water supplies, is a health hazard - particularly to young children.

Pretreatment and analysis of slurries to determine the nitrate content can lead to increased efficiency of application and reduced risk of pollution.

1.2 Methods of Analysis

There are a large number of techniques for carrying out the required measurements for either nitrate or dissolved oxygen analyses[2, 10-12]. These have included colourimetry[2], UV spectroscopy[2], potentiometry[13] and voltammetry for nitrate analysis while the Winkler titration[10,14], conductimetry[7], coulometry[15] and voltammetry have been widely used for dissolved oxygen measurement.

Some voltammetric nitrate reduction studies are described below, but the literature on the voltammetric reduction of dissolved oxygen is so vast that it will be only briefly mentioned.

1.2.1 The Voltammetric Reduction of Nitrate

The reduction of nitrate ions can be broadly divided into two categories;

(i) catalytic reduction,
and (ii) direct reduction.

(i) Catalytic Reduction

Electrochemical reduction has been studied using the catalytic waves obtained in the presence of cadmium (II), lanthanum (III), molybdate, dioxovanadium (V), ytterbium (III) and zirconyl ions, copper/cadmium codeposited on graphite and also in the presence of chromium (III) complexes of glycine[16-23].

The mechanisms of these reactions involve either the reduction of a complex formed between nitrate and the added species, or the enhancement of the cathodic current due to the reduction of

the added species - the reduced form of which is rapidly oxidized by nitrate. The latter is illustrated by the mechanism proposed for reduction using Cd^{2+} on a glassy carbon electrode(22):

Metallic cadmium is deposited on the electrode by an anodic to cathodic potential sweep;

$$Cd^{2+} + 2\bar{e} \longrightarrow Cd^{o} \qquad (1.3)$$

When the sweep is reversed then a cathodic peak is observed due to the reaction of the metal with nitrate;

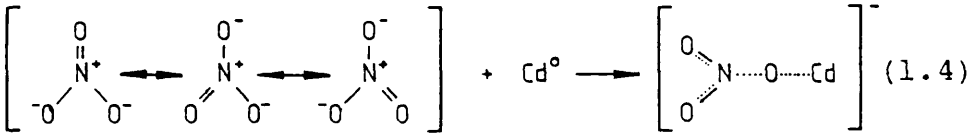

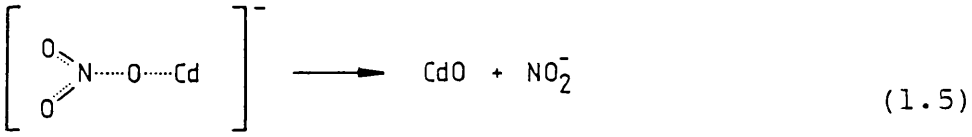

The Cd^{2+} is regenerated by dissolution of the cadmium oxide;

$$CdO + 2H^{+} \longrightarrow Cd^{2+} + H_2O \qquad (1.6)$$

In order to complete the catalytic cycle the last process must be faster than the formation of the oxide. In solutions which are not strongly acidic then the dissolution process is not sufficiently fast and the electrode becomes blocked with the oxide.

(ii) Direct Reduction

A variety of materials including Cd, Cr, Cu, Pb, Pt, Ti, Zn, Cu(Hg), Sn(Hg) have been investigated for their suitability as electrodes for the direct reduction of nitrate[24-34].

(a) Cadmium A rotating cadmium disc electrode has been used to examine nitrate reduction using hydrochloric acid (10 mmol dm^{-3}) as the supporting electrolyte. There was no separation of the cathodic and anodic currents, the anodic potential being limited by oxidation of the cadmium (-0.85V vs SCE) whilst the cathodic potential was limited by hydrogen evolution (-1.30V vs SCE).

At low rotation speeds and bulk nitrate concentrations the reduction currents were found to be limited by convective-diffusional mass transport and plots of the limiting current vs nitrate concentration were linear with zero intercept for $[NO_3^-] < 0.35$ mmoldm^{-3}.

Nitrite could also be reduced using this system but the reaction was found to be highly irreversible and the limiting current plateau was obscured by hydrogen evolution[24].

(b) Copper Pletcher et al. have used a rotating copper disc electrode to study nitrate reduction in aqueous acidic perchlorate and sulphate media[26]. The potential range was limited by copper dissolution (ca. OV vs SCE) at the anodic end and by hydrogen evolution (ca. -0.7V vs SCE) at the cathodic end, but below pH2 irreversible waves were observed with mass transfer control at high overpotentials. The half-wave potential was found to be pH dependant and also sensitive to halides such that $E_{\frac{1}{2}}$ was shifted to more negative potentials with increasing halide concentration.

Controlled potential electrolyses of nitrate gave an electron transfer number, n, of about 8. The solutions were analysed for both hydroxylamine and ammonia. No evidence was found of the former, but ammonia yields were in the range 64-88% after the passage of 8F mol^{-1}. In the presence of sufficient protons the overall reaction was taken to be;

$$NO_3^- + 8e^- + 9H^+ \longrightarrow 3H_2O + NH_3 \quad . \quad (1.7)$$

Nitrite could also be reduced using this system.

Copper was chosen for further investigation as a cathode for the direct reduction of nitrate because of its low cost and apparent simplicity. It also has the advantage of compatability in a greenhouse environment where the toxicity of Cd, Pb, Hg, etc. would not be appreciated.

1.2.2 Voltammetric Reduction of Dissolved Oxygen

Many materials have been investigated for their suitability as electrodes for dissolved oxygen reduction, e.g. Ag, Au, C, Hg, Pt[35-46]. The dropping mercury electrode has been extensively used since it has the advantage that the electrode surface is renewed every few seconds which minimises the effect of electrode contamination. The DME is cumbersome, however, and in many cases it is unsuitable due to the danger of poisoning.

Solid electrodes can be made into robust monitors but have the drawback that the surfaces are readily contaminated and are not easily renewed.

1.3 Membrane covered amperometric sensors

This type of sensor was pioneered by Clark in the 1950s[47-49] and since that time it has become perhaps the most widely used type of dissolved oxygen monitor. The concept is to separate the working electrode from the test solution by an oxygen permeable membrane, Fig.1.1.

The sensors may be either galvanic or voltammetric but perhaps the most successful has been the Mackereth electrode[50] which is based on a silver-lead galvanic couple. Oxygen is reduced at the silver cathode while lead (II) hydroxide is precipitated at the consumable lead anode;

$$O_2 + 2H_2O + 4\bar{e} \longrightarrow 4OH^- \qquad (1.8)$$

$$2Pb + 4OH^- \longrightarrow 2Pb(OH)_2 + 4\bar{e} \qquad (1.9)$$

1.3.1 Oxygen flux across the membrane

In a traditional Clark-type sensor the working electrode potential is sufficient to immediately reduce any oxygen arriving at the electrode surface;

$$O_2 + n\bar{e} \longrightarrow \text{reduction products} \qquad (1.10)$$

This imposes a concentration gradient across the membrane and consequently there is a continuous flux of oxygen across the membrane and electrolyte. Thus, a continuous current may be observed at the working electrode and, under suitable circumstance, the magnitude of this current is proportional to the external oxygen concentration.

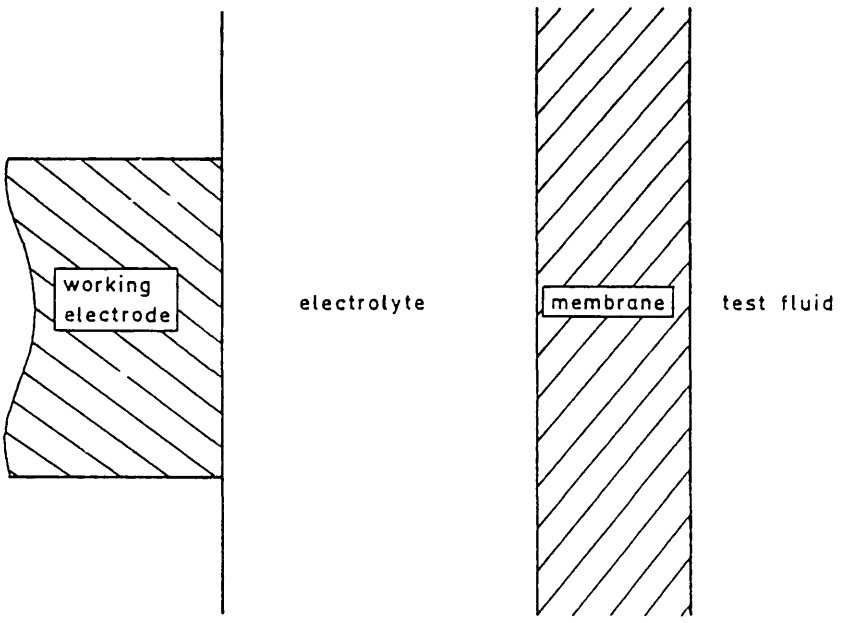

Fig.1.1. Schematic representation of a Clark-type electrode

1.3.2 Steady-State Current

At steady-state the flux of oxygen to the working electrode surface is the same in both the electrolyte and membrane phases. From Fick's first law of diffusion;

$$j/A = D_e(c_2 - c_1)/a \qquad (1.11)$$

$$= D_m(c_4 - c_3)/b \qquad (1.12)$$

where c_i is the boundary oxygen concentration, as defined in Fig.1.2

- j is the steady-state oxygen flux
- A is the electrode area
- D_i is the oxygen diffusion coefficient in phase i
- a is the electrolyte thickness
- b is the membrane thickness

For a simple, irreversible reaction

$$O + n\bar{e} \xrightarrow{k'} R \qquad (1.13)$$

the flux to the electrode is given by the rate of electron transfer;

$$j/A = k'c_1 \qquad (1.14)$$

From the distribution laws;

$$c_4 = \xi_m c_s / \xi_s \qquad (1.15)$$

and $$c_3 = \xi_m c_2 / \xi_e \qquad (1.16)$$

where ξ_i is the oxygen solubility in phase i. Using these relationships to substitute for c_3 and c_4 in (1.12) yields;

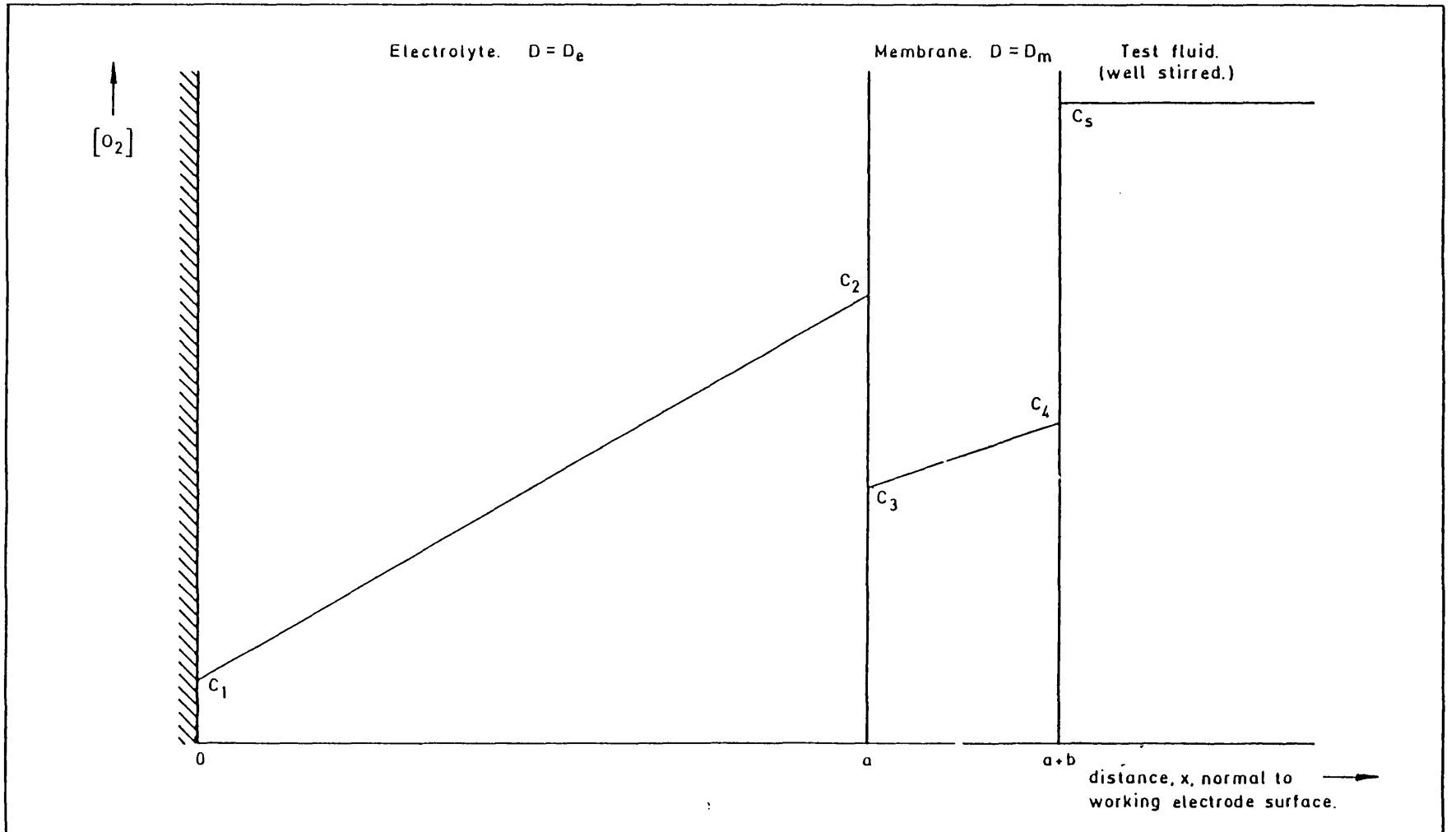

Fig.1.2. Steady-state oxygen profile across a Clark-type membrane electrode.

$$j/A = (\xi_m D_m/b)(c_s/\xi_s - c_2/\xi_e) \quad (1.17)$$

An expression for c_2 can be obtained by using (1.14) to substitute for c_1 in (1.11). Rearrangement yields;

$$c_2 = (aj/D_eA)(1 + D_e/ak') \quad (1.18)$$

This result can be used in (1.17) to give;

$$\frac{j}{A} = \frac{\xi_m D_m}{b}\left[\frac{c_s}{\xi_s} - \frac{aj}{\xi_e D_e A}\left[1 + \frac{D_e}{ak'}\right]\right] \quad (1.19)$$

Thus, $$\frac{j}{A}\left[1 + \frac{\xi_m D_m}{b}\left[\frac{a}{\xi_e D_e} + \frac{1}{k'}\right]\right] = \frac{\xi_m D_m c_s}{\xi_s b} \quad (1.20)$$

$$j\left[\frac{\xi_s b}{\xi_m D_m} + \frac{\xi_s a}{\xi_e D_e} + \frac{\xi_s}{\xi_e k'}\right] = Ac_s \quad (1.21)$$

and $$j = Ac_s\left[\frac{\xi_s b}{\xi_m D_m} + \frac{\xi_s a}{\xi_e D_e} + \frac{\xi_s}{\xi_e k'}\right]^{-1} \quad (1.22)$$

Now, if the electrode potential is sufficiently cathodic then k' will be very large and the flux will be diffusion controlled. The limiting flux, j_L, is given by;

$$j_L = Ac_s\left[\frac{\xi_s b}{\xi_m D_m} + \frac{\xi_s a}{\xi_e D_e}\right]^{-1} \quad (1.23)$$

Oxygen diffusion coefficients in polymers are generally two, or more, orders of magnitude less than that for an aqueous electrolyte[51]. Hence, the conditions in the average sensor are such that $b/P_m >> a/P_e$. Then, the limiting flux is given by;

$$j_L = Ac_s \xi_m D_m/\xi_s b \quad (1.24)$$

Now, if the test fluid is in the liquid phase, then

$$j_L = Ac_s P_m/b \qquad (1.25)$$

where P_m is the permeability coefficient given by;

$$P_m = \xi_m D_m / \xi_s \qquad (1.26)$$

In the gas phase, the limiting flux is given by;

$$j_L = ApP_m/b \qquad (1.27)$$

where P_m is the permeability coefficient given by;

$$P_m = \xi_m D_m \qquad (1.28)$$

and p is the oxygen partial pressure;

$$p = p_{O2}/p_{total} \qquad (1.29)$$

The corresponding diffusion-limited current, i_L, is given by;

$$i_L = nFAj_L \qquad (1.30)$$

Thus, for dissolved oxygen measurements;

$$i_L = nFAc_s P_m/b \qquad (1.31)$$

while for gas measurements;

$$i_L = nFApP_m/b \qquad (1.32)$$

These results show that the steady-state, diffusion-controlled current is linearly related to the oxygen concentration in the test-fluid.

Mancy, Okun and Reilley derived the former result by extrapolation of a time dependent series solution(52).

1.3.3 The Membrane

Clark-type sensors are distinguished from conventional electrochemical cells by the inclusion of a permeable membrane between the test solution and the electrodes which make up the cell.

The membrane serves several purposes:
(a) it contains the clean electrolyte in which the oxygen reduction occurs;
(b) it prevents the passage, from the test fluid to the electrolyte, of ionic species which may give rise to unwanted background currents or interfere with the reduction reaction;
(c) it excludes large molecules, such as proteins, which may poison the electrode surface;
(d) it prevents suspended solids in the test fluid from blocking the electrode surfaces;
(e) it allows the measurement of gas phase oxygen levels, if required.

Thus, the membrane imparts many advantages to the sensor and these have contributed to its popular use, but there are a number of disadvantages - the current observed is a function of:

(a) the membrane permeability - which is temperature sensitive[10];

$$P_m = P_o \exp(-E_p/RT) \qquad (1.33)$$

where E_p is the activation energy for permeation. The membrane may also undergo changes in its crystallinity and this will severely affect the magnitude of P_m;
(b) the membrane thickness - which is liable to change as the membrane either expands or relaxes;
(c) the amount of membrane fouling (if any); and

(d) the degree of stirring in the test fluid: friction between the membrane and the flowing fluid causes a hydrodynamic boundary layer, Z_H, to be formed. In the case of laminar flow with the direction of flow normal to the electrode axis, then

$$Z_H \approx xR_y^{-\frac{1}{2}} \qquad (1.34)$$

where R_y is the Reynolds number and x is the flow velocity. When the flow velocity is high then Z_H is very small and oxygen-transport is limited only by the membrane. Conversely, if the fluid is stagnant then oxygen-transport is governed by diffusion in both the medium and membrane[53].

These problems, (a)-(d), arise because the steady-state current is due to a flux of oxygen across the membrane.

1.3.4 Improved Clark Cells

The temperature dependence of the observed current can be compensated, to some extent, by incorporation of a temperature sensor into the dissolved oxygen monitor. The temperature signal can be used to suitably adjust the oxygen reduction signal[10, 54].

The flow dependence of the observed current can be reduced by using a thicker or less permeable membrane, but this reduces the electrode sensitivity and slows down its response time. An alternative strategy has been proposed by Ben-Yaakov and Ruth who have presented computer simulations and experimental results to show that a double layer membrane can dramatically reduce the flow-sensitivity while maintaining a reasonable response time. The outer membrane has to be relatively thick and very permeable. Best

results were obtained with a 2 mil Teflon/10 mil silicone rubber composite[55].

Micro-electrodes can also be used to reduce the flow dependence of membrane covered electrodes: if the electrode radius is much smaller than the membrane thickness then radial diffusion becomes important. Thus, the effective membrane area is increased and the flow sensitivity is reduced[56].

Current density increases as the electrode area is decreased and this puts a lower limit on the size of any such practical electrode. In order to overcome this problem several methods for boosting the steady-state current have been investigated. Butler et al. used a spiral of 40mm thick platinum as the cathode[57], but a more popular technique is to use a multicathode arrangement[53, 58].

Ross has patented a membrane-covered sensor with a porous anode placed between the cathode and the gas-permeable membrane. Oxygen is reduced at the cathode while a similar amount of oxygen is produced at the anode. The current is still a function of the external oxygen partial pressure, but at steady state there is no net oxygen flux across the membrane[59]. This eliminates the dependence on membrane properties, fouling, etc., but the observed current becomes critically dependent on the interelectrode distance which is subject to change.

The Ross concept was refined by Taylor et al. who used coplanar, interdigitated anodes and cathodes. This arrangement has the same advantages as the Ross electrode but, in addition, the current is no longer critically dependent on the interelectrode distance[60,61].

1.4 Summary

Measurements of nitrate and/or dissolved oxygen concentrations are very important. There are many areas of application and many methods of analysis. Development of voltammetric sensors for each of these species is described in this thesis. Published work on nitrate reduction is indicated and membrane-covered Clark-type electrodes are discussed.

CHAPTER 2

EXPERIMENTAL DETAILS

2.0 Introduction

This chapter contains details of some of the apparatus and procedures used to obtain experimental results laid out in Chapters 3 and 4. Other details are included in these later chapters when they are helpful to the discussion.

2.1 Disc Electrodes

Disc electrodes were of the form shown in Fig.2.1. For experiments involving controlled hydrodynamics the disc electrodes were rotated to give a well-defined diffusion layer, while for stationary electrode experiments the disc electrodes were used because of their availability and because of their well-defined planar geometry.

The disc as well as other electrodes were made by Michael Pritchard in the WJA Workshops at Imperial College.

2.1.1 Materials

Metals for the disc and other electrodes, were from Johnson Matthey. Gold was grade 2, and platinum grade 4 while both nickel and silver were Specpure.

Teflon or Kel-F were favoured as insulating materials for the sheath since they are resistant to non-aqueous solvents. However, in aqueous solution it was found that these plastics tended to promote the adhesion of gas bubbles on their surfaces and this could lead to spurious results.

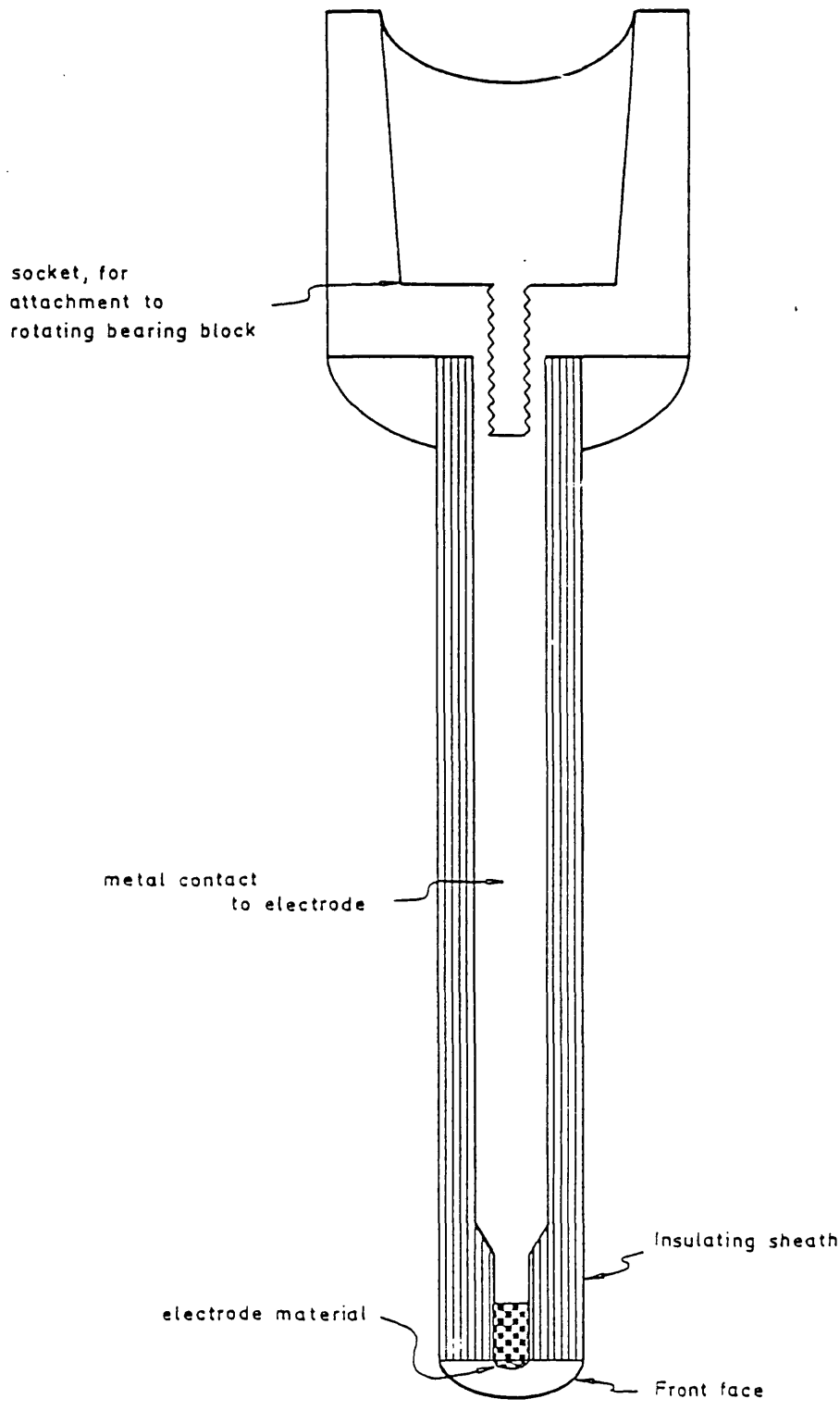

Fig. 2.1 . Projection of section through a typical disc electrode.

(Approximately twice actual size.)

Delrin and epoxy resin were less prone to this problem, but epoxy resin could not be used in organic solvents and Delrin was not recommended. Delrin was also found to be vigorously attacked by aqueous perchloric acid.

2.1.2 Dimensions

A travelling microscope, mounted on a jeweller's lathe, was used to measure the dimensions of disc and ring-disc electrodes with a precision of 0.001mm. At least twelve readings were taken about the circumference of the electrode and the mean values, together with the standard deviations, are reported in Table 2.1.

The miniature, gold disc electrodes 18 and 20 were slightly off-centre (ca.0.07 and 0.04mm. respectively), even when the electrode body was running true. The figures quoted in the Table are corrected for this eccentricity.

2.1.3 Preparation

The electrodes were polished to a mirror finish using the following procedures;

(i) machining marks and other gross surface imperfections were removed by using a glycerol slurry of 25μ aluminium oxide (Buehler Ltd., Lake Bluff, Il.) on a polishing pad with a rotating polishing table (Oxford Electrodes);

(ii) 6μ diamond lapping spray (Hyprez, Engis Ltd.), together with a water-based lubricant and a fresh polishing pad, were used to remove surface scratches;

(iii) a mirror finish was produced by manual application of 1μ polishing alumina (Banner

Electrode	Disc	Ring	Sheath	r_1 /mm	r_2 /mm	r_3 /mm	A_D /mm^2	A_R /mm^2
CU1	Cu	-	araldite	3.53±0.01	-	-	39.15±0.05	-
F	Ni	-	araldite	3.490±0.002	-	-	38.26±0.04	-
H	Pt	Pt	teflon	3.508±0.004	3.783±0.004	4.040±0.020	38.66±0.09	6.32±0.60
K	Pt	Pt	araldite	3.505±0.004	3.788±0.004	4 039±0.005	38.59±0.09	6.18±0.24
6	Au	Pt	delrin	1.424±0.005	1.554±0.005	1.844±0.004	6.37±0.05	3.12±0.08
10	Cd	-	delrin	3.488±0.003	-	-	38.22±0.06	-
14	Ni	-	PTFE	3.530±0.005	-	-	39.14±0.11	-
15	Au	-	teflon	3.520±0.002	-	-	38.93±0.04	-
18	Au	-	teflon	0.472±0.007	-	-	2.80±0.08	-
21	Au	-	teflon	0.484±0.010	-	-	2.94±0.12	-

Table 2.1. Disc and ring-disc electrode specifications.

r_1 - disc radius r_2 and r_3 - inner and outer ring radii

A_D - disc area A_R - ring area

Scientific, Coventry) using an aqueous slurry on a cotton wool pad;

(iv) the electrode was polished with 0.3μ alumina immediately prior to each experiment. This further reduced the surface roughness and produced a fresh, clean surface.

2.1.4 Rotation of the Electrodes

Disc and ring-disc electrodes were screwed on to a rotating bearing-block. Mercury wetted contacts provided the electrical contact. A DC servo-motor (Printed Motors Ltd.) was mounted on top of the bearing block. The position of a 10-turn analogue dial, on a motor controller (Oxford Electrodes), determined the rotation speed which was measured using optical feedback from a slotted i.r. opto-switch and slotted disc. The rotation speed was read from a four-digit LED display.

Rotation speeds up to 36Hz were continuously available, while speeds of up to 49Hz were available for short periods of time. Control below 1Hz could be erratic, depending on the particular rig.

The bearing block and motor assembly were mounted on a pair of steel pillars which allowed the electrode to be raised or lowered to any desired position.

2.2 Membrane electrodes

Membrane covered sensors were fabricated so as to contain working, reference and counter electrodes within the same body.

2.2.1 General purpose sensors

The general purpose design was that shown in Fig.2.2. All electrodes were coplanar on the front face of the sensor. Two working electrode materials (gold and platinum) were usually incorporated, so as to give some choice for a particular application. The reference electrode (q.v.) was silver chloride plated on to the silver disc. The counter electrode was a platinum ring. Working and reference electrode diameters were either 1.0 or 1.5 mm diameter.

The annular depression round the group of electrodes was used as an electrolyte reservoir - a few drops of the electrolyte were introduced on to the face of the sensor and a teflon membrane (12μ Radiometer D602) stretched over the top. The membrane was held in place by a rubber O-ring which was seated in the groove round the side of the sensor body.

2.2.2 Micro-electrodes

Two sensors were fabricated with micro-sized gold working electrodes. Wire with a diameter of 0.004" was used for this purpose. This gave an approximate working area of 8×10^{-5} cm^2. Both sensors incorporated silver/silver chloride reference electrodes and nickel hydroxide counter electrodes (q.v.).

The first design, Fig.2.3, was such that the three electrodes were coplanar and the working electrode sat close to the counter.

The second design, Fig.2.4, was such that;

(a) the counter and primary reference electrodes were set back from the front face and within the electrolyte reservoir,

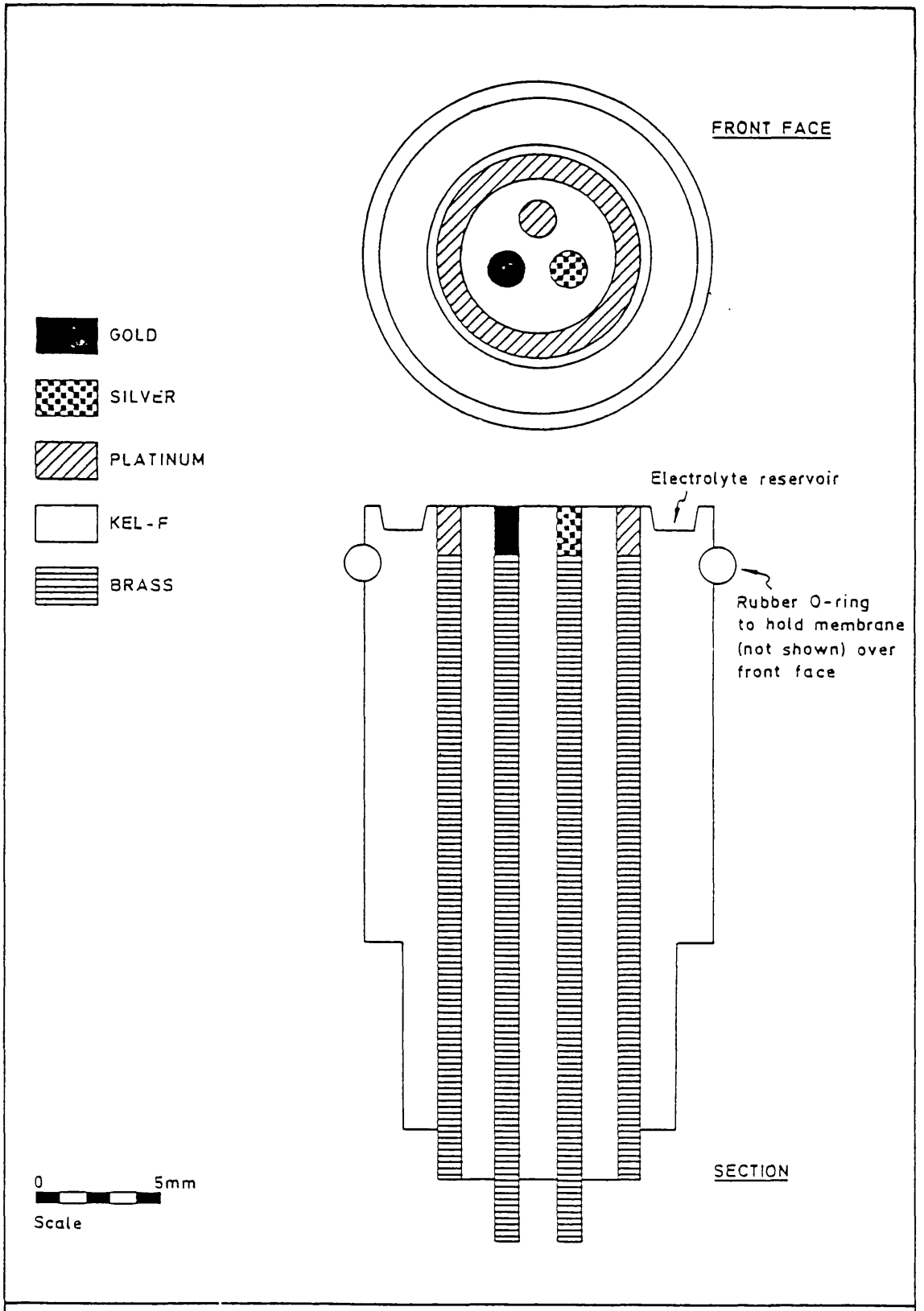

Fig. 2. 2. General purpose membrane-covered sensor.

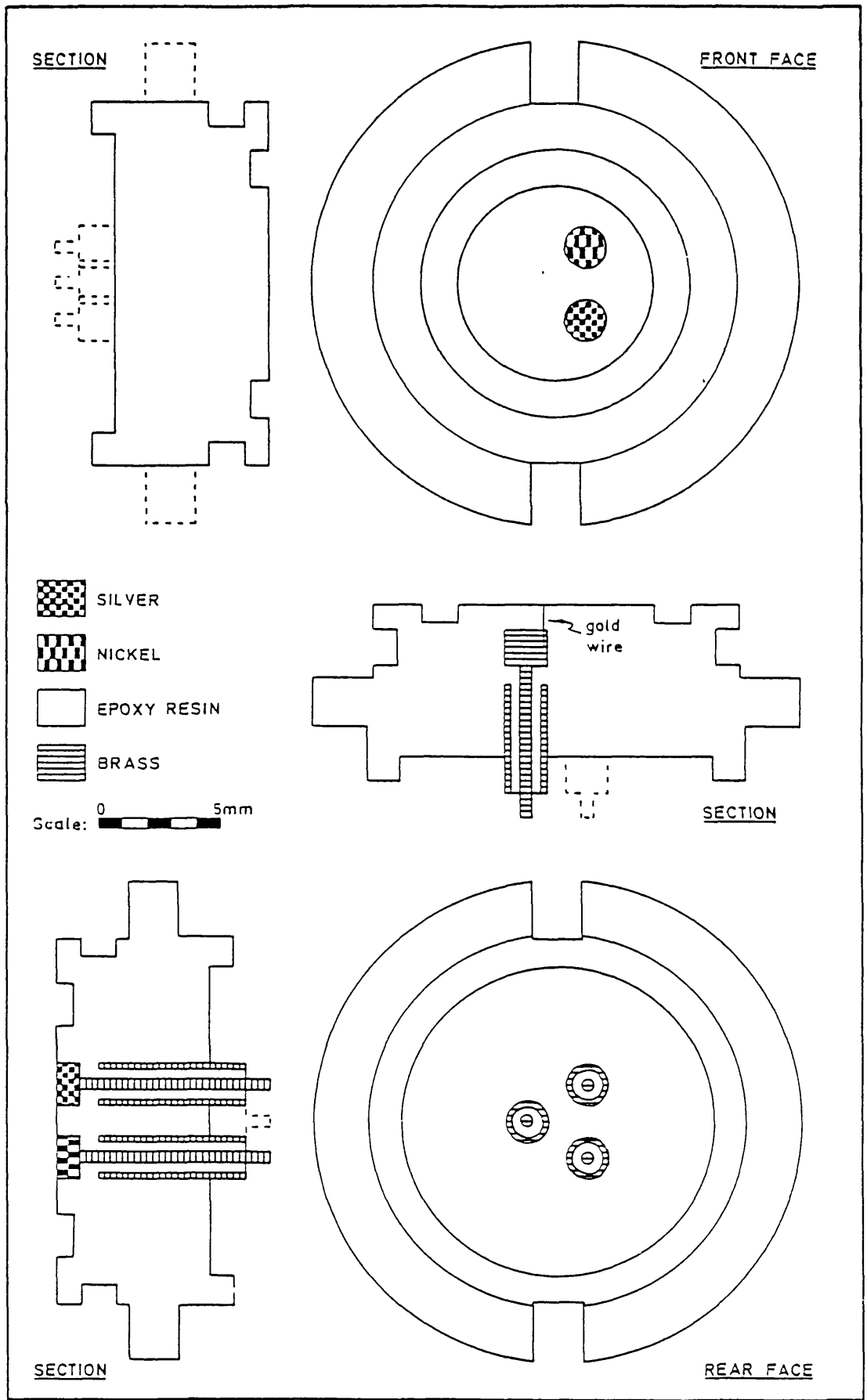

Fig.2.3. Construction of the membrane cell with micro-sized gold working electrode.

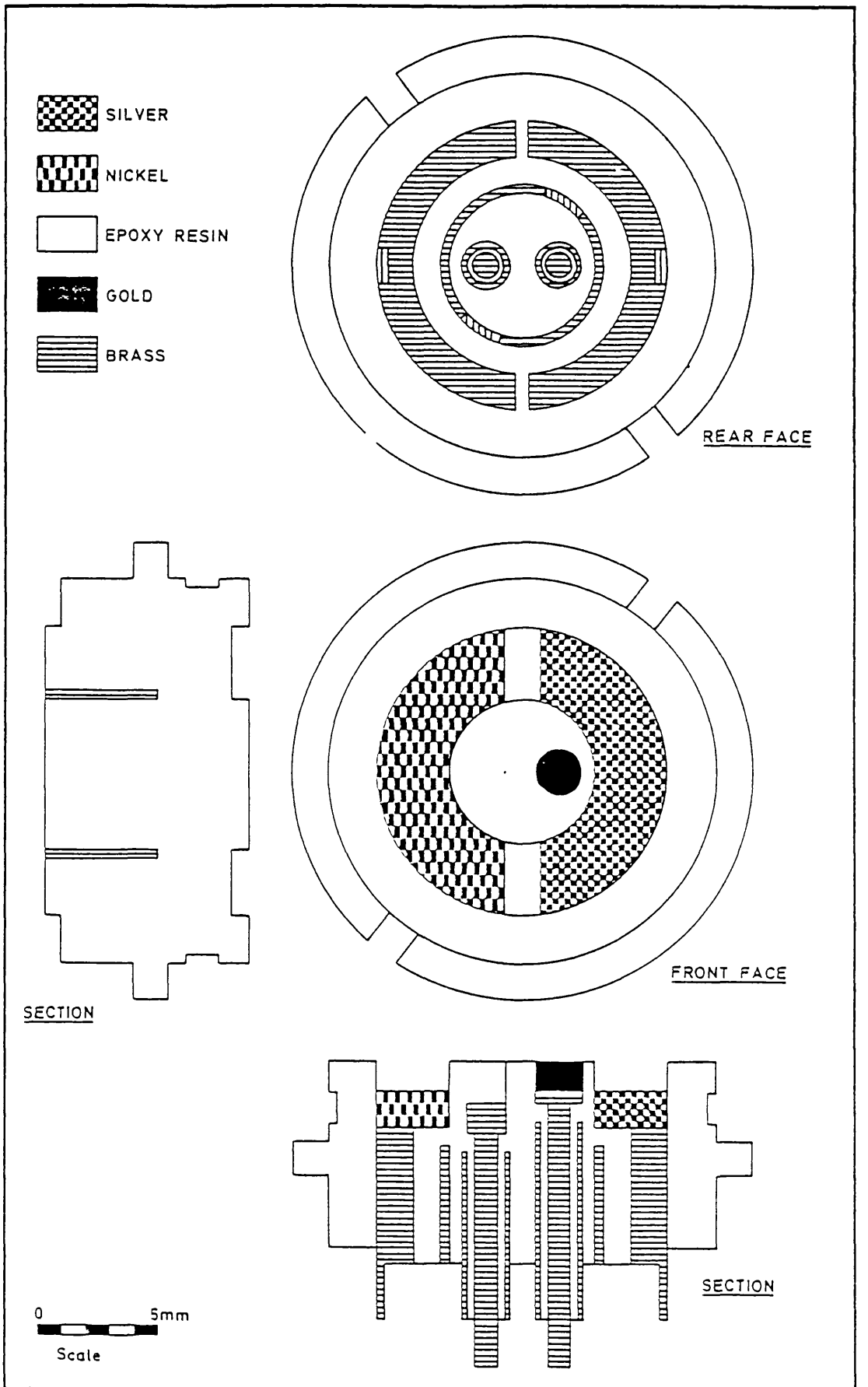

Fig. 2. 4. Construction of the double reference membrane electrode with micro-sized gold working electrode.

(b) a large gold quasi-reference electrode was incorporated in the front face of the sensor so as it sat close to the micro-electrode. It was coupled to the silver/silver chloride reference via a 22MΩ resistor and a 100nF capacitor[62].

This arrangement had two advantages;

(i) the front face of the sensor could be easily polished without depositing either nickel or silver on the working electrode, and

(ii) the close proximity of the quasi-reference to the working electrode reduced the uncompensated resistance.

Steady-state currents from the sensors were very small, so a number of precautions were taken to reduce the amount of noise;

(i) each electrode within the sensor was protected by a brass shield connected to the electrical common,

(ii) current-voltage conversion was carried out using a high quality Analog Devices AD515 amplifier placed immediately behind the working electrode,

(iii) all external connections were via low noise, shielded cables,

(iv) the amplifier and all connections were enclosed within a brass cylinder connected to the electrical common. It was araldited in position and the outside surface varnished so as to protect it from chemical attack.

These precautions allowed sub-nanoamp currents to be successfully measured.

A problem with this type of sensor was in maintaining the seal round the micro-electrode. The source of the problem is thought to have been differential expansion while making soldered joints. Sensors are now made with plug-in connectors.

2.2.3 Silver/silver chloride reference electrodes

Silver chloride was plated on to silver using a slight modification of the technique reported by Midgley and Torrence.[63] The electrode was placed in hydrochloric acid (10mmol dm^{-3}) and galvanostatted at a current density of 10-20mAcm^{-2} for a few minutes until the first traces of silver chloride could be seen. The current density was then reduced to 0.1 - 0.2mAcm^{-2} for 24 hours.

With membrane covered electrodes it was found that the chloride concentration, if any, in the bulk electrolyte made little, if any difference to the reference potential. One problem, however, was that colloidal silver tended to migrate to the working electrode. This problem was particularly acute in basic, aqueous electrolytes but the effect has not been noted in non-aqueous solvents.[64]

2.2.4 Nickel hydroxide counter electrodes

This material was chosen as a counter electrode because of its ability to pass large quantities of charge before the onset of oxygen evolution. This property was particularly important when making dissolved oxygen measurements because evolution at the counter electrode could lead to spurious results.

Nickel hydroxide has been extensively studied[65-70] because of its importance in battery technology, but there is still much discussion over the exact chemical transformations. At its simplest the reaction may be described as;

$$Ni(OH)_2 + OH^- \rightleftharpoons NiO(OH) + H_2O + e \quad (2.1)$$

Thus, there is a solid-state transformation but no oxygen evolution.

Thick oxide films could be made using the Wynne-Jones method.[65] The roughened nickel surface was galvanostatted at a current density of $1mAcm^{-2}$ for ca.2 mins in nickel nitrate (1 mol dm^{-3}). Very large peaks were observed initially but these became smaller until they reached a stable magnitude, Fig.2.5.

At alternative technique was to grow the hydroxide film by potential cycling the roughened nickel surface in sodium hydroxide (1 mol dm^{-3})[67]. This gave lower charge capacity but the procedure was often more convenient.

The counter electrode could only be used at pH>11.

2.2.5 Other Electrodes

A stationary, gold microdisc electrode (ø = 0.004") was fabricated, Fig.2.6. Measures were taken to increase the signal-noise ratio, as with the other micro-electrodes (section 2.2.2).

Where possible, saturated calomel electrodes were used as references. These were either manufactured in house or purchased from Radiometer.

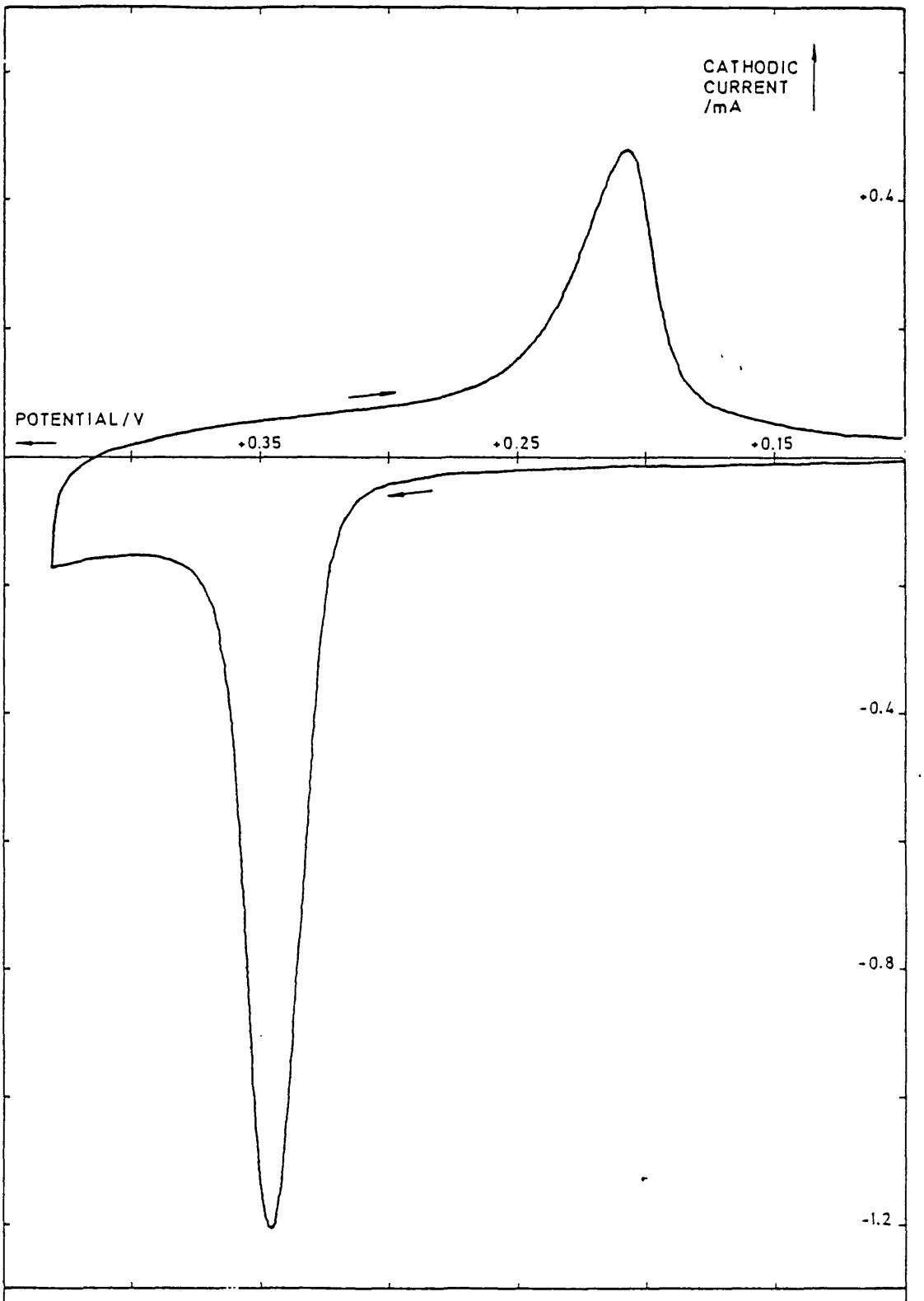

Fig. 2.5. Cyclic voltammogram of nickel hydroxide electrode in sodium hydroxide (1 mol dm^{-3})

A = 1.8 mm^2 v = 5 mV s^{-1}

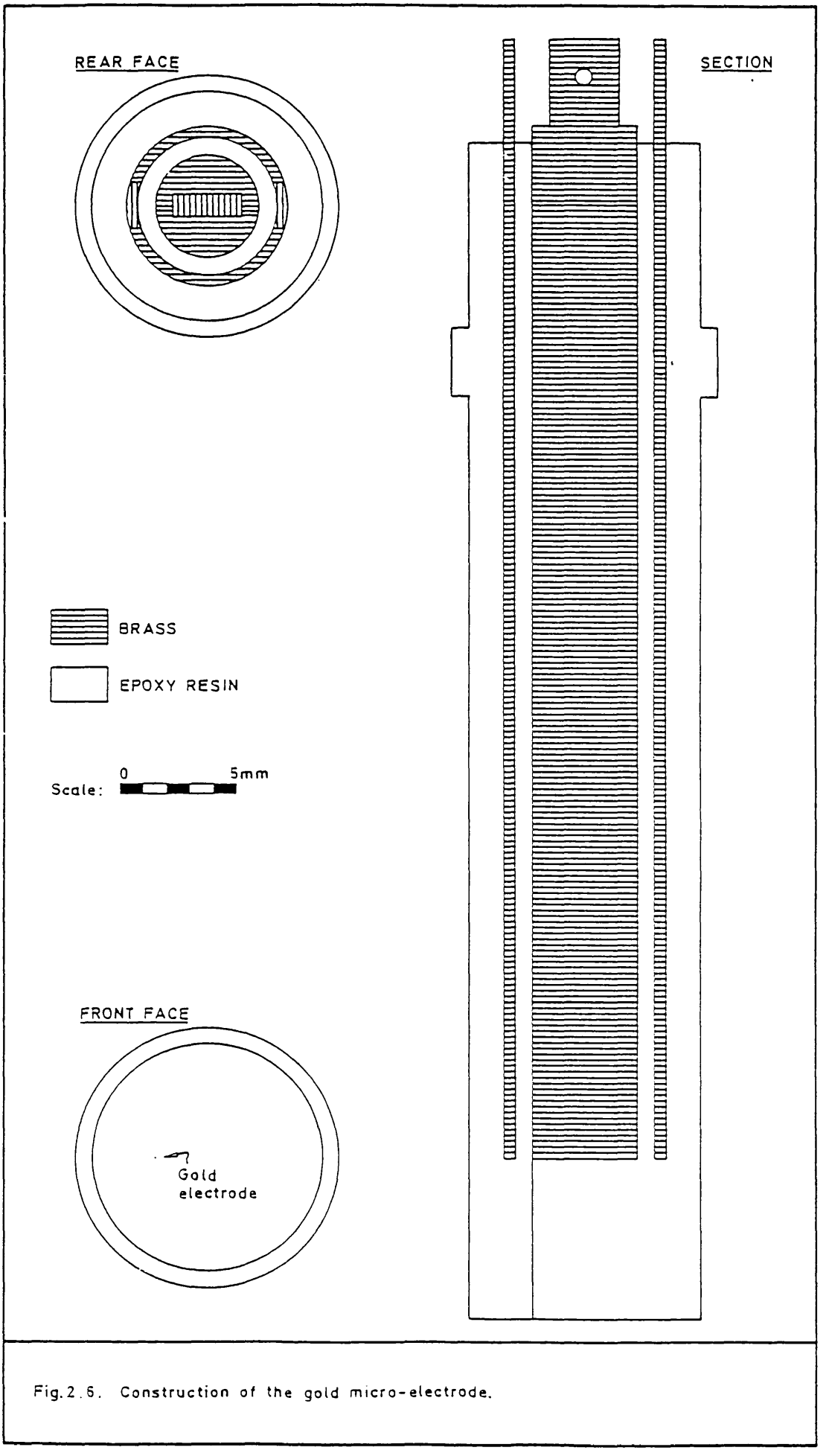

Fig. 2.6. Construction of the gold micro-electrode.

2.3 The Electrochemical Cell

A cell of the type shown in Fig.2.7 was used for many of the electrode studies. Water from a thermostatted tank was circulated between the double walls of the vessel and this allowed the temperature of the test solution to be maintained at 25.0 ± 0.3°C.

A saturated calomel electrode (SCE) was generally used as the reference electrode and this and the working electrode were located through holes in the closely fitting Teflon lid. A platinum gauze counter electrode was kept behind a sintered glass frit, in the side arm compartment.

The gas bubbler was used to deoxygenate, or otherwise equilibrate, the test solution with the required gas mixture. A further hole in the lid allowed the gas to be passed over the solution, rather than disturbing the solution, when measurements were being recorded.

2.4 Gas Mixtures

Mixtures of oxygen, in a carrier gas, were obtained by using an array of flowmeters (GEC Marconi/Fisher Controls Series 1100) or both channels of a Signal Instruments 852 blender or two of the three channels of a Signal 853 blender.

2.4.1 Flowmeters

The flowmeters were operated by using a needle valve to control the flow of gas through a tube, the flow rate being indicated by the position, on an arbitrary scale, of a metal float in the tube. The tubes were calibrated using

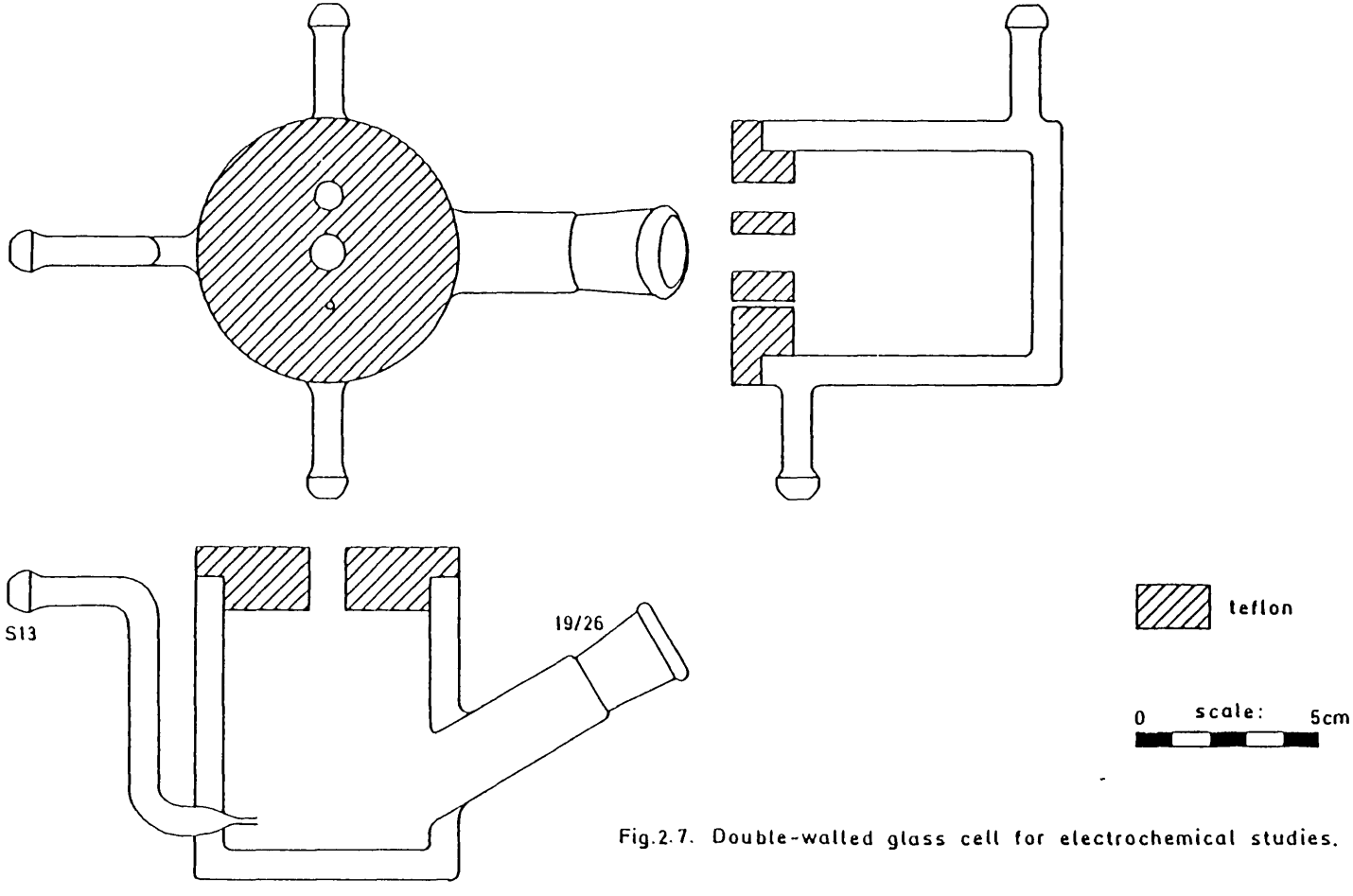

Fig.2.7. Double-walled glass cell for electrochemical studies.

bubble flowmeters[71] and the particular gas for which the tube was intended (Figs 2.8, 9, 10).

The behaviour of tube 336859/03 was idiosyncratic. The float position could not be adjusted, from below, to read above 20. Instead, the float would shoot off scale and the needle valve would have to be closed, a little, in order to bring the float back on to scale. The calibrated flow followed one curve, if the float was not allowed to exceed 20, while if the float hit the top stop then all subsequent readings followed another calibration curve, Fig.2.8, until the gas flow was completely shut off. The reproducibility of this effect was verified by three independent calibrations.

Oxygen concentrations were calculated using the following expression;

$$[O_2] \ / \ \text{vol\%} = f_{O2} \ / \ (f_{O2} + f_{N2}) \qquad (2.2)$$

where f_{O2} is the oxygen flow rate and f_{N2} is the flow rate of the carrier gas (nitrogen). When changes in oxygen concentration were necessary, then it was usual to maintain a constant total flow rate. This was achieved by the iterative adjustment of the positions of both the oxygen and nitrogen floats, since these were, to some extent, interdependent. This was a tedious procedure and experiments involving oxygen concentration changes were greatly simplified when the gas blenders became available.

2.4.2 Gas Blenders

The blenders manufactured by Signal Instruments were fixed flow devices, either 1 or 5 $dm^3\ min^{-1}$ output. They were operated, in the case of the 852 machines, by a 20-turn analogue dial

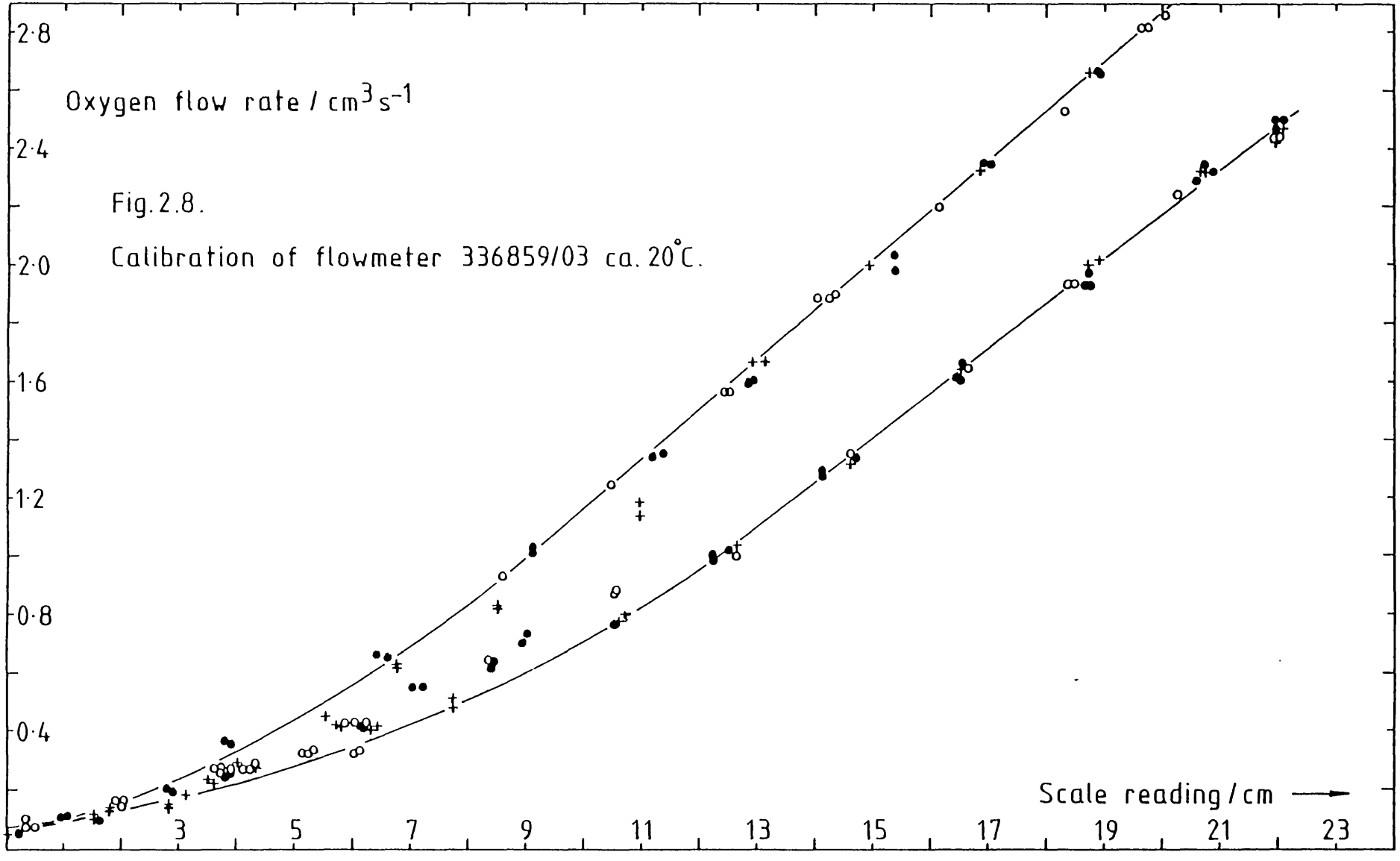

Fig. 2.8.

Calibration of flowmeter 336859/03 ca. 20°C.

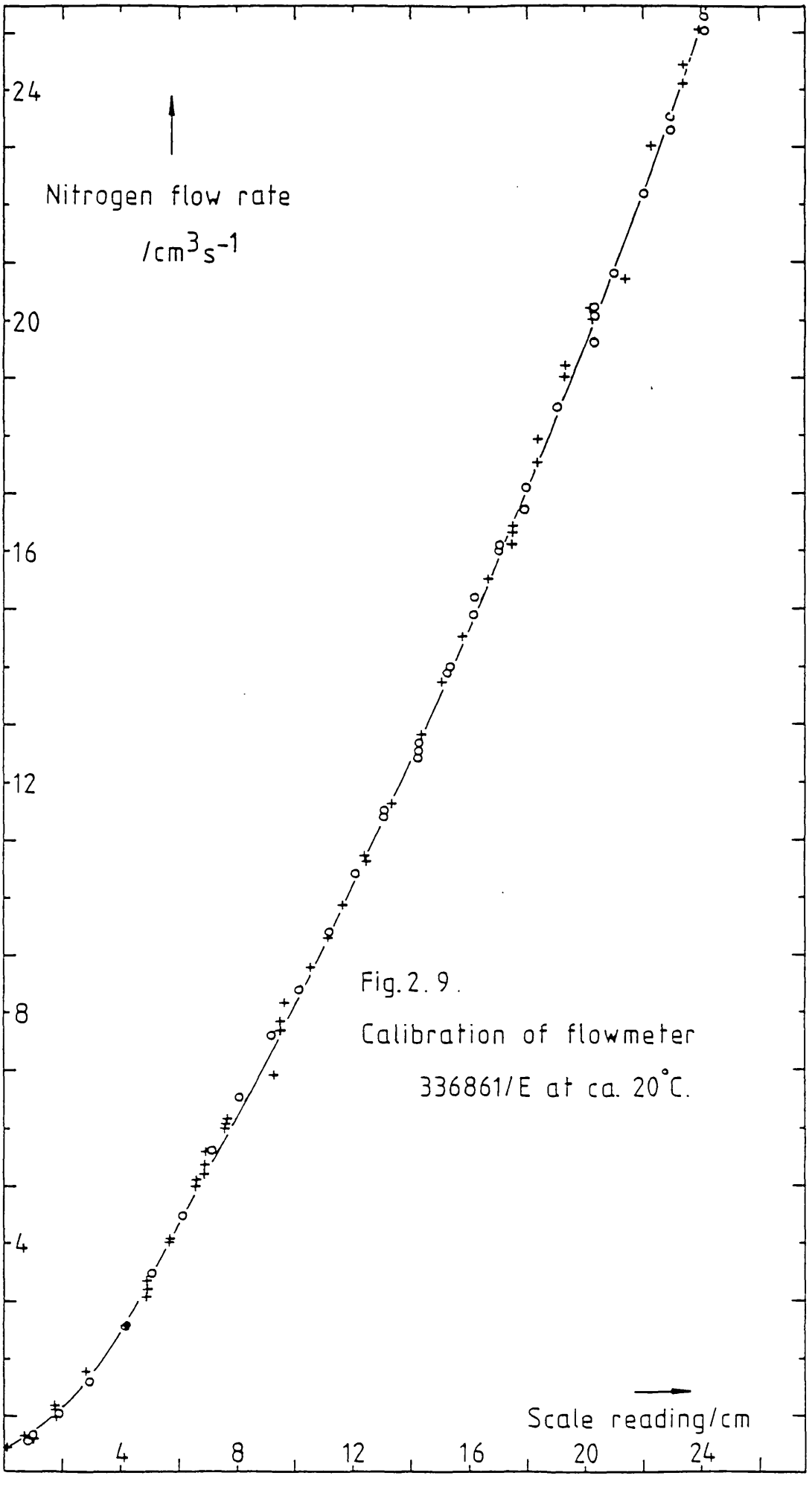

Fig. 2. 9.
Calibration of flowmeter
336861/E at ca. 20°C.

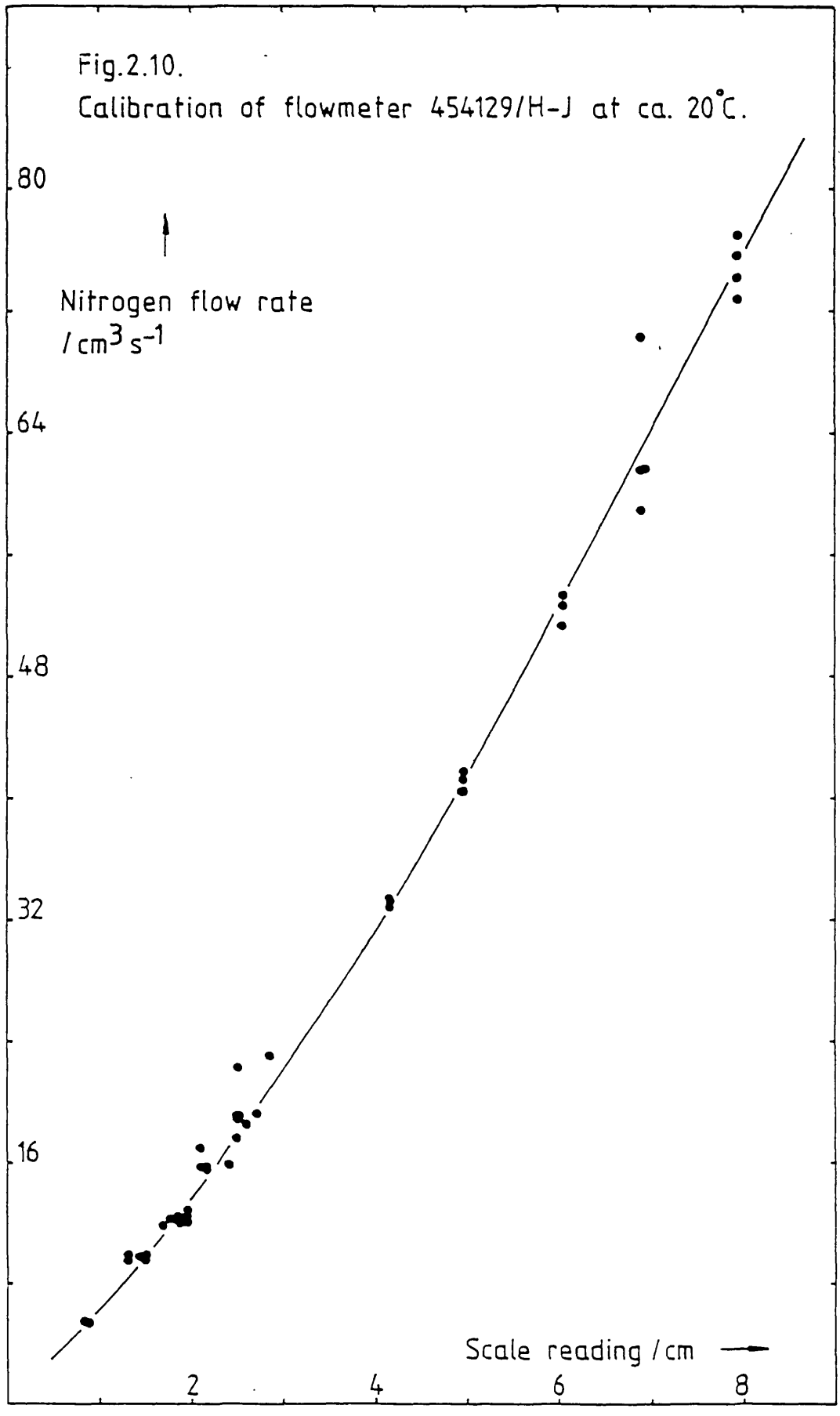
Fig.2.10.
Calibration of flowmeter 454129/H-J at ca. 20°C.
80
64
48
32
16
Nitrogen flow rate
/ cm3 s-1
Scale reading / cm
2
4
6
8

or, in the case of the 853 machine, by computer controlled servo-motors using digital-analogue convertors. Either mechanism determined the contribution of oxygen to the total flow, the remainder being automatically made up by the carrier gas.

The blenders were factory calibrated using compressed air on all inlet streams. A trace of propane was added to the stream to be calibrated and a flame ionisation detector was used to determine the ratio of propane in the inlet and outlet streams. The results were used to prepare calibration curves for the analogue dials or tables of concentration output vs potential input for the servo motors.

It was impractical to further deoxygenate the carrier gas used in the glenders since the inlet operating pressure was either 30 or 50 p.s.i., depending on the machine. Thus, high purity argon (BOC99.9999%) was used as the diluent.

From Graham's Law, the flow of gas through an orifice is inversely proportional to the square-root of the density, ρ , of the gas,

$$\text{flow rate, } f \propto \rho^{-\frac{1}{2}} \qquad (2.3)$$

The calibration curves supplied by Signal Instruments had to be corrected for this effect. The correction factor, CF, for oxygen in an argon stream, is given by;

$$CF = [100\% * (\rho_{O2}/\rho_{air})^{\frac{1}{2}}]^{-1}.$$

$$[D(O2) * (\rho_{O2}/\rho_{air})^{\frac{1}{2}} + (100\% - D(O2)) * (\rho_{Ar}/\rho_{air})^{\frac{1}{2}}] \qquad (2.4)$$

where D(O2) is the desired oxygen concentration. The experimentally determined factors, $(\rho_i/\rho_{air})^{1/2}$, as supplied by Signal Instruments, were used in practice.

gas,i	$(\rho_i/\rho_{air})^{1/2}$	
	theoretical	experimental
air	1.000	1.000
O_2	0.952	0.961
Ar	0.78	0.860

Table 2.2. Square-root density ratios

Then the concentration, S, to be read from the Signal Instruments calibration is given by;

$$S = CF * D(O2) \qquad (2.5)$$

Tabulated dial settings/DAC voltages are given in Tables 2.3, 4, 5. Useful oxygen in argon ratios are given and the corresponding percentages of propane labelled air (air*) are also included.

2.5 Chemicals

2.5.1 Purified Water

A mixed bed ion-exchange column (Model 3C Deioniser, Houseman (Burnham) Ltd.) was used in order to provide water of resistivity greater than $2M\Omega\ cm^{-1}$. This was then distilled twice from consecutive glass stills with silica sheathed heating elements.

% O_2 in Ar/(v/v)	% air* in air / (v/v)	dial setting	% O_2 in Ar/(v/v)	% air* in air / (v/v)	dial setting	% O_2 in Ar/(v/v)	% air* in air / (v/v)	dial setting	% O_2 in Ar/(v/v)	% air* in air / (v/v)	dial setting
0.0	0.00	20.00									
1.0	0.895	14.46	11.0	9.97	12.11	21.0	19.2	10.64	55.0	52.3	6.92
2.0	1.79	14.03	12.0	10.8	12.00	22.0	20.1	10.50	60.0	57.4	6.40
3.0	2.69	13.79	13.0	11.8	11.81	23.0	21.1	10.36	65.0	62.6	6.00
4.0	3.59	13.51	14.0	12.7	11.63	24.0	22.0	10.23	70.0	67.7	5.50
5.0	4.50	13.26	15.0	13.6	11.48	25.0	23.0	10.10	75.0	73.0	5.04
6.0	5.40	13.03	16.0	14.5	11.33	30.0	27.7	9.50	80.0	78.3	4.63
7.0	6.31	12.83	17.0	15.5	11.19	35.0	32.6	8.95	85.0	83.6	4.20
8.0	7.22	12.61	18.0	16.4	11.05	40.0	37.4	8.36	90.0	89.0	3.83
9.0	8.13	12.42	19.0	17.3	10.95	45.0	42.3	7.88	95.0	94.5	3.46
10 0	9.05	12.26	20.0	18.3	10.79	50.0	47.3	7.36	100	100	0.00

Table 2.3. Calibration of Signal blender 852P6S No. 1951 corrected for O_2 in Ar (23 June 83)

% O_2 in Ar / (v/v)	% air* in air / (v/v)	dial setting	% O_2 in Ar / (v/v)	% air* in air / (v/v)	dial setting	% O_2 in Ar / (v/v)	% air* in air / (v/v)	dial setting	% O_2 in Ar / (v/v)	% air* in air / (v/v)	dial setting
0 0	0.00	20.00									
1.0	0.895	14.53	11.0	9.97	12.26	21.0	19.2	10.92	55.0	52.3	7.12
2.0	1.79	14.11	12.0	10.8	12.13	22.0	20.1	10.79	60.0	57.4	6.66
3.0	2.69	13.87	13.0	11.8	12.00	23.0	21.1	10.64	65.0	62.6	6.16
4.0	3.59	13.62	14.0	12.7	11.87	24.0	22.0	10.50	70.0	67.7	5.73
5.0	4.50	13.40	15.0	13.6	11.70	25.0	23.0	10.36	75.0	73.0	5.22
6 0	5.40	13.17	16.0	14.5	11.55	30.0	27.7	9.80	80.0	78.3	4.80
7.0	6.31	13.00	17.0	15.5	11.40	35.0	32.6	9.19	85.0	83.6	4.32
8.0	7.22	12.79	18.0	16.4	11.27	40.0	37.4	8.66	90.0	89.0	3.92
9 0	8.13	12.60	19.0	17.3	11.14	45.0	42.3	8.11	95.0	94.5	3.45
10.0	9.05	12.43	20.0	18.3	11.00	50.0	47.3	7.63	100	100	0.00

Table 2.4. Calibration of Signal blender 852VIS No. 3039 corrected for O_2 in Ar (9 September 83)

% O_2 in Ar/(v/v)	% air* in air/(v/v)	DAC output/V	% O_2 in Ar/(v/v)	% air* in air/(v/v)	DAC output/V	% O_2 in Ar/(v/v)	% air* in air/(v/v)	DAC output/V	% O_2 in Ar/(v/v)	% air* in air/(v/v)	DAC output/V
0.0	0.00	0.00									
1.0	0 895	2.92	11.0	9.97	4.00	21.0	19.2	4.74	55.0	52.3	6.52
2.0	1.79	3.11	12.0	10.8	4.09	22.0	20.1	4.80	60.0	57.4	6.75
3.0	2.69	3.25	13.0	11.8	4.17	23.0	21.1	4.86	65.0	62.6	6.96
4.0	3.59	3.37	14.0	12.7	4.26	24.0	22.0	4.93	70.0	67.7	7.21
5.0	4.50	3.48	15.0	13.6	4.34	25.0	23.0	4.98	75.0	73.0	7.43
6.0	5.40	3.57	16.0	14.5	4.40	30.0	27.7	5.27	80.0	78.3	7.64
7.0	6.31	3.67	17.0	15.5	4.48	35.0	32.6	5.55	85.0	83.6	7.83
8.0	7.22	3.75	18.0	16.4	4.54	40.0	37.4	5.80	90.0	89.0	8.02
9.0	8.13	3.83	19.0	17.3	4.61	45.0	42.3	6.04	95.0	94.5	8.19
10.0	9 05	3.92	20.0	18.3	4.68	50.0	47.3	6.29	100	100	10.0

Table 2.5. Calibration of Signal blender 853V13 No. 3038 corrected for O_2 in Ar (29 September 83)

The distillation apparatus was latterly replaced by a Milli-Q Type 1 Reagent Grade Water System with four filter cartridges: (1) Super-C, activated carbon to remove organic contaminants and residual chlorine; (2) and (3) Ion-ex, a mixed bed ion-exchange resin to further remove dissolved inorganic electrolytes; (4) Organex-Q, a filter to remove trace organic material. This system was capable of producing water of resistivity 18 MΩ cm^{-1} at 25°C.

The deionised and doubly distilled water will be referred to as DDW, while the water produced by the Milli-Q system will be referred to as MQW.

2.5.2 Chemicals and Solutions

Chemicals were of AnalaR grade, except silver perchlorate (general purpose reagent, > 98%), and all were used without further purification. Solutions were prepared with either DDW or MQW, as available.

When necessary, solutions were deoxygenated with either high purity argon, without further purification, or with white spot nitrogen (BOC Gases) which was further deoxygenated by passing through three Dreschel bottles containing a solution of sodium anthraquinone-2-sulphonate ($2gdm^{-3}$) over zinc amalgam. The amalgam reduced the yellow suspension to produce the red semi-anthraquinone which reacts rapidly with oxygen.(72)

2.6 Analogue Electronics

The analogue electronics used for measurement and control were based on integrated circuit operational amplifiers.(73)

Typical specifications, of three of the amplifiers used most often, are given in Table 2.6. The input offset voltage of the LH0042CD could be trimmed, using an external circuit, but these amplifiers were almost entirely phased out in favour of the more rugged, laser trimmed LM11C which was less expensive and more stable. The AD515 is particularly suitable for measuring very low currents and was used for remote applications in microelectrode sensors.

2.6.1 Decoupling

All amplifiers were decoupled using a pair of capacitors at each power input pin, Fig.2.11. This reduced noise on the power lines and attenuated spikes due to power surges on switching.

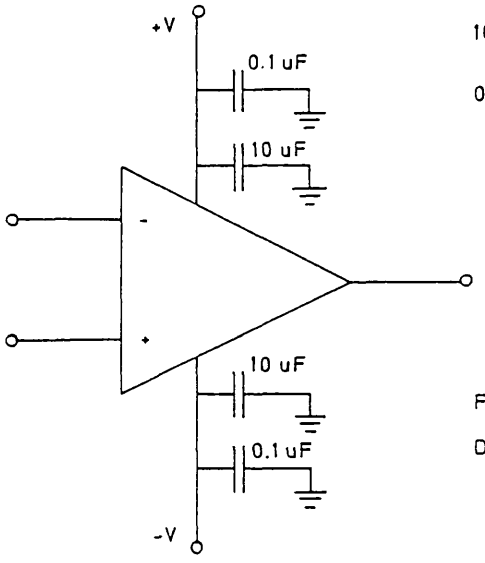

10 uF 35V tantalum, eg. RS102-702.

0.1 uF 30V ceramic, eg. RS125-806.

Fig.2.11.
Decoupling of operational-amplifiers.

2.6.2 Modules

Some of the most commonly employed feedback circuits were built in modular form for incorporation in a rack system.

Table 2.6. Typical operational amplifier specifications

Op-amp :	National Semiconductor LM11C	Analog Devices AD515K	(Radiospares) LH0042CD
Supply voltage / V	+/- 2.5 to 20	+/-5 to 18	+/-5 to 22
Short circuit current / mA	15	25	?
Open loop gain (2kΩ load) / db	109	92	100
Input impedance / Ω	10^{11}	10^{13}	10^{12}
Input offset voltage / mV	0.2	0.4	5
Input bias current / pA	40	0.15	10
Input offset current / pA	1	?	1
Slew rate / $V\mu s^{-1}$	0.3	?	3

Circuit boards were prepared using an ultra-violet light source to transfer circuits composed on acetate sheets to photosensitive copper-clad board. These were assembled, after developing and etching, and mounted on steel panels which could be screwed into an aluminium rack.

A +/- 15V DC power supply was connected via a 3-pin DIN socket at the rear of each module. Complex circuits could be made by interconnecting the modules using 4mm sockets in the top of each module which could be accessed via the lid of the box in which the rack was mounted. External connections were via BNC sockets in the front panel.

The aluminium box was connected directly to the earth of the mains supply so as it acted as a Faraday cage, but the +/- 15V supply was completely floating from the mains so as to avoid earth loops. BNC sockets were isolated from the box using teflon inserts and the BNC shields were individually wired to the supply common. These precautions, together with the decoupling, greatly reduced the number of problems associated with the electronics, as compared to boxes which were less carefully constructed.

Mechanical construction of the box was by John Hooper at Imperial College.

2.6.3 The Oxford Box

The 'Oxford Box' preceded the rack system, described above, and was used for some of the early work described in this thesis. It was a simple system consisting of two potential sources, six operational amplifiers and a selection of feedback elements, all mounted on a single panel. Individual feedback circuits were constructed using external connections via 4mm sockets.

2.7 The Chemistry Microprocessor Unit Interface System

A software controlled interface system (IS) was developed by Dr N J Goddard in the Chemistry Microprocessor Unit (CMU) at Imperial College. The CMUIS was operated by the Research Machines 380Z microcomputer and was based on a standard 19", 6U rack and a 19", 3U power rack. Each rack contained a controller board which was used to buffer and decode an extension of the computer's bus so as to identify the position of each rack in a daisy-chain system.

The CMUIS became available part way through the period of work described in this thesis and was an invaluable tool used in conjunction with the analogue electronics.

2.7.1 Function Boards

The standard rack contained slots for up to sixteen double-eurocard size, 5E wide function boards, while the power rack provided slots for up to four 20E wide, standard eurocard size modules. Each type of board was given a type number and if more than one board of a given type was present in the rack then each board was uniquely identified by its relative position. Thus, the lefthand most board (as viewed from the front of the rack) was numbered one, the next board of the same type on its right was numbered two, and so on.

a) DAC1

Board type 1. This contained two 12-bit digital-analogue convertors (accessed via ports 0 and 2 when writing to DACa and DACb respectively). Their output was either unipolar 0-10V or bipolar +/- 10V. The useful range was -2048 to 2047.

Values larger than this caused the value to be repeated approximately modulo 2048, i.e. 2048 was equivalent to 0 and -2049 equivalent to -1. The Hybrid Systems DAC336C12 was used, with an output impedance of 0.2 ohms and a current capability of 5mA.

b) ADC2

Board type 4. This provided a fast 12-bit successive approximation analogue-digital converter with integral sample and hold. The Datel ADC-HS12BMC could be configured in three bipolar input modes; +/- 2.5V, +/- 5V or +/- 10V. The ADC had a conversion and acquisition time of ca.20 s and an imput impedance of 100 megahms.

c) PIO1

Board type 2. This provided 32 parallel I/O lines programmable as either input or output in group of eight. The board was used to power a digital plotter.

d) TIMER 1

Board type 12. This provided a 32 bit, 8 decade timer.

e) 4 DC SWITCHES

Board type 64. This module was designed to fit the power rack and provided four 0.5A 24V DC switched outputs under computer control.

2.7.2 Combination of digital and analogue electronics

Several boards, other than those described above, were designed for the interface rack. A potentiostat board and a multiplexer board, with programmable offset and gain, were amongst these, but in practice it was found that these function boards were of limited use because of the large amounts of digital noise which corrupted the analogue electronics. High frequency noise was transmitted both through space and through the power bus.

The pragmatic solution was to separate the digital and analogue electronics. Combination of the Chemistry Microprocessor Unit Interface System with the analogue electronics, previously described, provided a very versatile and extremely powerful tool for measurement, analysis and control.

The analogue electronics were placed as far as practically possible from the CMUIS and signals to and from the rack were scaled by the analogue electronics so as to use as much as possible of the dynamic range of the DACs and ADCs. The digital noise was reduced to an acceptable level by taking these precautions.

2.7.3 Software for the CMUIS

Several assembly language routines were supplied with the interface system for control of the function boards. The routines were accessible from the BASIC programming language using the CALL command.

a) CALL "IDENT", A1, A2

This routine performs a number of functions;

(i) it initialises the interrupt system,

(ii) it creates tables in memory which are used to identify the board from which an interrupt originated,

(iii) it identifies all of the boards in all of the racks and lists them on the VDU and/or printer if these devices are enabled. A1=1 enables the VDU, while A1=0 disables the device. A2 acts similarly for the printer.

b) CALL "WRITE8", T,N,P,D

This routine writes an unsigned, 8-bit integer D to port P of board number N of type T.

c) CALL "WRIT16", T,N,P,D

This routine is similar to WRITE8 but transfers a signed or unsigned 16-bit integer to ports P and P+1.

d) CALL "STROBE", T,N

This routine is used to give start signals to a timer, DAC or ADC, as specified by the board type, T, and the number, N.

e) CALL "SETTR", T,N,TR,CB

This routine sets the interrupt trigger source and spare control bit to the values in TR and CB. TR specifies one of four trigger sources (0 to 3) but this value, as well as that of CB, depends on the board type.

f) CALL "TIMER", N,D

This routine sends out a trigger from the Nth timer board after D milliseconds. The timer is activated on CALL, but SETTR can be used to select single-shot or repeat mode of the timer board.

g) CALL "MTIMER", N,D

This routine is similar to TIMER except that the unit of time is microseconds rather milliseconds.

h) CALL "INADC", N,VARADR(X)

This routine reads the conversion from ADC number N to the variable X.

i) CALL "PULSE1", ND,NA,NT,NP,VARADR(V), VARADR(I)

This routine writes V to DAC number ND and reads I from ADC number NA using timer number NT to control the duration between the number of points NP. V and I would normally be dimensioned arrays.

2.8 Commercial Instrumentation

Many pieces of commercial instrumentation were used during the course of this work and some of the most important items are described in the main text. There are, however, additional items which deserve a mention:

1) A Princeton Applied Research PAR-174 was used for some of the nitrate reduction studies employing linear and triangle sweep waveforms.

2) Nitrate reduction potential step transients were recorded using a Gould OS4000 digital storage oscilloscope and hardcopies were obtained using an OS4001 output unit.

3) A Bryans 6000A4 XYt chart recorder was used for most voltammograms, etc.

4) Data acquired using the 380Z microcomputer and stored on disc was subsequently output on to a Watanabe WX4651 A3 digi-plotter.

CHAPTER 3

The Development of a Voltammetric Nitrate Sensor

3. Introduction

Pletcher et al. have shown that nitrate can be easily reduced at a copper cathode in aqueous, acidic solution[26]. It is cheap, readily available and environmentally acceptable, as compared to other materials, e.g. Cd, which have been investigated as candidates for a cathode suitable for nitrate reduction. Thus, copper was chosen as a material worthy of further investigation as to the possibility of its incorporation in a voltammetric sensor for the quantitative determination of nitrate.

3.1. Copper Foil Electrodes

Inital voltammetric investigations were carried out on copper foil electrodes which were easily made in the laboratory. A strip of foil, about 120mm x 5mm, was cut from a sheet (AnalaR, BDH Chemicals Ltd). One end was soldered to a length of shielded cable. The joint and most of the copper strip were contained in a glass tube, the ends of which were subsequently sealed with epoxy resin. The exposed piece of copper foil was cut to the desired size, while the shielded cable was used to connect the electrode to the electronics.

3.1.1 Cyclic Voltammetry at Foil Electrodes

Irreproducible results were obtained on electrodes which received no pretreatment other than polishing with 0.3μ alumina. Better results were obtained if the electrode was held in the

hydrogen evolution region for a period of time prior to recording the voltammograms. Potential cycles between about 0 and -0.6V showed an irreversible wave on the sweep towards more cathodic potentials but the reverse scan displayed little evidence of any wave (Fig.3.1).

Pu[74] has put forward a hypothesis to account for the enhancement of the nitrate reduction wave. He suggests that nitrate is reduced most readily at a clean copper surface and that adsorbed oxygen, Cu(O), is removed by pretreatment in the hydrogen evolution region;

$$Cu(O) + 2H^+ + 2\bar{e} \longrightarrow Cu + H_2O \qquad (3.1)$$

Evidence in support of this sort of mechanism is indirect:

(a) surface oxidation of copper readily occurs and if the electrode is left to stand in background electrolyte, then the electrode becomes completely deactivated towards nitrate reduction.

(b) the catalytic reduction of nitrate by cadmium operates by a similar mechanism. A Cd-O bond is formed using one of the nitrate oxygens[16] and cadmium metal is regenerated by reduction of the cadmium ion formed by dissolution of the oxide;

$$CdO + 2H^+ \longrightarrow Cd^{2+} + H_2O \qquad (3.2)$$

$$Cd^{2+} + 2\bar{e} \longrightarrow Cd^{o} \qquad (3.3)$$

3.1.2 Linear Sweep Voltammetry at Foil Electrodes

The working electrode potential was maintained in the hydrogen evolution region for several seconds before switching to 0V vs SCE;

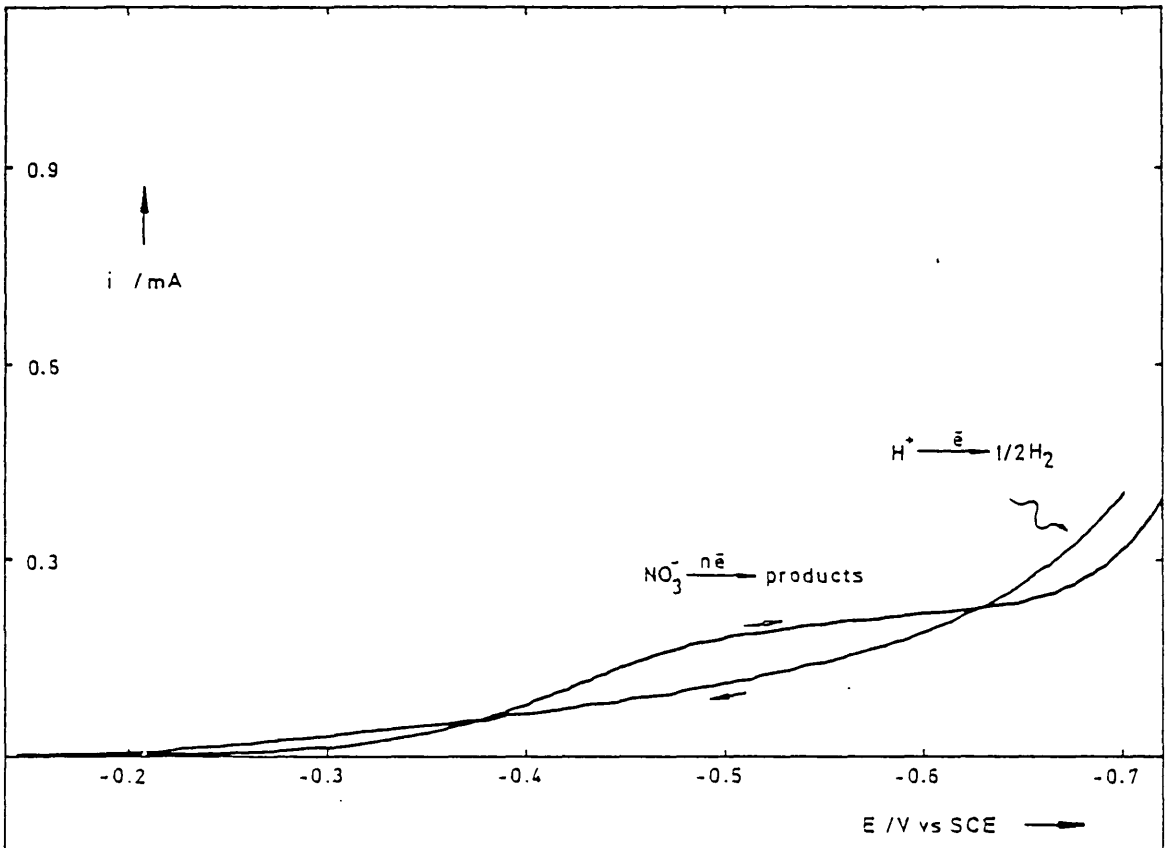

Fig.3.1. Nitrate reduction on a stationary, pretreated copper foil electrode.

$[NaNO_3] = 5\,mmol\,dm^{-3}$, $[HClO_4] = 1{\cdot}0\,mol\,dm^{-3}$, $A \simeq 0{\cdot}09\,cm^2$, $v = 10\,mV\,s^{-1}$.

The electrode was polished with 1μ alumina and its potential maintained at -0·7V for ca. 5mins before recording the voltammogram.

bubbles were then removed from the working and counter electrodes and the potential was ramped negative until the start of the hydrogen evolution wave when the sweep was reversed, Fig.3.2.

Current maxima were observed in the forward scans, as predicted by the theory of linear sweep voltammetry. For irreversible reactions [75, 76];

$$i_p = 0.4958nFAc_\infty(\alpha FD_O v/RT)^{\frac{1}{2}} \qquad (3.4)$$

where i_p is the peak current
- n is the number of electrons transferred in the overall reduction reaction
- F is the Faraday constant
- A is the electrode area
- c_∞ is the bulk concentration of the oxidized species
- α is the electron transfer coefficient
- D_O is the diffusion coefficient of the oxidized species
- v is the potential sweep rate
- R is the gas constant
- T is the absolute temperature.

Thus, a plot of i_p vs $v^{\frac{1}{2}}$ should be a straight line, through the origin, with slope given by:

$$d(i_p)/d(v^{\frac{1}{2}}) = 0.4958nFAc_\infty(\alpha FD_O/RT)^{\frac{1}{2}} \qquad (3.5)$$

Fig.3.3(a) shows such a plot, but there is a significant intercept - only part of which can be accounted for by the background current in the absence of nitrate.

From Fig.3.3(a);

$$\text{slope} = (9.7 \pm 0.3) \times 10^{-3} \quad A(Vs^{-1})^{-\frac{1}{2}} \qquad (3.6)$$

$$\text{intercept} = (4.3 \pm 0.4) \times 10^{-4} \quad A \qquad (3.7)$$

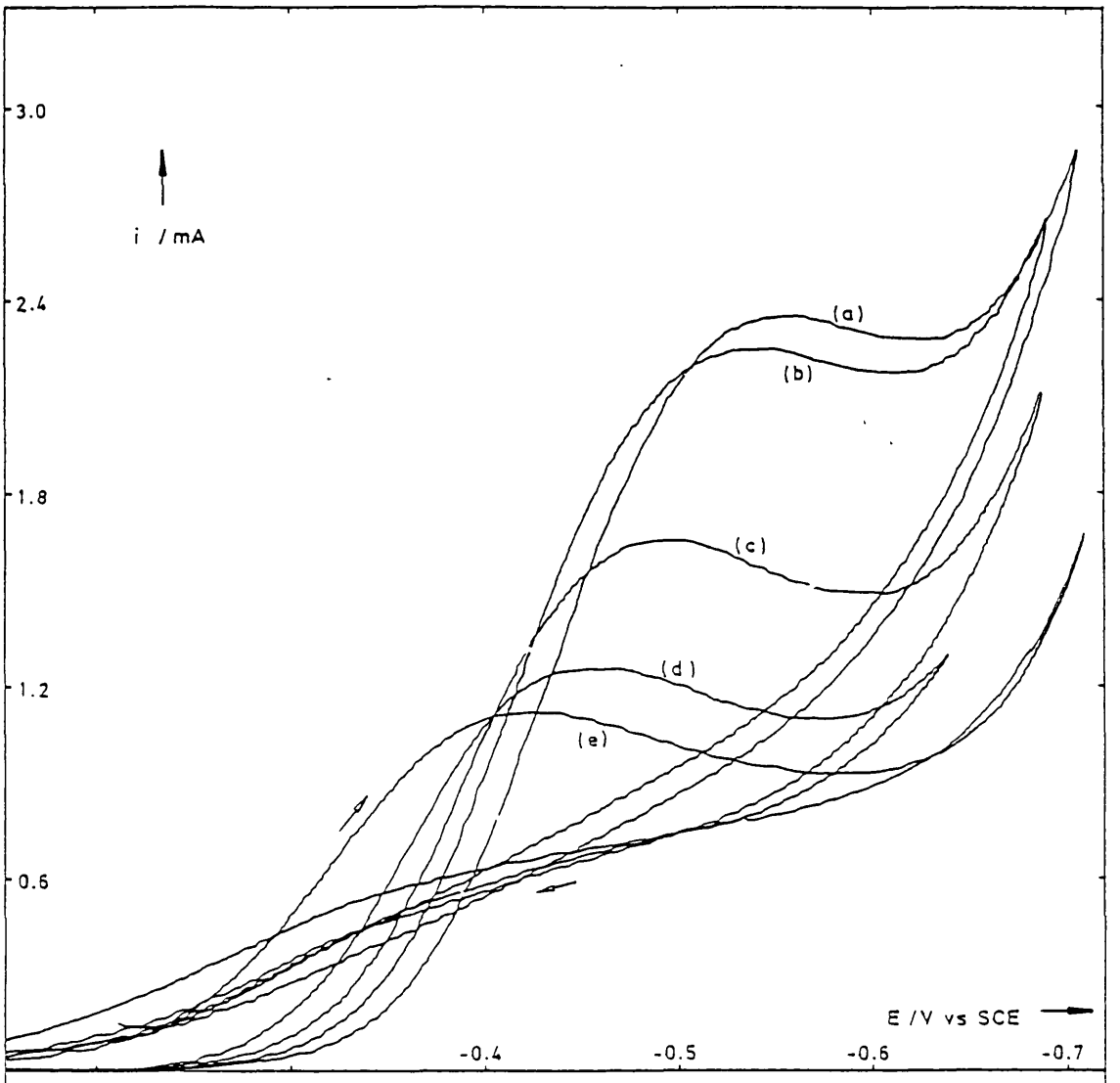

Fig.3.2. The effect of potential sweep rate, v, on the nitrate reduction current using a stationary copper foil electrode.

v / mVs^{-1}; (a) 40, (b) 33, (c) 15·4, (d) 7·4, (e) 5.

$[NaNO_3] = 5\,mmol\,dm^{-3}$, $[HClO_4] = 1{\cdot}0\,mol\,dm^{-3}$, $A \simeq 0{\cdot}9\,cm^2$.

The electrode was polished with 1μ alumina, its potential held in the hydrogen evolution region (-0·7V) for a period of time (3min for the 1st curve (e) and 1min for others), the potential switched to 0V, bubbles were removed from the working and counter electrodes before recording the voltammograms.

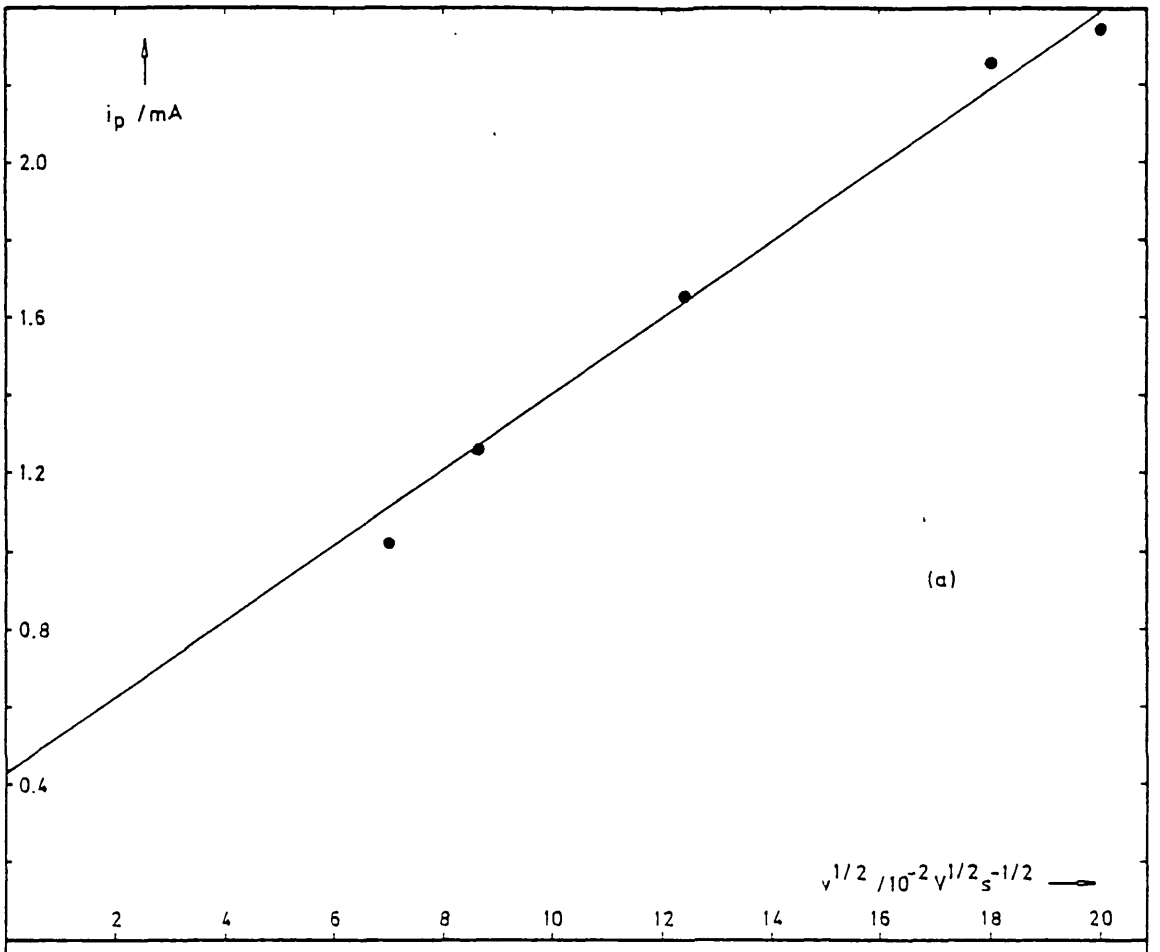

Fig.3.3. (a) i_p vs $v^{1/2}$. (b) $\ln(i_p)$ vs E_p for nitrate reduction on a copper foil electrode.

Data from Fig.3.2.

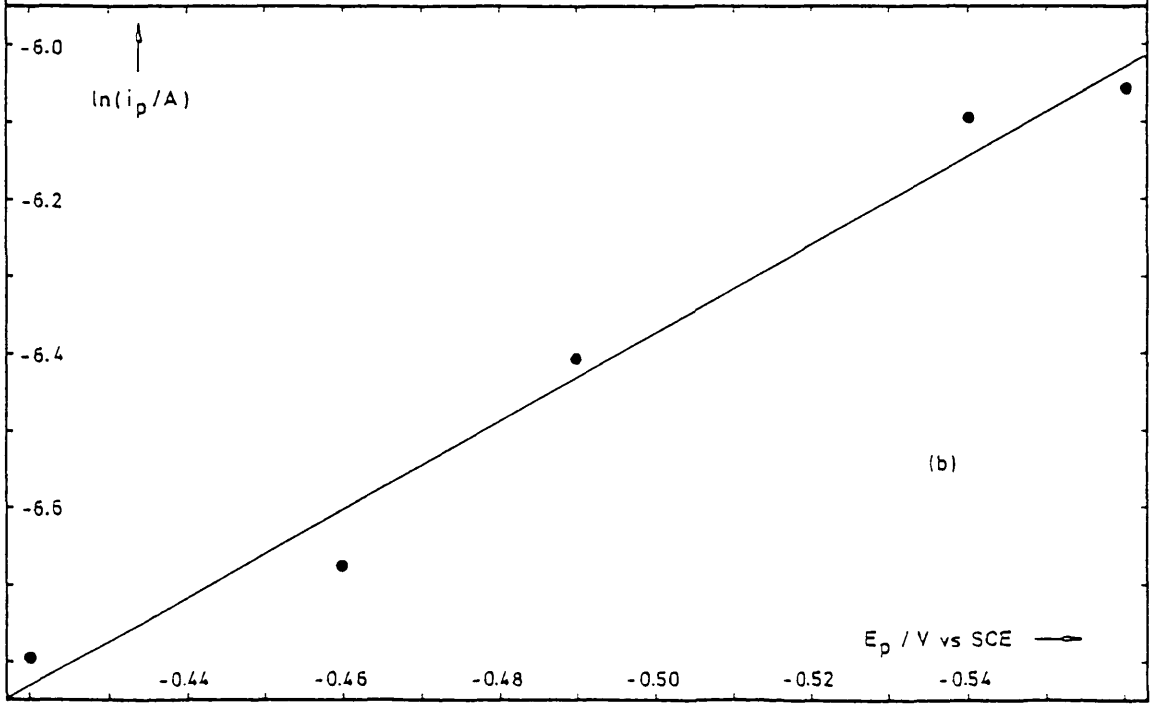

An estimate of the product $n\alpha^{\frac{1}{2}}$ was calculated from the slope, using (3.5);

$$n\alpha^{\frac{1}{2}} = 1.7 \pm 0.1 \qquad (3.8)$$

while an estimate of α was obtained by using the relationship (89d);

$$\ln(i_p) = \ln(0.227nFAc_\infty k_o') + (\alpha F/RT)(E^o - E_p) \qquad (3.9)$$

where E_p is the peak potential

E^o is the formal electrode potential

k_o' is the electrochemical rate constant when $E=E^o$.

This indicates that a plot of $\ln(i_p)$ vs E_p should be linear, with

$$\text{slope} = -\alpha F/RT \qquad (3.10)$$

and $$\text{intercept} = \ln(0.227nFAc_\infty k_o') + \alpha FE^o/RT \qquad (3.11)$$

The intercept is of little practical use unless either k_o' or E^o can be determined independently, but the slope allows α to be calculated. Fig.3.3(b) shows the data from Fig.3.2 plotted according to (3.9). The slope of this plot yields;

$$\alpha = 0.15 \pm 0.01 \qquad (3.12)$$

This value can be substituted into (3.8) to give;

$$n = 4.3 \pm 0.4 \text{ electrons} \qquad (3.13)$$

3.1.3 Mixed Perchlorate Electrolyte

Pletcher et al. found that when nitrate was subject to constant current electrolysis then an electrolyte of perchloric acid and sodium perchlorate (1:9) gave a greater yield of ammonia than the equivalent concentration of perchlorate all in the acid form.

In this laboratory, the mixed electrolyte was found to give better shaped reduction waves and this mixture was used in all of the experiments subsequently reported here.

3.2 The Stationary Copper Disc Electrode

The design and dimensions of the copper disc electrode, CU1, have been reported in the experimental section. The copper surface could be activated by maintaining its potential so as to pass a small anodic current for a short while prior to recording the voltammograms, Fig.3.4. This treatment works by removing the top few layers of copper atoms so as to produce a fresh, clean surface.

3.2.1 Linear Sweep Voltammetry (LSV)

Linear sweep voltammograms were obtained by using a Princeton Applied Research PAR-174. Plots of i_p vs $v^{\frac{1}{2}}$ and $\ln(i_p)$ vs E_p are shown in Figs.3.5 & 6 respectively. The first graph shows that the peak current is not linearly dependent on the square root of the sweep rate over the full range employed. The peak currents at high sweep rates are less than would be predicted by extrapolation of the currents at slower rates. By analogy with

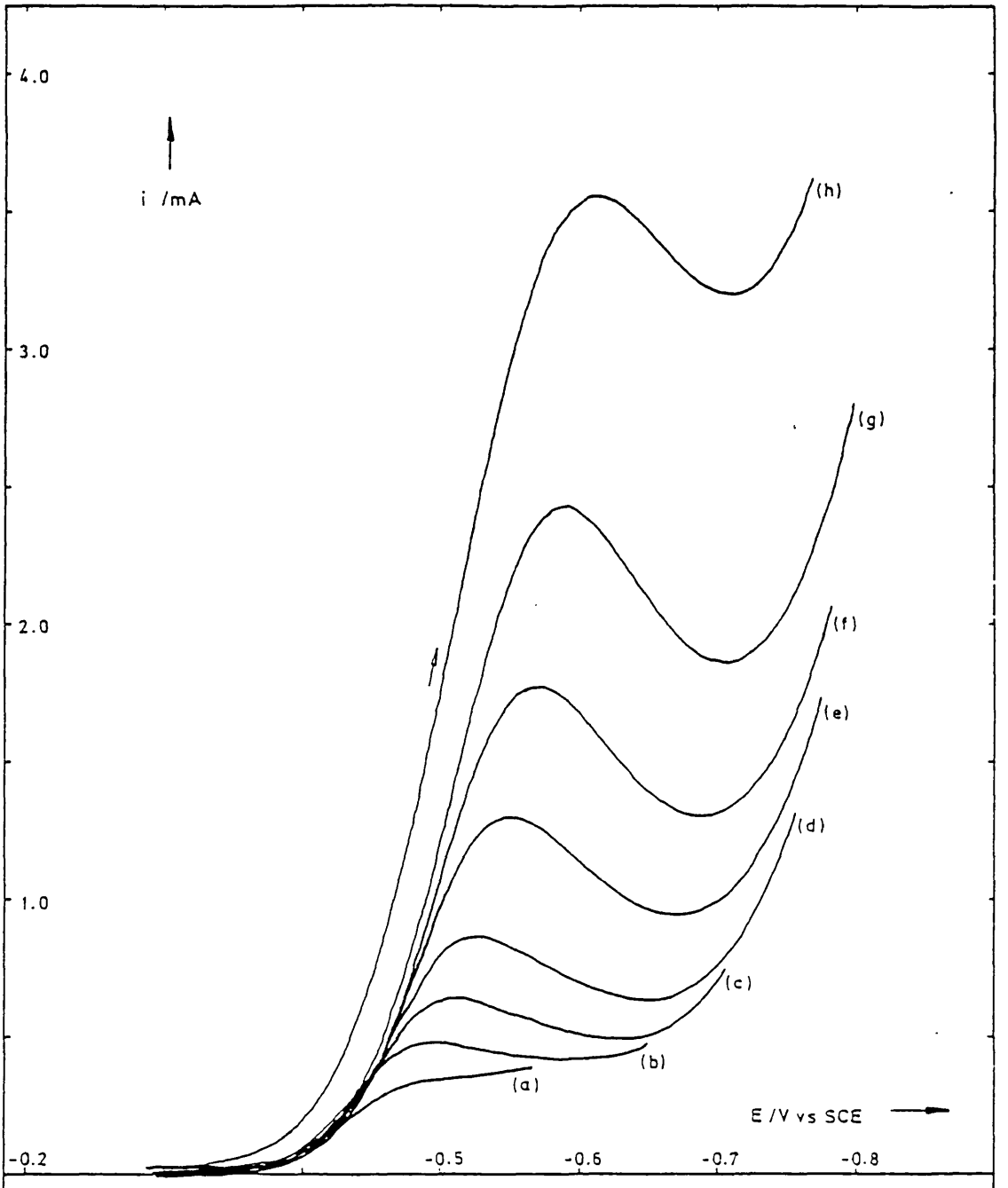

Fig.3.4. The effect of potential sweep rate, v, on the nitrate reduction current using a stationary copper disc electrode.

v /mVs^{-1}; (a) 2, (b) 5, (c) 10, (d) 20, (e) 50, (f) 100, (g) 200, (h) 500.

[$NaNO_3$] = 2 mmoldm^{-3}, [$HClO_4$] = 0.1 moldm^{-3}, [$NaClO_4$] = 0.9 moldm^{-3}, A = 0.3915 cm^2.

Copper ions were stripped from the electrode surface before each sweep, so as to provide a fresh surface, by maintaining the potential at +0.1V vs SCE for 10s before beginning each linear scan at -0.1V.

Fig.3.5. Nitrate reduction: linear sweep voltammetry

Plot of peak current vs square root of sweep rate

$[NaNO_3] = 2mM$, $[HClO_4] = 0{\cdot}1M$, $[NaClO_4] = 0{\cdot}9M$, $A = 0{\cdot}3915\ cm^2$

Electrode held at +0·1V vs SCE prior to each sweep.

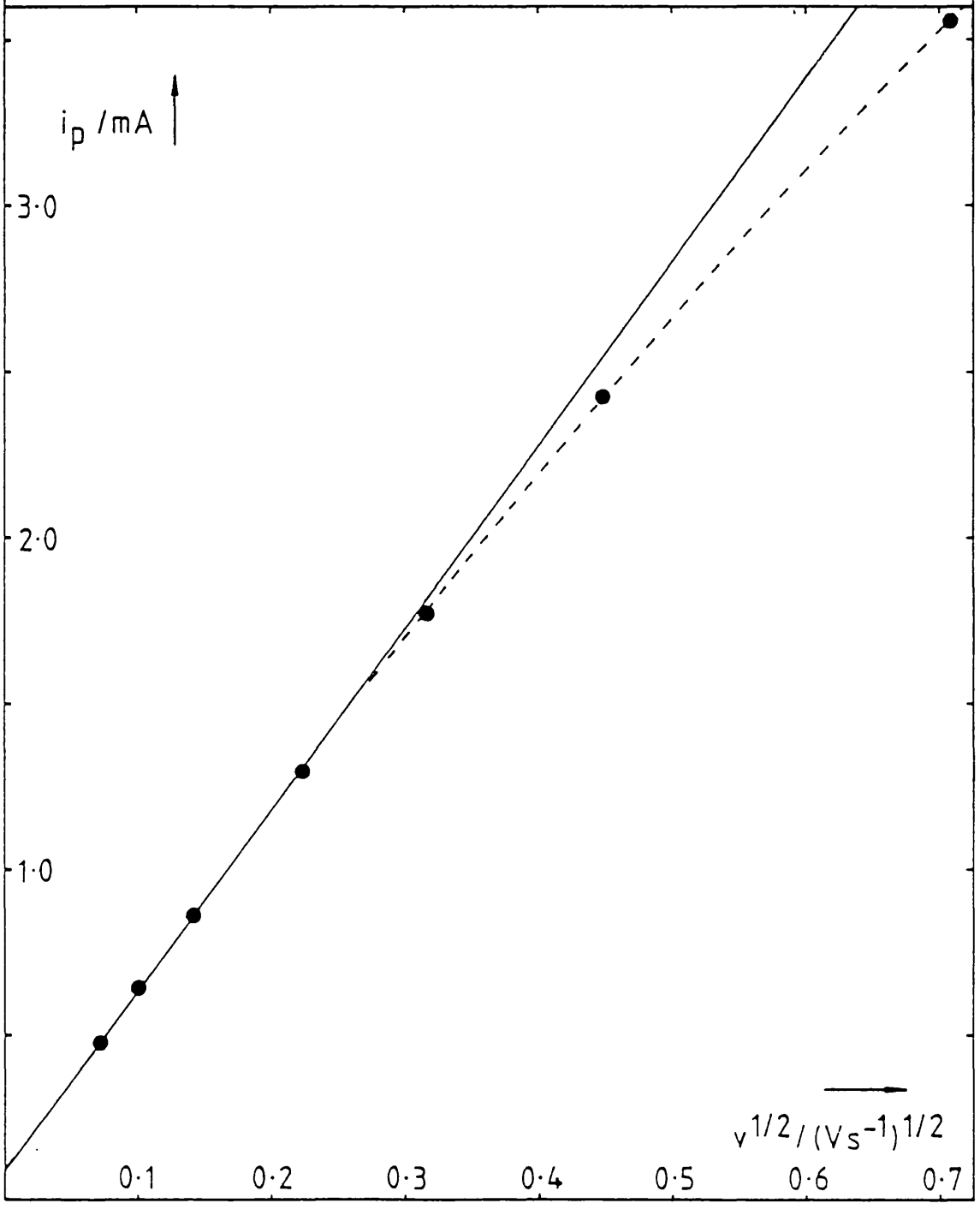

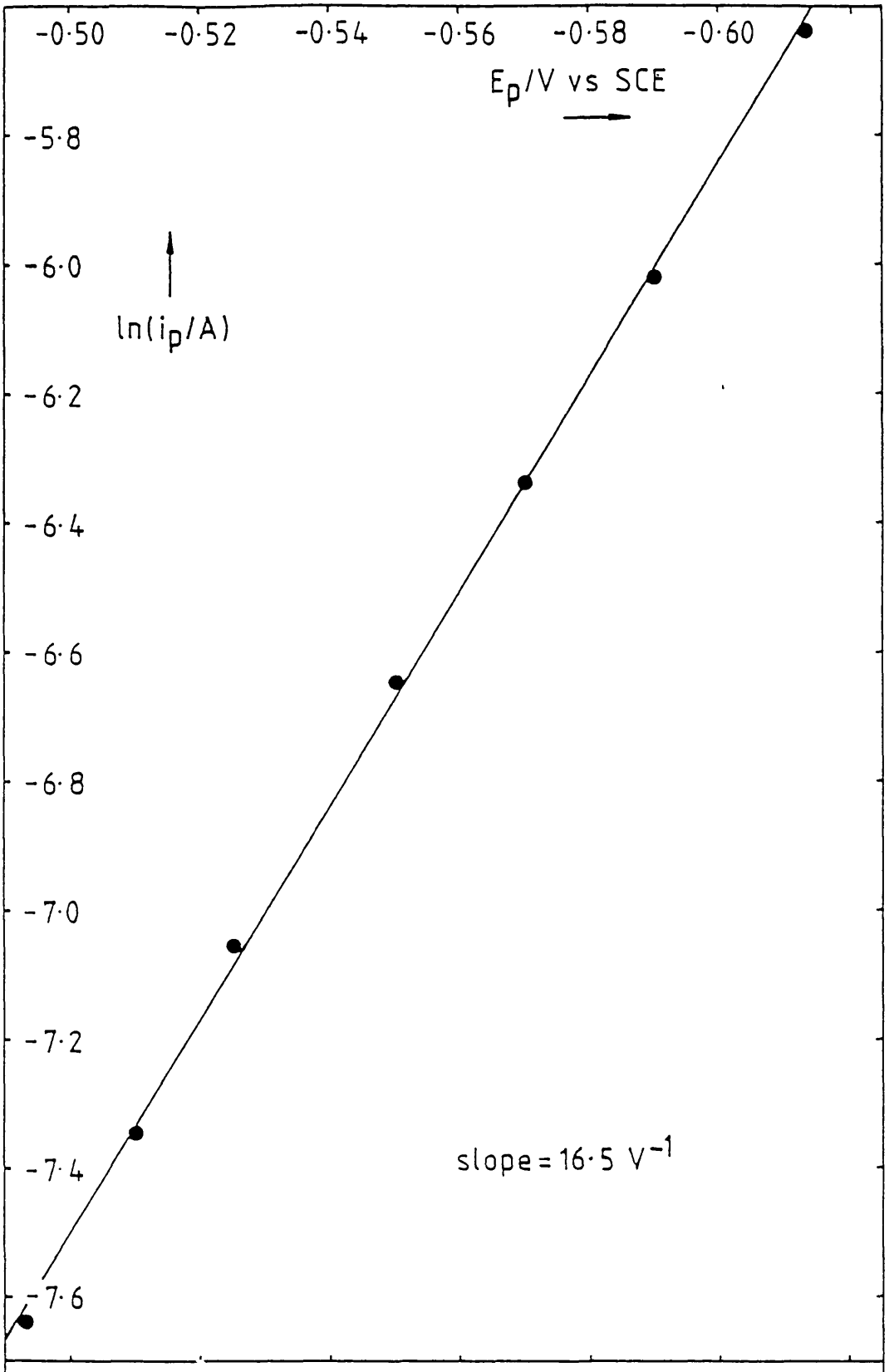

Fig.3.6. Nitrate reduction: linear sweep voltammetry.
Plot of ln(peak current) vs peak potential.
[$NaNO_3$] = 2mM, [$HClO_4$] = 0·1M, [$NaClO_4$] = 0·9M, A = 0·3915 cm^2.
Electrode held at +0·1V vs SCE for 10s prior to sweep.

the work of Cruz-Carrera and Arancibia [16] on cadmium, this effect could be explained by the rate of supply of nitrate to the electrode exceeding the rate of dissolution of the oxides formed by the nitrate reduction;

$$Cu + NO_3^- \longrightarrow Cu(O) + NO_2^- \qquad (3.14)$$

$$Cu(O) + 2H^+ + 2\bar{e} \xrightarrow{rds} Cu + H_2O \qquad (3.15)$$

An estimate of $n\alpha^{\frac{1}{2}}$ can be obtained, from the initial slope of the i_p vs $v^{\frac{1}{2}}$ plot, using the relation;

$$n\alpha^{\frac{1}{2}} = \text{slope}.[(RT)^{\frac{1}{2}}(0.4958F^{3/2}Ac_\infty D_O)^{-1}] \qquad (3.16)$$

Now, from Fig.3.5,

$$\text{slope} = 5.34 \pm 0.06 \text{ mA}(Vs^{-1})^{-\frac{1}{2}} \qquad (3.17)$$

Thus,

$$n\alpha^{\frac{1}{2}} = 5.5 \pm 0.1 \qquad (3.18)$$

An estimate of α can be obtained from

$$\text{slope} = \alpha F/(RT) \qquad (3.19)$$

$$= 16.5 \pm 0.2 \ V^{-1} \qquad (3.20)$$

Thus,

$$\alpha = 0.42 \pm 0.01 \qquad (3.21)$$

This result can be substituted into (3.18) to yield;

$$n = 8.5 \pm 0.2 \text{ electrons} \qquad (3.22)$$

This compares well with the result of Pletcher who obtained n=8 electrons using a rotating copper disc electrode.

3.2.2 Concentration dependence of the peak current

Aliquots of concentrated sodium nitrate (0.5 mol dm^{-3}) in perchloric acid (0.1 mol dm^{-3}), sodium perchlorate (0.9 mol dm^{-3}) were added to a known volume of the background electrolyte. A linear sweep voltammogram was recorded after each addition, Fig.3.7(a). From Fig.3.7(b) it can be seen that there is a linear relationship between the magnitude of the peak current and the concentration of nitrate in the solution;

$$\text{slope} = 0.700 \pm 0.005 \text{ mA(mmol dm}^{-3})^{-1} \quad (3.23)$$

$$\text{intercept} = 0.07 \pm 0.01 \text{ mA} \quad (3.24)$$

The relationship between the peak current and the nitrate concentration can be obtained from (3.4) which may be differentiated to yield;

$$d(i_p)/d(c_\infty) = 0.4958nFA(\alpha FD_O v/RT)^{\frac{1}{2}} \quad (3.25)$$

Taking the values $n\alpha^{\frac{1}{2}} = 5.5 \pm 0.1$, from above, $D_O = (1.7 \pm 0.1) \times 10^{-5}$ $cm^2 s^{-1}$(26), $A = 0.3915$ cm^2, $v = 5 \times 10^{-2}$ Vs^{-1} and $T = 298K$, then

$$d(i_p)/d(c_\infty) = 0.59 \pm 0.04 \text{ mA(mmol dm}^{-3})^{-1} \quad (3.26)$$

The observed and calculated slopes are in fair agreement, being within three sigma limits of each other. The magnitute of the observed slope was confirmed by repetition of the experiment.

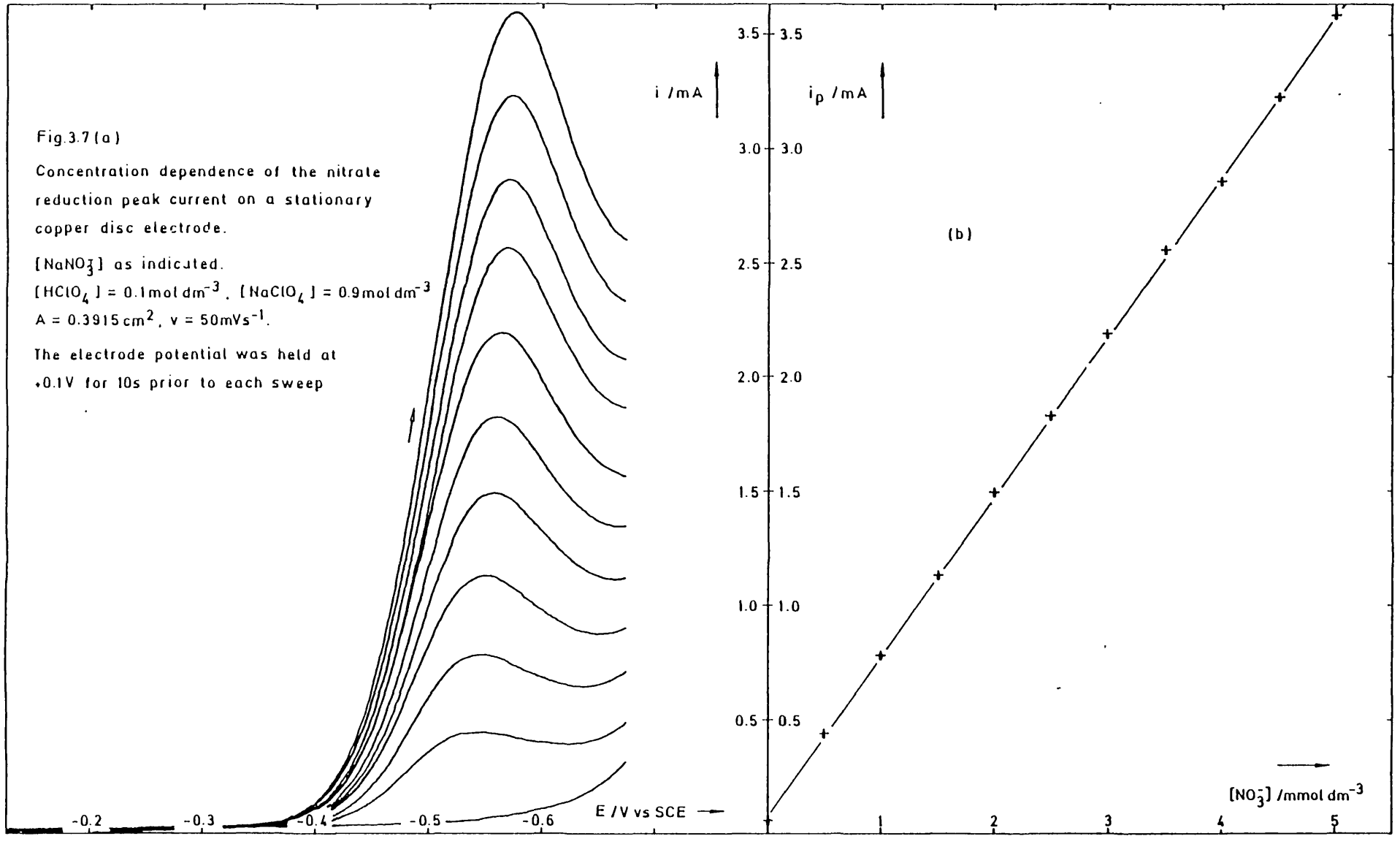

Fig.3.7(a)

Concentration dependence of the nitrate reduction peak current on a stationary copper disc electrode.

$[NaNO_3]$ as indicated.
$[HClO_4] = 0.1 mol\,dm^{-3}$, $[NaClO_4] = 0.9 mol\,dm^{-3}$
$A = 0.3915\,cm^2$, $v = 50 mVs^{-1}$.

The electrode potential was held at +0.1V for 10s prior to each sweep

3.2.3 Nitrite Reduction

Nitrite is generally accepted to be an intermediate in the cathodic reduction of nitrate. To check on the electrode response, small aliquots of sodium nitrite (0.5 mol dm^{-3}), in perchloric acid (0.1 mol dm^{-3}), sodium perchlorate (0.9 mol dm^{-3}), were added to a known volume of the background electrolyte and a linear sweep voltammogram recorded after each addition, Fig.3.8. The experiments were complicated by the evolution of gas (77, 78).

$$HClO_4 \rightleftharpoons H^+ + ClO_4^- \qquad (3.27)$$

$$NO_2^- + H^+ \rightleftharpoons HNO_2 \qquad (3.28)$$

$$HNO_2 + H^+ \rightleftharpoons H_2NO_2^+ \qquad (3.29)$$

$$H_2NO_2^+ \rightleftharpoons NO^+ + H_2O \qquad (3.30)$$

$$NO^+ + HNO_2 \rightleftharpoons N_2O_3(g) + H^+ \qquad (3.31)$$

$$N_2O_3(g) \longrightarrow NO(g) + NO_2(g) \qquad (3.32)$$

The stock nitrite solution was made up immediately before use and depletion of nitrite is unlikely to have been significant, but it might have been better to use an aqueous solution without the background electrolyte because gas bubbles formed in the barrel of the syringe used to deliver the solution.

If the electron transfer number for the reduction of nitrate is taken to be eight, then the transfer number for nitrite is likely to be six. Further assuming αn and D_o to be the same as for nitrate, then the response of the peak current to nitrite concentration should be three-

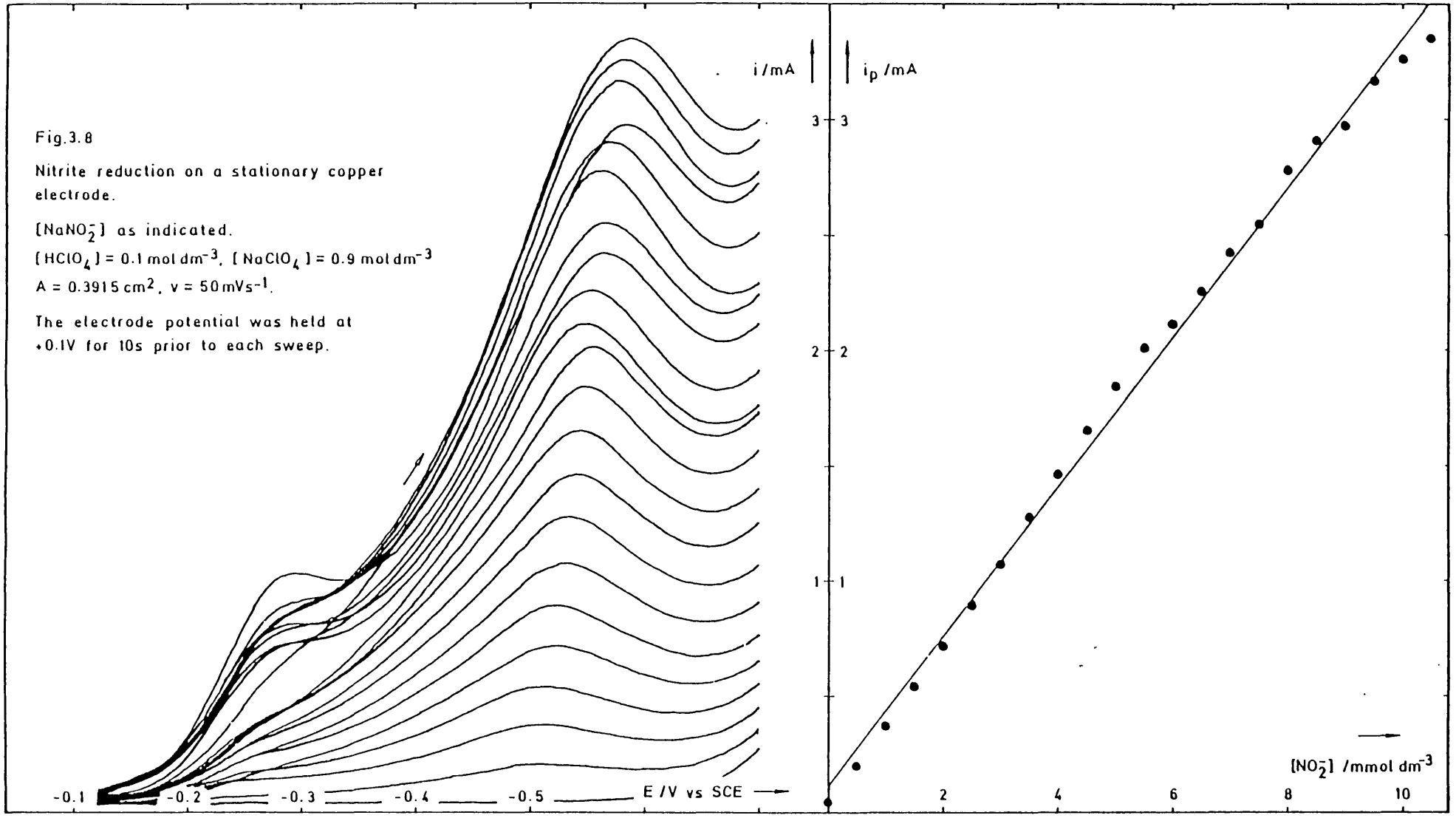

Fig.3.8

Nitrite reduction on a stationary copper electrode.

$[NaNO_2^-]$ as indicated.

$[HClO_4] = 0.1\ mol\ dm^{-3}$, $[NaClO_4] = 0.9\ mol\ dm^{-3}$

$A = 0.3915\ cm^2$, $v = 50\ mVs^{-1}$.

The electrode potential was held at +0.1V for 10s prior to each sweep.

quarters that of the nitrate response, calculated above. Hence,

$$d(i_p)/d(c_\infty) = 0.44 \pm 0.03 \text{ mA (mmol dm}^{-3})^{-1} \quad (3.33)$$

This can be compared to the experimentally observed value, calculated from the data shown in Fig.3.8(b);

$$d(i_p)/d(c_\infty) = 0.324 \pm 0.008 \text{ mA (mmol dm}^{-3})^{-1} \quad (3.34)$$

This value is less that the one calculated above, but this will certainly be due in part to the depletion of nitrite via gaseous evolution and in part due to overestimation of the volume of nitrite added to the test solution because of bubble formation in the syringe barrel.

The potentials of the nitrite reduction peaks are a little more positive than the corresponding nitrate peaks, but there is a reduction wave at -250 ± 30 mV vs SCE which is not present in the nitrate reduction voltammograms. This is probably due to the reduction of a species in the nitrite reaction sequence, above, which is not formed in the direct reduction of nitrite.

3.2.4 The effect of chloride on the nitrate reduction peak

A number of workers have noted an adverse effect on the voltammetric reduction of nitrate when halides are present in the test solution. This can be attributed to adsorption of the halide on the electrode surface. Fig. 3.9 shows the result of increasing chloride concentration on the nitrate reduction peak. The peak shifts to more

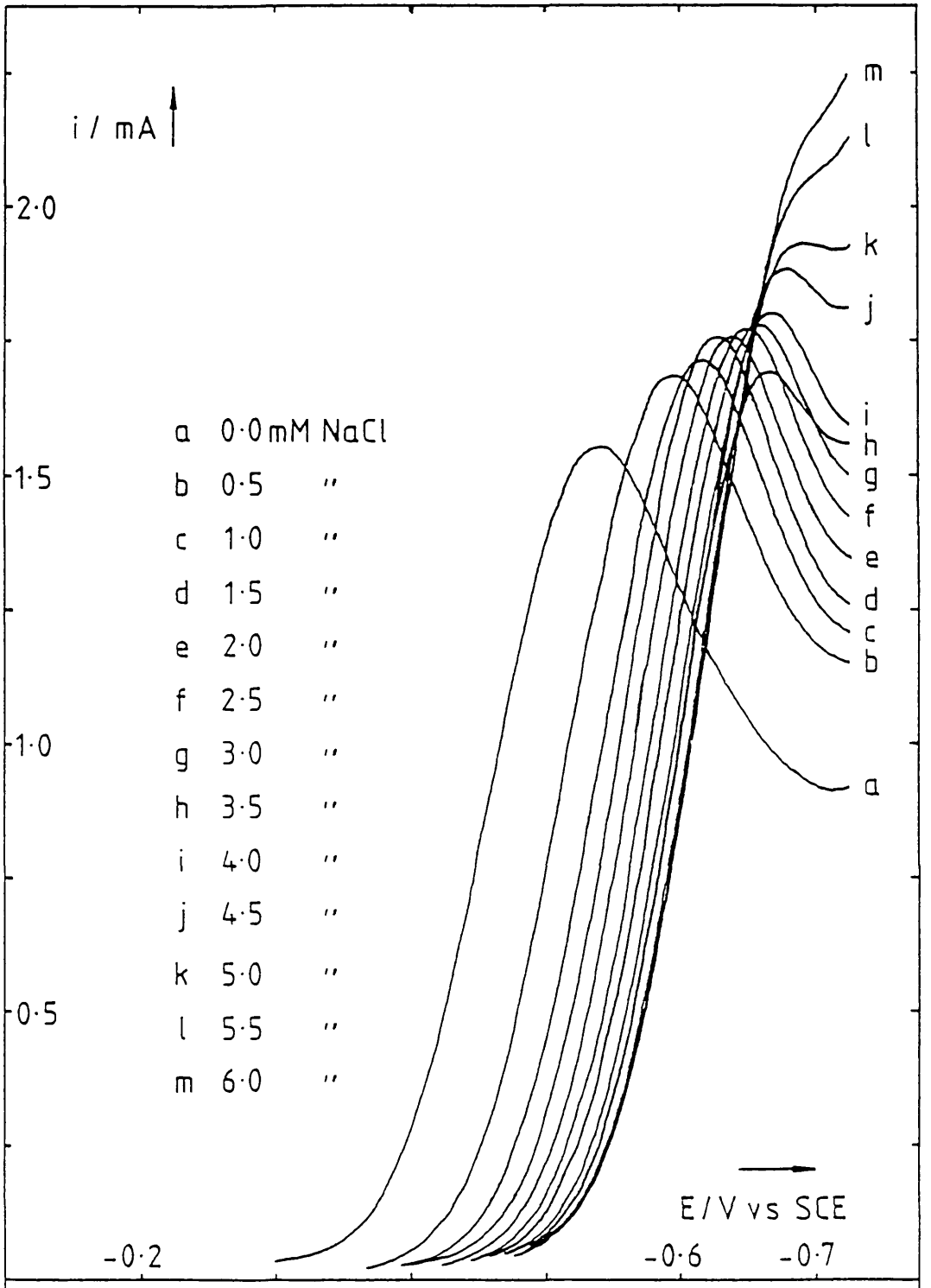

Fig.3.9. Nitrate reduction: linear sweep voltammetry. The effect of chloride on the peak potential. $[NaNO_3] = 2{\cdot}5\,mM$, $[HClO_4] = 0{\cdot}1\,M$, $[NaClO_4] = 0{\cdot}9\,M$, $A = 0{\cdot}3915\,cm^2$, $v = 50\,mVs^{-1}$. Electrode held at +0·1V for 10s prior to sweep.

negative potentials as the concentration increases, and the shape of the peaks suggests a change in E^{o} rather than a change in α . The rise in the magnitude of the peak current can be accounted for by the increase in the background current.

Plants grown using the hydroponic technique have been found to suffer from the accumulation of chloride in the water reservoir. Consequently, the tank has to be periodically emptied and refilled with fresh water. For tomatoes, the recommended limit for chloride has been 400 ppm (ca. 11 mmol dm^{-3}). At this upper limit the nitrate peak would be obscured by hydrogen evolution, but it should be possible to overcome this by diluting the samples, with the perchlorate reagent, since nitrate is required in relatively high concentrations (ca. 3 to 21 mmol dm^{-3}) [8].

3.3 The Rotating Copper Disc Electrode (RCuDE)

Rotating disc electrodes (RDEs) provide a simple method for controlling solution hydrodynamics. Flow towards the disc is imposed by the motion of the electrode and the rate of mass transfer is determined by the rotation speed,

The disc current is given by;

$$i = nFAj \qquad (3.35)$$

where j is the flux of electroactive material at the disc surface.

$$j^{-1} = (k' c_{\infty})^{-1} + (k_D c_{\infty})^{-1} \qquad (3.36)$$

where k' is the electrochemical rate constant and k_D is the rate of diffusion;

$$k' = k'_o \exp[-\alpha nF(E-E^o)/RT] \quad (3.37)$$

$$k_D = D/x_D \quad (3.38)$$

where x_D is the diffusion layer thickness.

Transport limited flux, j_L, is obtained when $k' >> k_D$, then

$$j_L = k_D c_\infty \quad (3.39)$$

and $$x_D = Z_D \quad (3.40)$$

where Z_D is the limiting diffusion layer thickness, given by;

$$Z_D = 0.643\, \omega^{-\frac{1}{2}}\, \upsilon^{1/6}\, D^{1/3} \quad (3.41)$$

where υ is the kinematic viscosity of the solution.

The corresponding limiting current, i_L, is given by combination of (3.37), (3.39) and (3.40) to yield the Levich equation[79];

$$i_L = 1.554nFAD^{2/3}\upsilon^{-1/6}c_\infty\omega^{\frac{1}{2}} \quad (3.42)$$

The Levich equation is strictly valid only when the electrode potential is fixed since it takes no account of sweep rate, v. For LSV on the RDE peak-shaped voltammograms would intuitively be expected when the sweep rate was high since the depletion layer set up would be much thinner than the diffusion layer, Z_D. Conversely, sigma-shaped voltammograms would be expected for slow sweep rates since the thickness of the depletion layer would be bounded by Z_D [80, 81, 104-6].

3.3.1 Sweep Rate Dependence of the Reduction Current

Nitrate reduction voltammograms, at different sweep rates, are shown in Fig.3.10. These results were typical but sometimes peak-shaped voltammograms were obtained at high sweep rates and sigma-shaped voltammograms were obtained at low sweep rates. The results cannot be explained by simple theory, but indicate again the importance of surface condition.

When cyclic rather than linear scan was employed then the hysteresis at intermediate sweep rates was less than at low scan rates, Fig.3.11.

3.3.2 Concentration Dependence of the Reduction Current

The effect of nitrate concentration on the limiting or peak current is summarised in Fig.3.12. It shows that there is a linear concentration dependence at all but the lowest sweep rate ($2mVs^{-1}$), with the highest correlation at the fastest sweep rates.

3.3.3 Rotation Speed Dependence of the Reduction Current

The effect of rotation speed on the nitrate reduction voltammogram is shown in Fig.3.13. Several things can be noted from this diagram. Firstly, the half-wave potential shifts to more negative potentials as the rotation speed increases. This is indicative of an irreversible reaction. Secondly, the amount of hysteresis increases with rotation speed, or the amount of charge passed. Thirdly, the relationship between the limiting

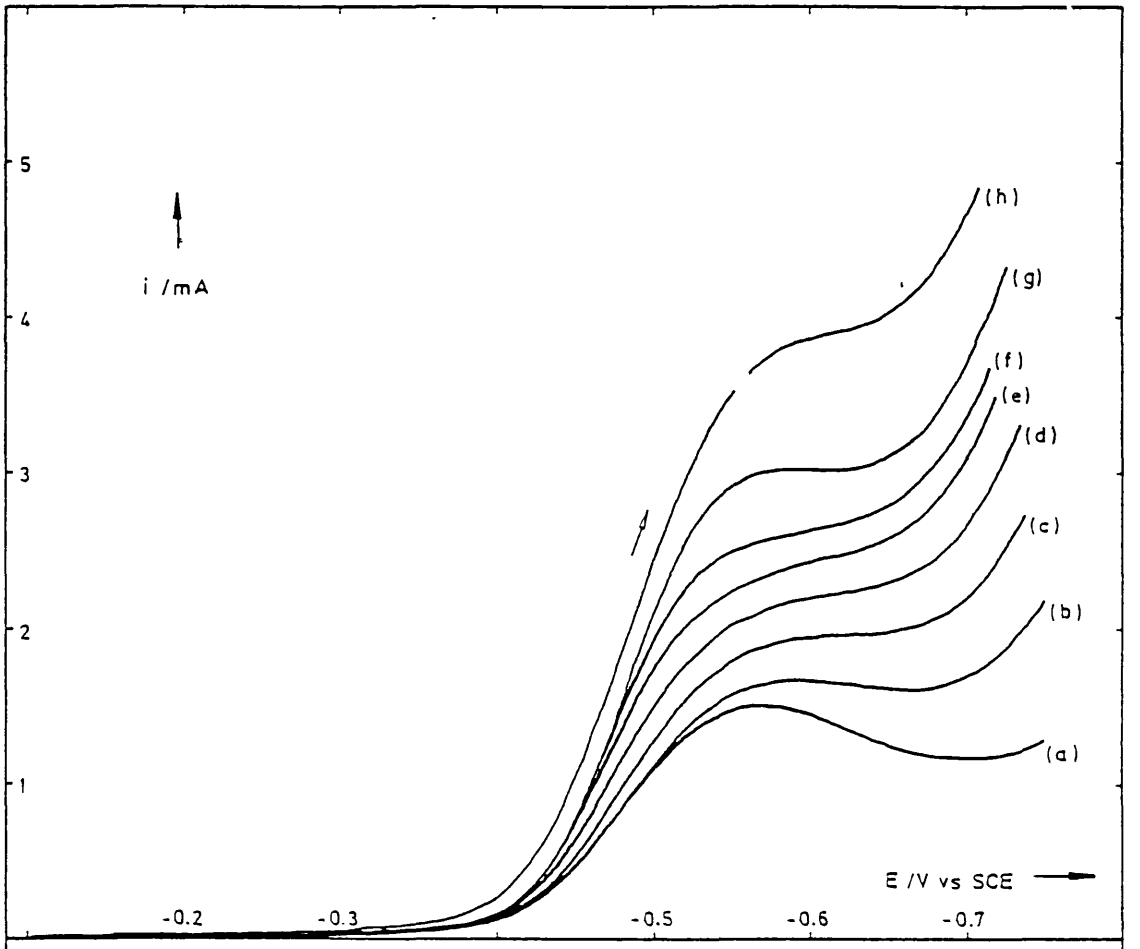

Fig.3.10. The effect of potential sweep rate on the nitrate reduction voltammogram.

v /mVs^{-1}; (a) 2, (b) 5, (c) 10, (d) 20, (e) 50, (f) 100, (g) 200, (h) 500.

[$NaNO_3$] = 2 mmol dm^{-3}, [$HClO_4$] = 0·1 mol dm^{-3}, [$NaClO_4$] = 0·9 mol dm^{-3}

ω = 4 Hz, A = 0·3915 cm^2.

The electrode was held at +0·1V vs SCE for 10s so as to obtain a fresh surface prior to each sweep.

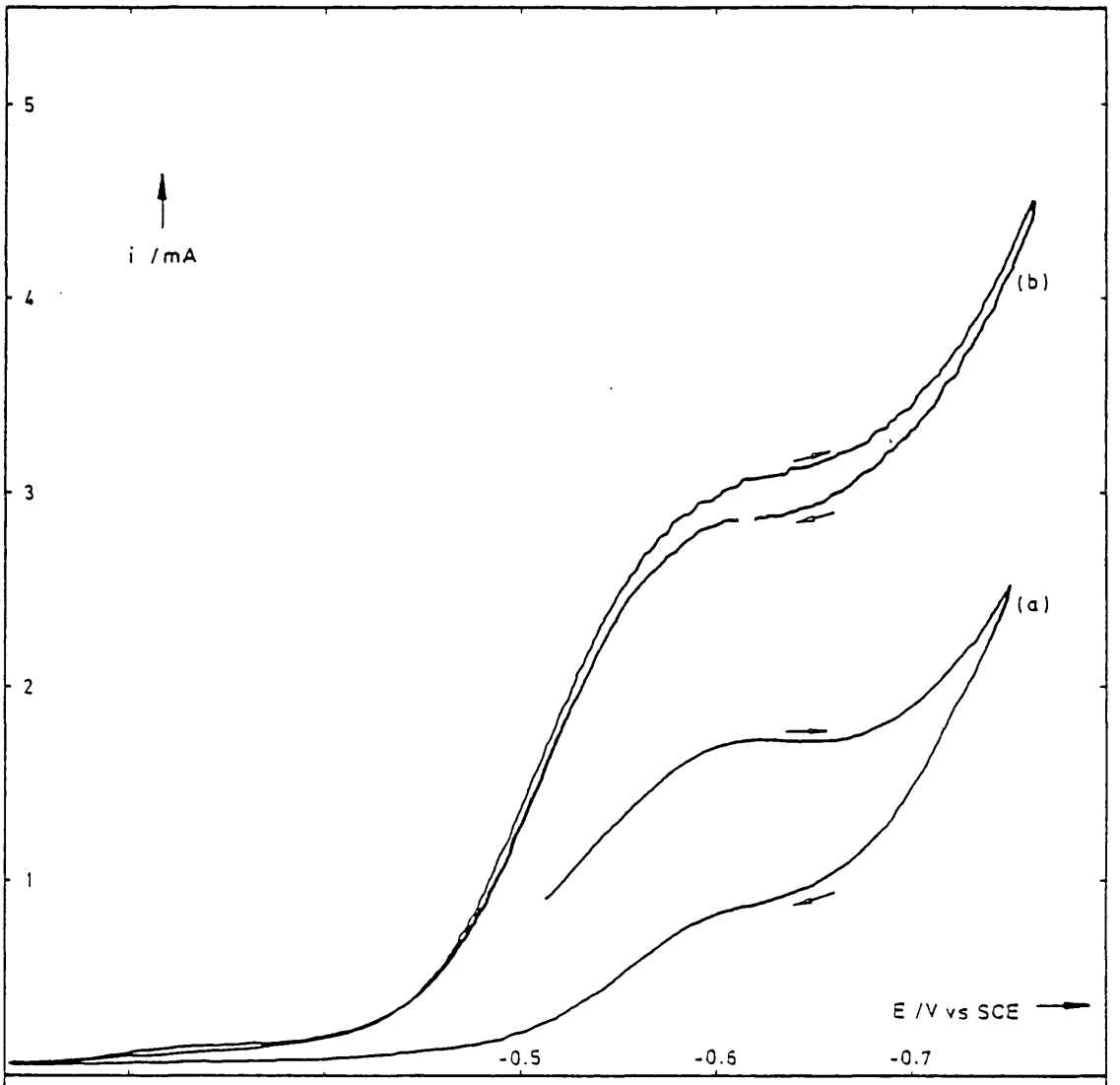

Fig.3.11. Nitrate reduction on a rotating copper disc electrode.

ω = 4Hz, A = 0.3915 cm^2, $[HClO_4]$ = 0.1 $moldm^{-3}$, $[NaClO_4]$ = 0.9 $moldm^{-3}$.

(a) The electrode, which had previously been used for recording other voltammograms, was held at +0.1V vs SCE for 10s, so as to strip copper ions from the surface, before starting the voltammogram at 0V.
$[NaNO_3]$ = 2 $mmoldm^{-3}$, v = 1 mVs^{-1}.

(b) The electrode was freshly polished with 0.3μ alumina, then its potential in the solution held at +0.1V for 40s before recording the voltammogram starting at 0V.
$[NaNO_3]$ = 2.25 $moldm^{-3}$, v = 5 mVs^{-1}.

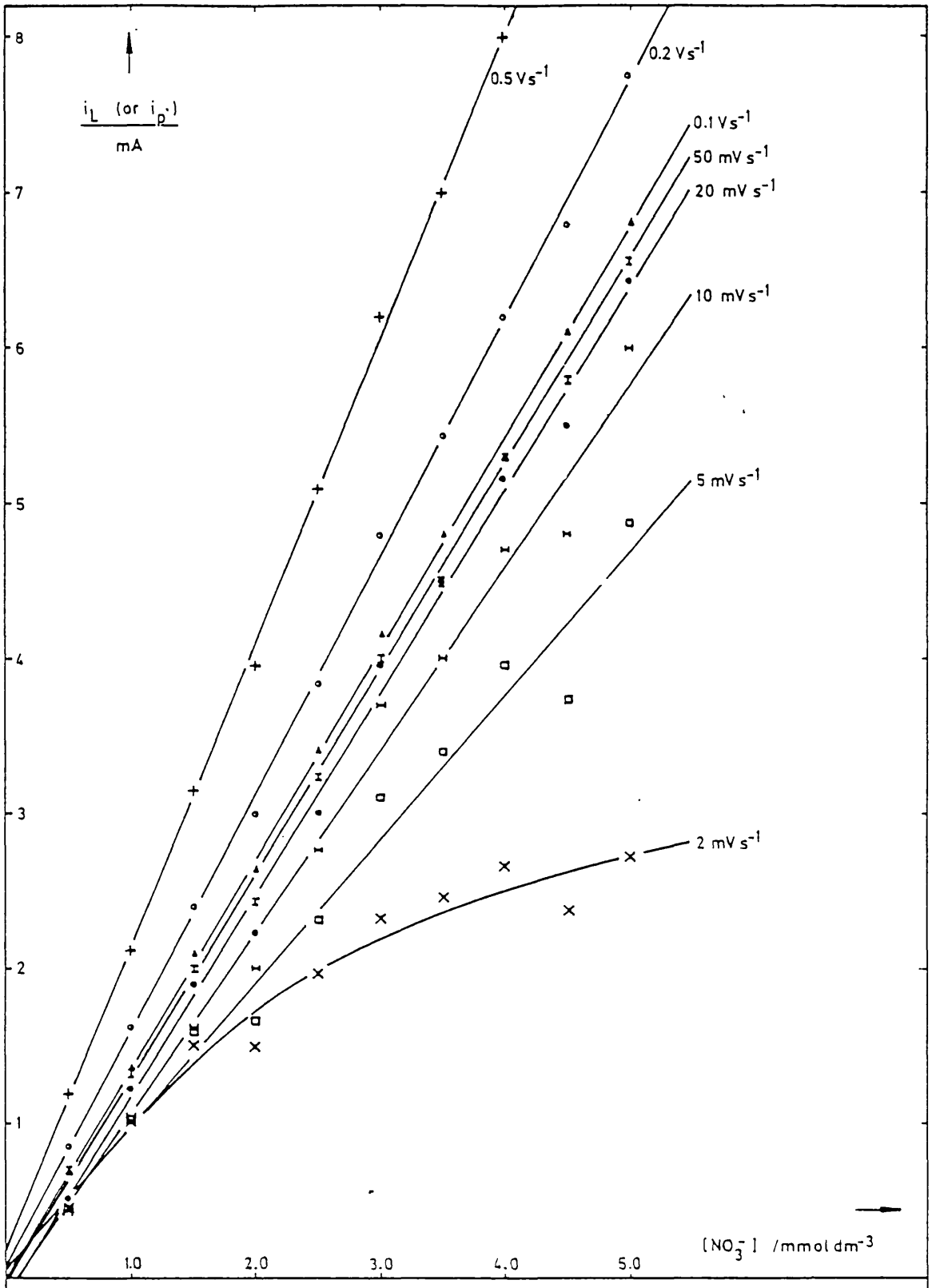

Fig.3.12. The effect of sweep rate on the magnitude of the nitrate limiting reduction current on a rotating copper disc electrode.

$[HClO_4] = 0.1\,mol\,dm^{-3}$, $[NaClO_4] = 0.9\,mol\,dm^{-3}$, $A = 0.3915\,cm^2$, $\omega = 4\,Hz$.

A fresh surface was obtained for each voltammogram by stripping copper ions from the electrode at the anodic limit (+0.1V vs SCE) for 10s

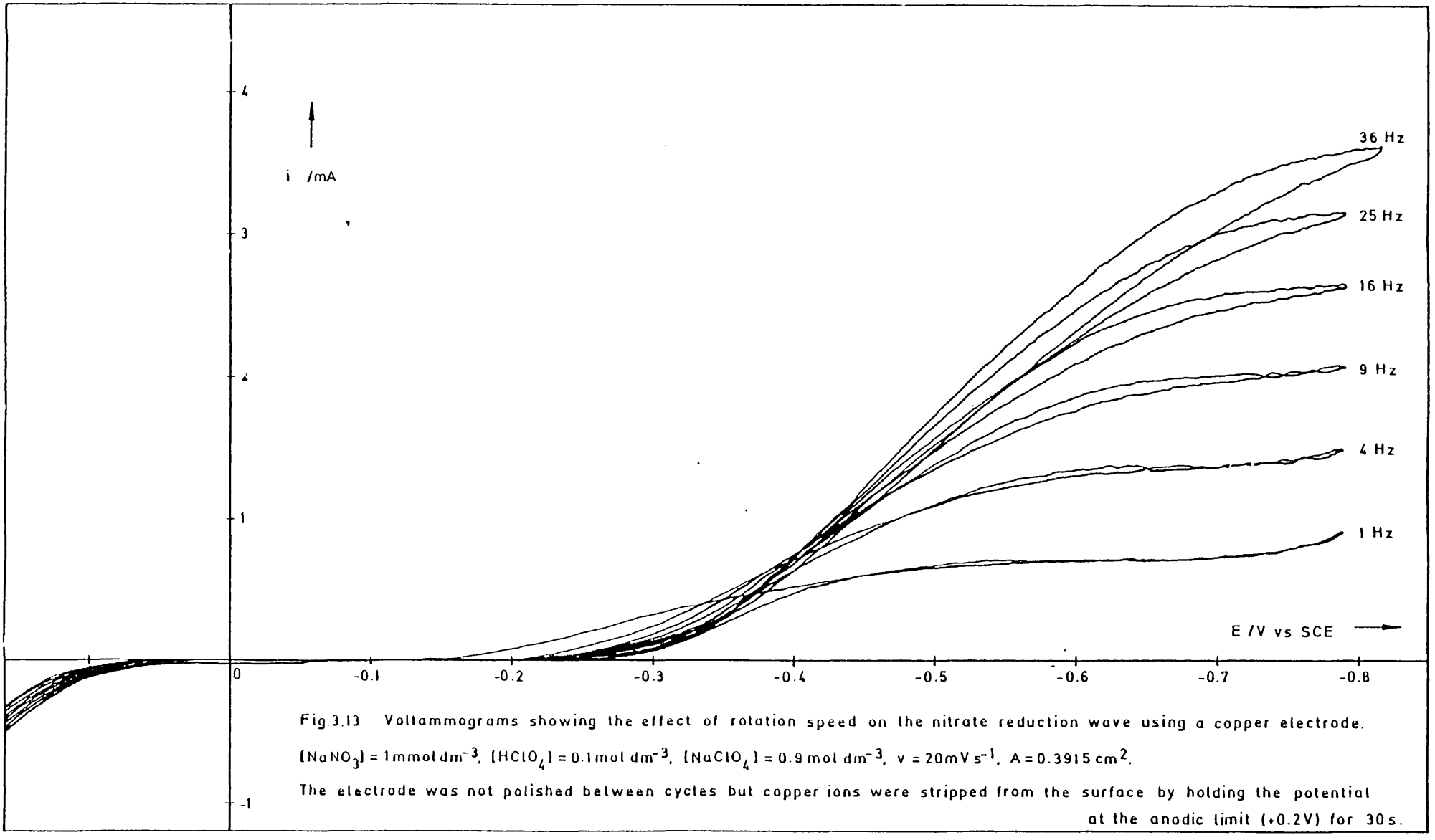

Fig.3.13 Voltammograms showing the effect of rotation speed on the nitrate reduction wave using a copper electrode. $[NaNO_3] = 1\,mmol\,dm^{-3}$, $[HClO_4] = 0.1\,mol\,dm^{-3}$, $[NaClO_4] = 0.9\,mol\,dm^{-3}$, $v = 20\,mV\,s^{-1}$, $A = 0.3915\,cm^2$. The electrode was not polished between cycles but copper ions were stripped from the surface by holding the potential at the anodic limit (+0.2V) for 30 s.

current and the square-root of the rotation speed is not linear, as would be predicted by the Levich equation. Fig.3.14(a) shows a plot of i_L vs $\omega^{\frac{1}{2}}$. From the initial slope;

$$n = 8.4 \pm 0.4 \text{ electrons} \qquad (3.43)$$

which is in good agreement with the value calculated by Pletcher [26].

The Levich equation assumes that the plateau current is limited by diffusion alone. Other potential-independent rate processes are taken into account by the Koutecky-Levich equation [82, 83];

$$i_L^{-1} = (nFAc_\infty k_?)^{-1} + (1.554nFAD^{2/3}\upsilon^{-1/6}c_\infty \omega^{\frac{1}{2}})^{-1} \qquad (3.44)$$

where $k_?$ is the rate of the unknown process(es).

From this equation, a plot of i_L^{-1} vs $\omega^{-\frac{1}{2}}$ should be linear with;

$$\text{slope} = (1.554nFAD^{2/3}\upsilon^{-1/6}c_\infty)^{-1} \qquad (3.45)$$

$$\text{and} \quad \text{intercept} = (nFAc_\infty k_?)^{-1} \qquad (3.46)$$

Fig.3.14(b) shows the same data as in (a) but plotted according to the Koutecky-Levich equation. Linearity is good and calculation yields;

$$n = 8.6 \pm 0.3 \text{ electrons} \qquad (3.47)$$

$$\text{and} \quad k_? = (8 \pm 1) \times 10^{-3} \text{ cm s}^{-1} \qquad (3.48)$$

The number of electrons is again in good agreement with Pletcher, but the source of $k_?$ is ambiguous. There is evidence to suggest that the electrode is being poisoned by the nitrate reduction, but in the

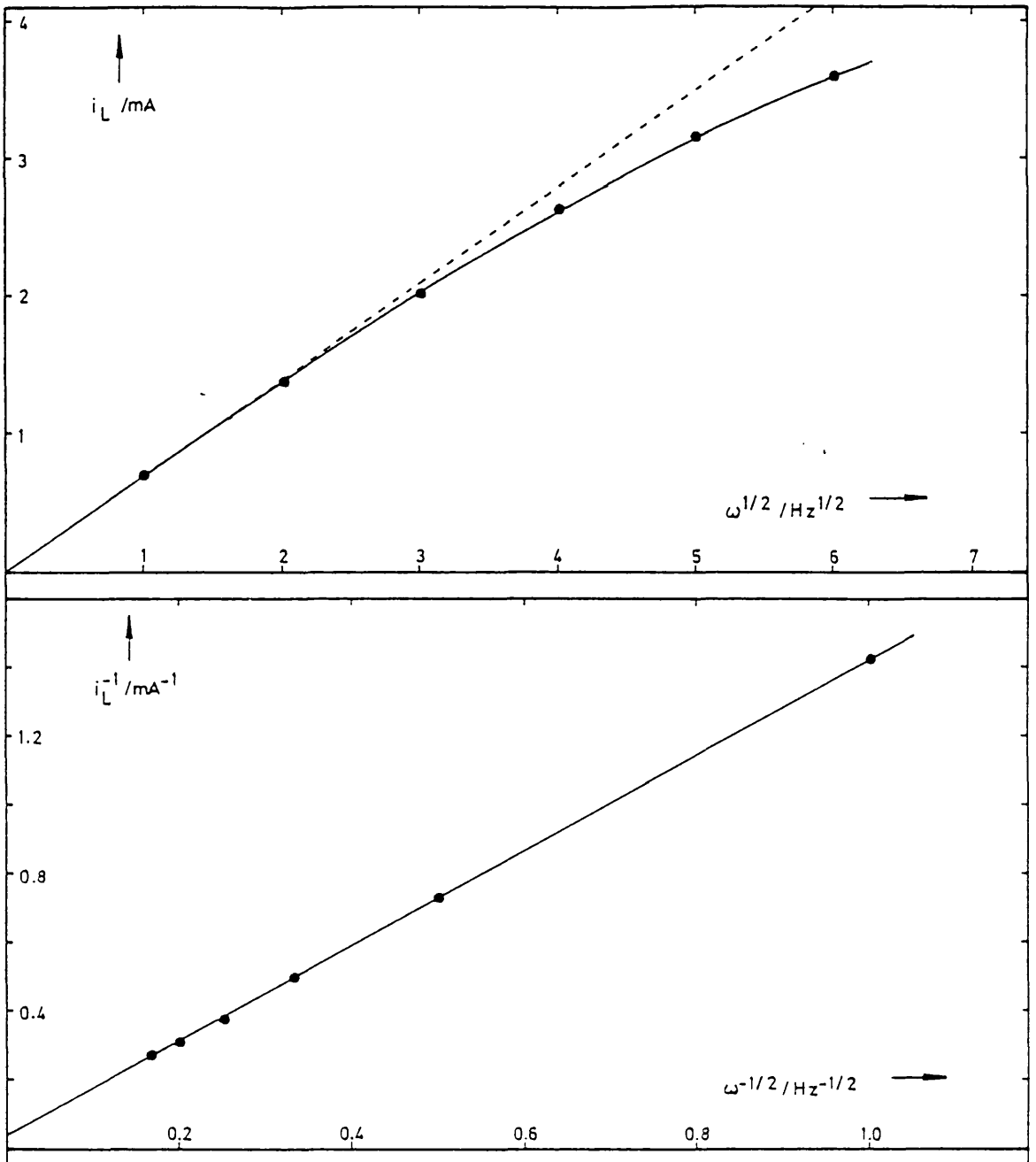

Fig.3.14. (a) i_L vs $\omega^{1/2}$, (b) i_L^{-1} vs $\omega^{-1/2}$ for nitrate reduction on a rotating copper disc electrode.

$[NaNO_3] = 1\,mmol\,dm^{-3}$, $[HClO_4] = 0{\cdot}1\,mol\,dm^{-3}$, $[NaClO_4] = 0{\cdot}9\,mol\,dm^{-3}$, $A = 0{\cdot}3519\,cm^2$, $v = 20\,mVs^{-1}$. A fresh electrode surface was provided between voltammograms by holding the potential at the anodic limit (+0·2V vs SCE) for 30s.

case of the data shown it may be that the potential was not made sufficently negative at the higher rotation speeds to give a truely diffusion controlled current, then $k_?$ would contain an element due to the electrochemical rate constant.

3.3.4 Poisoning of the Electrode Surface

The magnitude of the nitrate reduction current is acutely dependent on the scan number if the electrode surface is not regenerated between potential sweeps, Fig.3.15. There is little or no change in the E^o potential for the reaction, but the reduction wave does decay dramatically and peak-shaped voltammograms are eventually obtained.

For each of the sigmoid curves, the transfer coefficient, α , can be calculated by combining (3.36) and (3.38) to yield;

$$j^{-1} - j_L^{-1} = (k' c_\infty)^{-1} \qquad (3.49)$$

Substituting for the electrochemical rate constant using (3.37) gives;

$$(j^{-1} - j_L^{-1})^{-1} = k'_o c_\infty \exp[-\alpha nF(E-E^o)/RT] \qquad (3.50)$$

Using the relationship (3.35) yields;

$$[nFA(i^{-1} - i_L^{-1})]^{-1} = k'_o c_\infty \exp[-\alpha nF(E-E^o)/RT] \qquad (3.51)$$

or $$\ln(i^{-1} - i_L^{-1}) = (\alpha nF/RT)(E-E^o) - \ln(nFAk'_o c_\infty) \qquad (3.52)$$

Thus, a plot of $\ln(i^{-1} - i_L^{-1})$ vs E should be a straight line with;

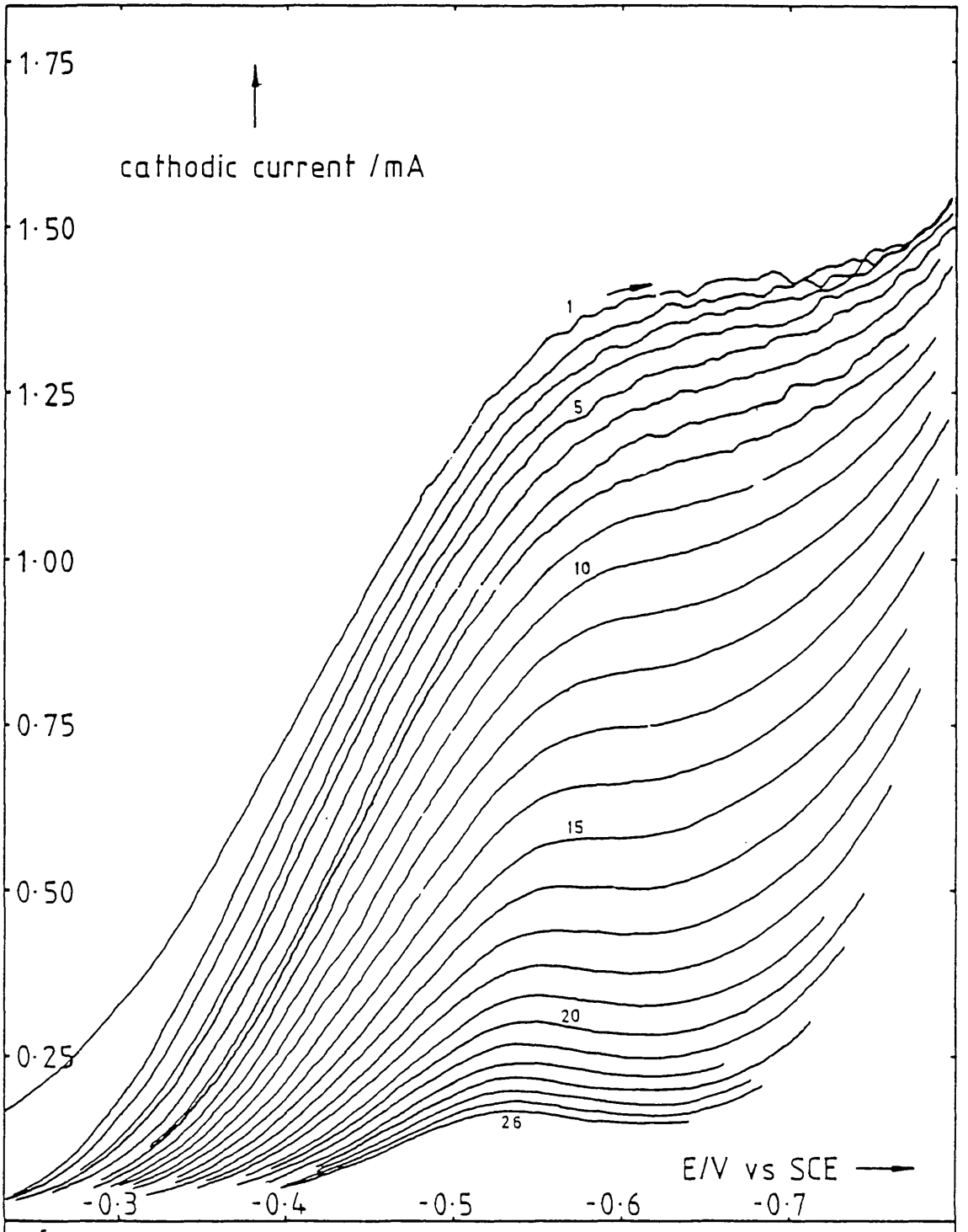

Fig. 3.15. Decay of the nitrate reduction wave on the rotating copper disc electrode (only the potential sweeps +'ve to -'ve were recorded).

$[NaNO_3] = 1mM$, $[HClO_4] = 0{\cdot}1M$, $[NaClO_4] = 0{\cdot}9M$, $\omega = 4\,Hz$, $v = 20\,mVs^{-1}$, $A = 0{\cdot}3915\,cm^2$. The electrode was polished with 0·3μ alumina and potential cycled between 0 and -0·8V vs SCE.

$$\text{slope} = \alpha nF/RT \qquad (3.53)$$

$$\text{and intercept} = -\ln(nFAk_o'c_\infty) - \alpha nFE^o/RT \qquad (3.53b)$$

Hence, α can be calculated from the slope of the plot, if n is known. Such a plot is shown in Fig.3.16. It can be seen that the data deviates from linearity at both the foot and the top of the reduction wave. The reduction transfer coefficient can be extracted, however, from the linear section and the results for the series of voltammograms in Fig.3.15 are summarised in Table 3.1.

scan number	α	scan number	α
1	0.042	9	0.056
2	0.047	10	0.058
3	0.051	11	0.061
4	0.052	12	0.061
5	0.054	13	0.062
6	0.055	14	0.063
7	0.056	15	0.063
8	0.057	16	0.063

Table 3.1. The reduction transfer coefficient as a function of scan number. Data from Fig.3.15.

These results indicate that the effective electrode area decreases, but the activity increases, as nitrate reduction proceeds.

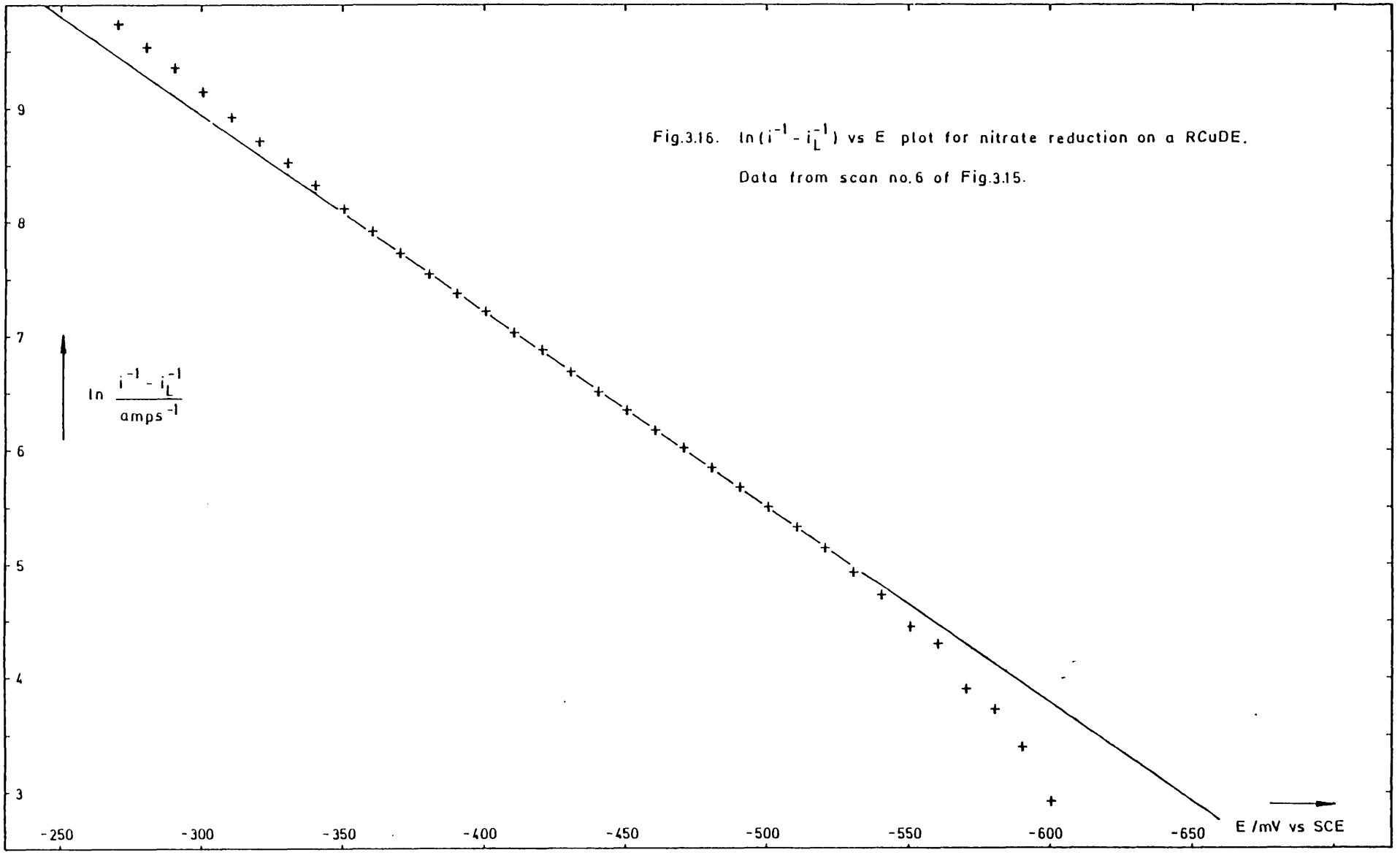

Fig.3.16. $\ln(i^{-1} - i_L^{-1})$ vs E plot for nitrate reduction on a RCuDE.

Data from scan no.6 of Fig.3.15.

3.3.5 Electrode poisoning at constant potential

The poisoning process could be clearly seen if the electrode was carefully polished and then maintained at a fixed potential in the limiting current region, Fig.3.17. The decay curve can be divided into three parts; (i) an initial part where the current is little changed with time, (ii) a region where the current decays rapidly with time and (iii) a final part where the current decays relatively slowly.

The current i- very responsive to rotation speed during the initial period. An estimate of the electron transfer number, n, can be made from the initial slope of the i_L vs $\omega^{\frac{1}{2}}$ plot, Fig.3.18(a);

$$n = 9.2 \pm 0.2 \text{ electrons} \qquad (3.54)$$

From the Koutecky-Levich plot, Fig.3.18(b);

$$n = 10 \pm 1 \text{ electrons} \qquad (3.55)$$

and $k_? = (6.6 \pm 0.8) \times 10^{-2} \text{ cm s}^{-1}$ (3.56)

The magnitude of $k_?$ shows that there is a significant poisoning process, while the two electron transfer numbers are in reasonable agreement with previous calculations and with Pletcher's value of eight electrons.

During the period of rapid decay it is difficult to determine the rotation speed dependence of i_L, but the rate of decay does accelerate with increasing rotation speed.

During the later stages of decay there is a linear relationship between i_L and $\omega^{\frac{1}{2}}$, but there is a significant intercept when the current is extrapolated to zero rotation speed, Fig.3.19.

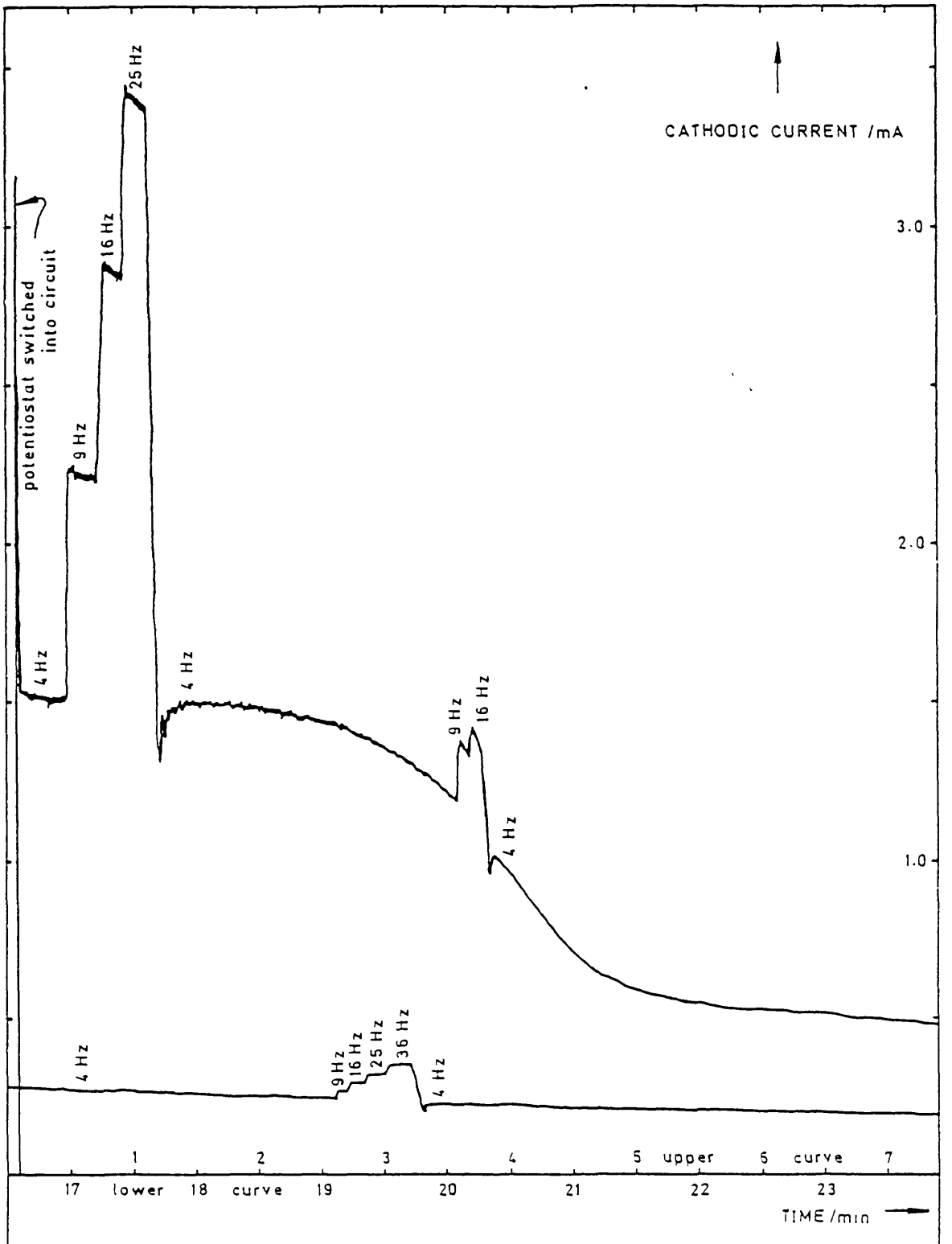

Fig.3.17. The effect of rotation speed during different stages of the nitrate reduction current decay at a rotating copper disc electrode.
$[NaNO_3] = 1mM$, $[HClO_4] = 0{\cdot}1M$, $[NaClO_4] = 0{\cdot}9M$, $A = 0{\cdot}3915\,cm^2$, disc potential = -0·75V vs SCE. Electrode polished with 0·3μ alumina immediatly before use.

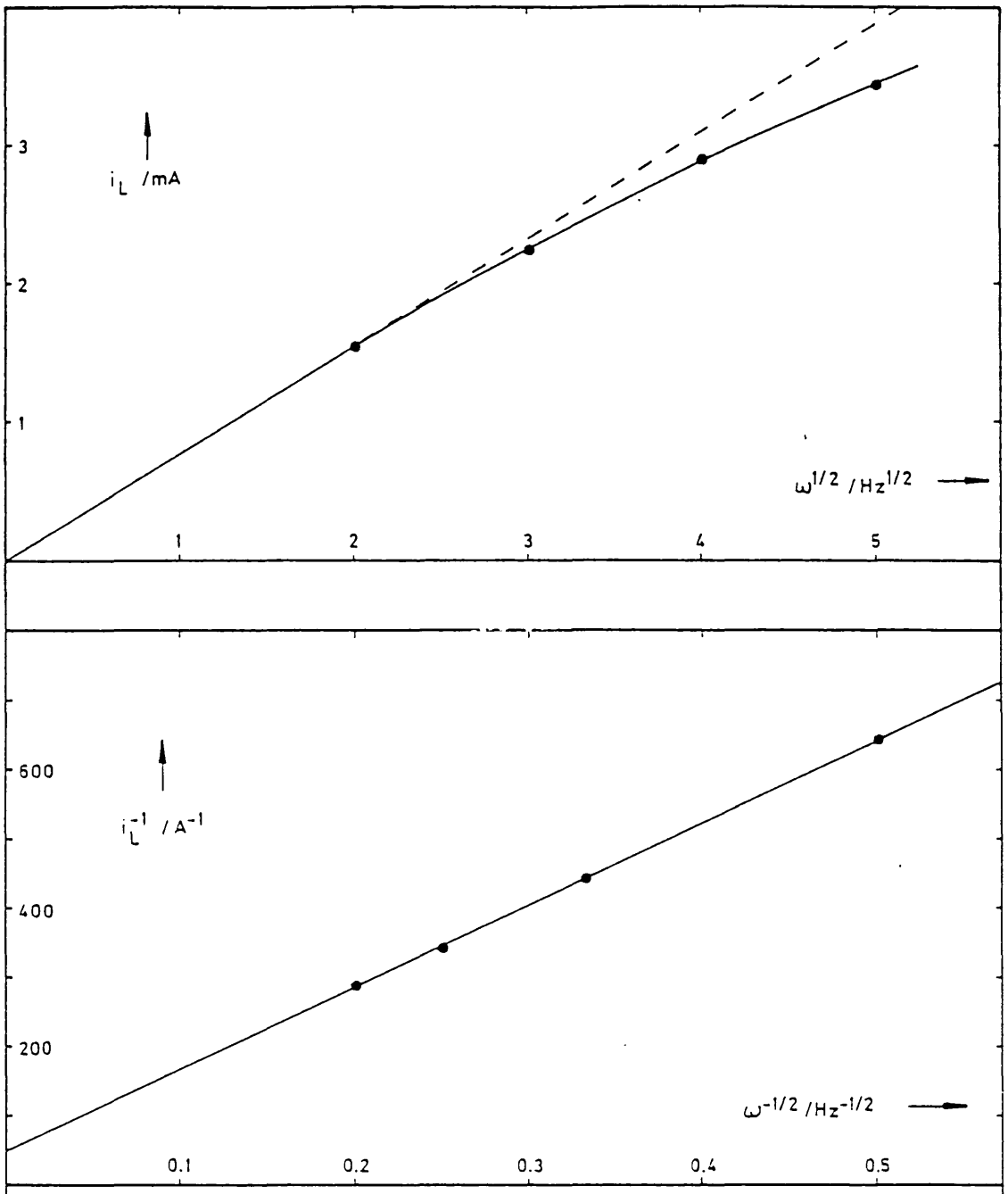

Fig.3.18. (a) i_L vs $\omega^{1/2}$, (b) i_L^{-1} vs $\omega^{-1/2}$ for nitrate reduction on a freshly polished rotating copper disc electrode with fixed potential.

Data from Fig.3.17.

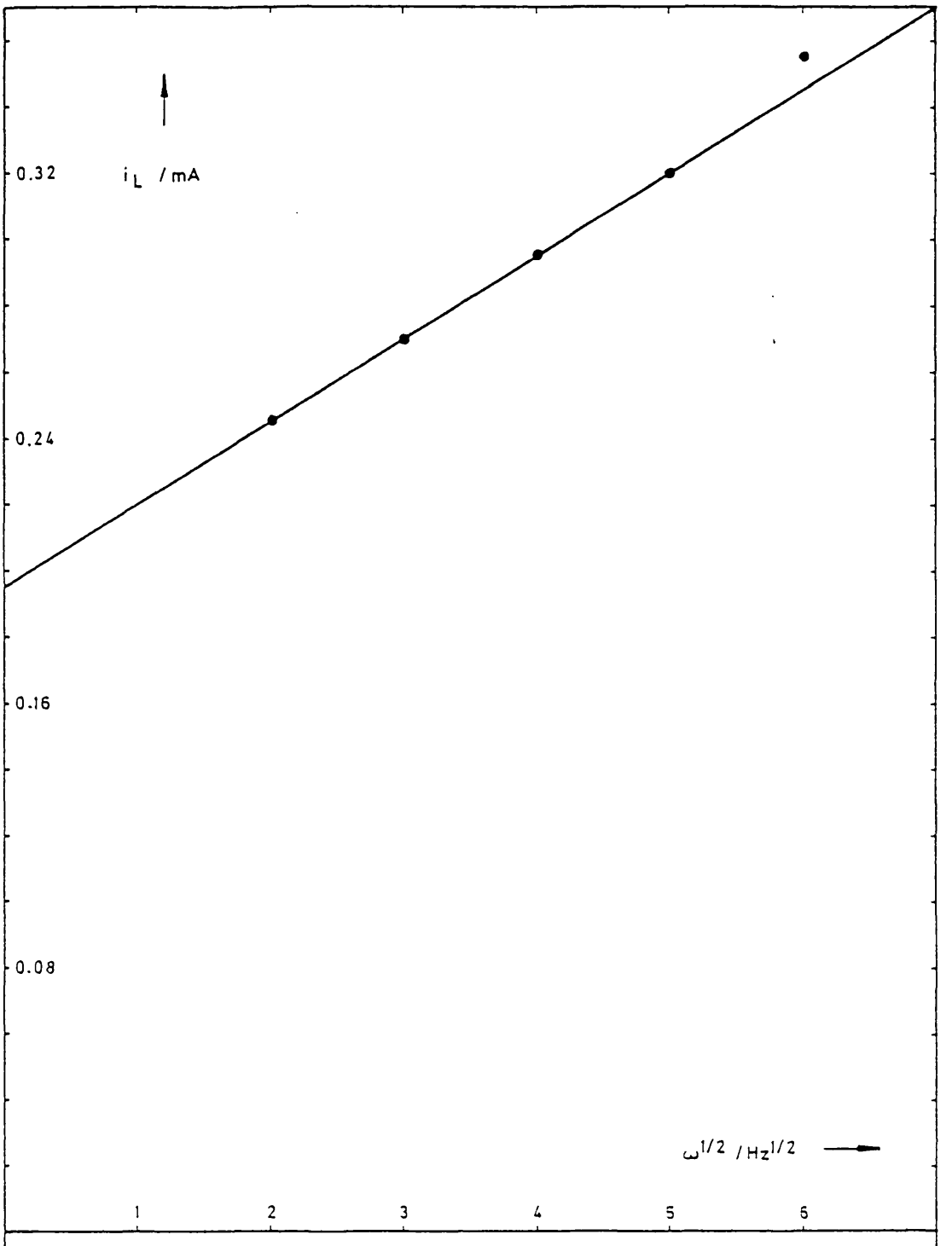

Fig.3.19. Rotation speed dependence of the limiting current during later stages of nitrate reduction on the RCuDE.

Data from Fig.3.17.

3.3.6 First order model for the electrode poisoning

In the steady state, the flux, j, of material reacting at the electrode surface must equal the flux through the diffusion layer. Hence, for the electrode reaction;

$$j = k'c_*(1 - f) \tag{3.57}$$

while, for the transport process;

$$j = D(dc/dx)_* \tag{3.58}$$

$$j = D(c_\infty - c_*)/ x_D \tag{3.59}$$

where k' is the electrochemical rate constant

c_* is the nitrate concentration at the double layer boundary

f is the fraction of deactivated electrode sites

$(dc/dx)_*$ is the concentration gradient at the double layer boundary

x_D is the diffusion layer thickness

Combining (3.57) and (3.59) yields;

$$c_* = c_\infty /[1 + k'(1 - f)(x_D/D)] \tag{3.60}$$

Using this result in (3.57) and rearranging yields;

$$c_\infty /j = 1/k_D + 1/[k'(1 - f)] \tag{3.61}$$

When $k'(1 - f) >> k_D$, then the corresponding flux is transport limited;

$$j_L = Dc_\infty / x_D \tag{3.62}$$

Thus, (3.61) may be rewritten as;

$$c_\infty / j = c_\infty / j_L + 1/[k'(1 - f)] \tag{3.63}$$

It remains to find an expression for f. Now, if the poisoning of the electrode obeys first-order kinetics then the rate of change of deactivated sites is given by;

$$df/dt = k_p(1 - f) - k_R f \tag{3.64}$$

where k_p is the rate of poisoning and k_R is the rate of regeneration.

In Laplace space this equation can be written as;

$$s\bar{f} = k_p/s - (k_p + k_R)\bar{f} \tag{3.65}$$

Rearrangement yields;

$$\bar{f} = k_p/(k_p + k_R).[1/s - 1/(s + k_p - k_R)] \tag{3.66}$$

Inverse transformation yields;

$$f = k_p/(k_p + k_R).[1 - 1/\exp[(k_p + k_R)t]] \tag{3.67}$$

or

$$1 - f = [k_R + k_p \exp[-(k_p + k_R)t]]/(k_p + k_R) \tag{3.68}$$

Using this result in (3.63) yields;

$$c_\infty/j = c_\infty/j_L + \frac{k_P + k_R}{k'(k_R + k_P \exp[-(k_P + k_R)t]} \quad (3.69)$$

or

$$(c_\infty/j - c_\infty/j_L)^{-1} = k'k_R/(k_P + k_R) + \frac{k'k_P \exp[-(k_P + k_R)t]}{k_P + k_R} \quad (3.70)$$

Now, as time tends towards infinity then the second term tends towards zero. Thus,

$$(c_\infty/j_\infty - c_\infty/j_L)^{-1} = k'k_R/(k_P + k_R) \quad (3.71)$$

where j_∞ is the flux as time tends towards infinity.

Substituting this result back into (3.70) yields;

$$(c_\infty/j - c_\infty/j_L)^{-1} = (c_\infty/j_\infty - c_\infty/j_L)^{-1} + k'k_P \exp[-(k_P + k_R)t]/(k_P + k_R) \quad (3.72)$$

$$= (c_\infty/j_\infty - c_\infty/j_L)^{-1} + [k_P/(k_P + k_R)].\ k'\exp[-(k_P + k_R)t] \quad (3.73)$$

$$= (c_\infty/j_\infty - c_\infty/j_L)^{-1} + [1 - k_R/(k_P + k_R)].k'\exp[-(k_P + k_R)t] \quad (3.74)$$

$$= \frac{1 - \exp[-(k_P + k_R)t]}{c_\infty/j_\infty - c_\infty/j_L} + k'\exp[-(k_P + k_R)t] \quad (3.75)$$

An expression for the electrochemical rate constant can be found by substituting t=0 into (3.69) which yields;

$$c_\infty/j_o = c_\infty/j_L + 1/k' \tag{3.76}$$

or

$$k' = [c_\infty/j_o - c_\infty/j_L]^{-1} \tag{3.77}$$

where j_o is the flux when time is zero.

Using this result in (3.75) yields;

$$\frac{1}{c_\infty/j - c_\infty/j_L} = \frac{1 - \exp[-(k_p + k_R)t]}{c_\infty/j_\infty - c_\infty/j_L} + \frac{\exp[-(k_p + k_R)t]}{c_\infty/j_o - c_\infty/j_L} \tag{3.78}$$

or

$$(1/j - 1/j_L)^{-1} = (1/j_\infty - 1/j_L)^{-1} + \exp[-k_p + k_R)t].$$

$$[(1/j_o - 1/j_L)^{-1} - (1/j_\infty - 1/j_L)^{-1}] \tag{3.79}$$

Now, $j_o \simeq j_L$ and if j is reasonably removed from j_o, then;

$$\ln[(1/j - 1/j_{o\simeq L})^{-1} - (1/j_\infty - 1/j_{o\simeq L})^{-1}] \simeq$$

$$\ln[(1/j_o - 1/j_L) - (1/j_\infty - 1/j_L)] - (k_p + k_R)t \tag{3.80}$$

Now, the fluxes can be directly replaced by the corresponding currents since the two are linearly related by (3.35). It can also be noted that the second term in the logarithm on the right-hand side is comparatively small. Thus, a plot of $\ln[(1/i - 1/i_o)^{-1} - (1/i_\infty - 1/i_o)^{-1}]$ vs t should be a straight line with;

$$\text{slope} = -(k_p + k_R) \tag{3.81}$$

and

$$\text{intercept} = \ln[1/(1/i_o - 1/i_L)] \qquad (3.82)$$

The electrochemical rate constant can be obtained from the intercept by using the following relationship;

$$k' = \exp(\text{intercept})/(c_\infty nFA) \qquad (3.83)$$

The regeneration rate can be obtained by rearranging (3.71) to give;

$$k_R = [(k_p + k_R)/k'].[c_\infty nFA(1/i_\infty - 1/i_L)]^{-1} \qquad (3.84)$$

$$= - [\text{slope}/\exp(\text{intercept})].(1/i_\infty - 1/i_L)^{-1} \qquad (3.85)$$

The poisoning rate can be calculated from the relationship;

$$k_p = - \text{slope}.[1 + (1/i_\infty - 1/i_L)^{-1}. \exp(- \text{intercept})] \qquad (3.86)$$

Several semi-logarithmic plots, according to (3.80), are shown in Figs.3.20(a) and 3.20(b). Linearity is good, but in some cases there is a break in the slope. In each of these cases the position of the break corresponds to the foot of the decay curve and indicates the onset of some other mechanism, which is not well understood. Values of k', k_p and k_R calculated from the first linear sections are shown in Table 3.2.

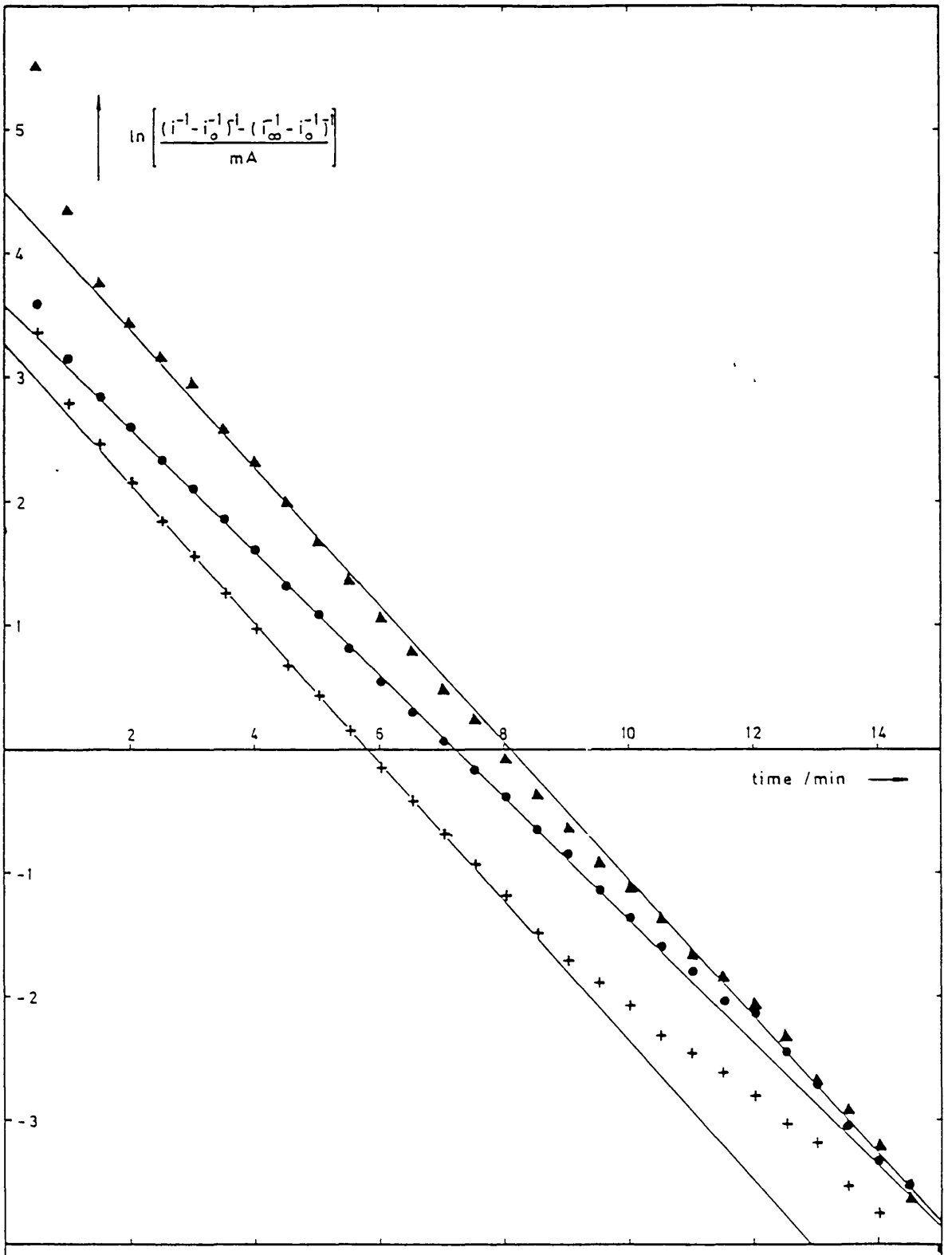

Fig. 3.20(a) Plots describing the first-order decay of the nitrate reduction limiting current on the RCuDE.

$[NaNO_3] = 1 mmol\,dm^{-3}$, $[HClO_4] = 0.1 mol\,dm^{-3}$, $[NaClO_4] = 0.9 mol\,dm^{-3}$

$\omega = 4 Hz$, $A = 0.3915 cm^2$, $E = -0.6 V$ vs SCE.

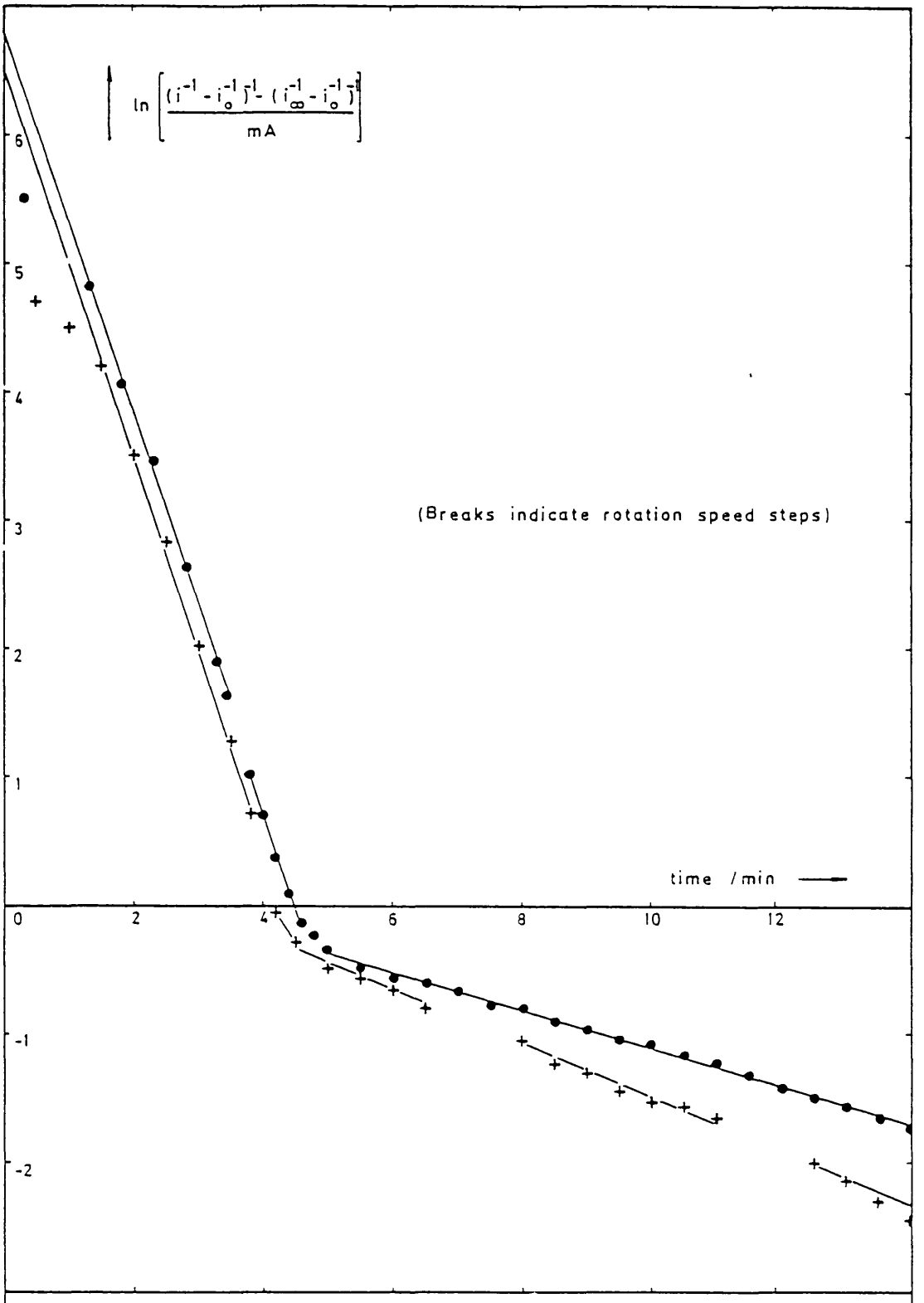

Fig.3.20(b) Plots describing the first-order decay of the nitrate reduction limiting current on the RCuDE.

$[NaNO_3] = 1 mmol dm^{-3}$, $[HClO_4] = 0.1 mol dm^{-3}$, $[NaClO_4] = 0.9 mol dm^{-3}$

$\omega = 4 Hz$, $A = 0.3915 cm$, $E = -0.75 V$.

E /mV vs SCE	k' /cm s^{-1}	k_R /10^{-8} s^{-1}	k_P /10^{-3} s^{-1}	$t_{f=0.999}$ /min
-600	0.28	35	9.3	12.3
-600	0.083	63	9.4	12.3
-600	0.11	40	8.2	14.0
-750	2.1	16	25	4.6
-750	2.3	10	25	4.7

Table 3.2. Measured values of k', k_R, and k_P.

It can be seen that the regeneration rate is negligible, while both the electrochemical and the poisoning rates increase with the applied potential.

The initial number of active sites is determined by the degree of electrode polishing. This is reflected by the duration of the initial, horizontal portion of the decay curve. The top part of the curve was not observed at all if the electrode was not carefully polished immediately before use. It can be seen, from the table, that the poisoning rate is effectively unchanged by the initial surface condition, but the electrochemical rate is severely effected since the initial number of sites is a factor in this rate.

The fraction of deactivated sites can be calculated from (3.67), with the simplification that $k_R << k_p$. Then;

$$f = 1 - \exp(k_p t) \qquad (3.87)$$

The times taken to increase this value to 0.999 are included in Table 3.2. The effective electrode area is very small at this level and if the remaining active sites are spread throughout the geometric area then the electrode would behave as a collection of micro-electrodes with radial diffusion making a contribution to the flux. This could explain the large intercept when the current is extrapolated to $\omega = 0$, Fig.3.19.

3.3.7 Potential Step Transients

Linear and cyclic sweep voltammetry has shown that a clean copper surface makes a good cathode for nitrate reduction, but the surface is quickly poisoned by the reduction process and this makes it impossible to obtain a reliable continuous measurement. Thus, the feasibility of intermittent measurements was investigated.

There is a potential separation between the copper stripping and nitrate reduction processes. Hence, a potential step between the two should, in principle, provide the nitrate with a fresh surface. The resultant, cathodic current transient could be interrogated, in order to measure the nitrate concentration, and the potential then returned to the copper stripping region so as to provide a fresh surface for the next measurement.

A pulse unit, based on a chain of LM555CN timers and LF398H sample and hold integrated circuits, was used for this work [84].

3.3.8 Concentration Dependence of Potential Step Transients

The electrode response to nitrate concentration is shown in Figs.3.21 and 3.22. There is a significant response even after an extended period of use, but the relationship between sampled current and concentration is not linear and there is a very large intercept at zero nitrate concentration. The background current can be attributed to;

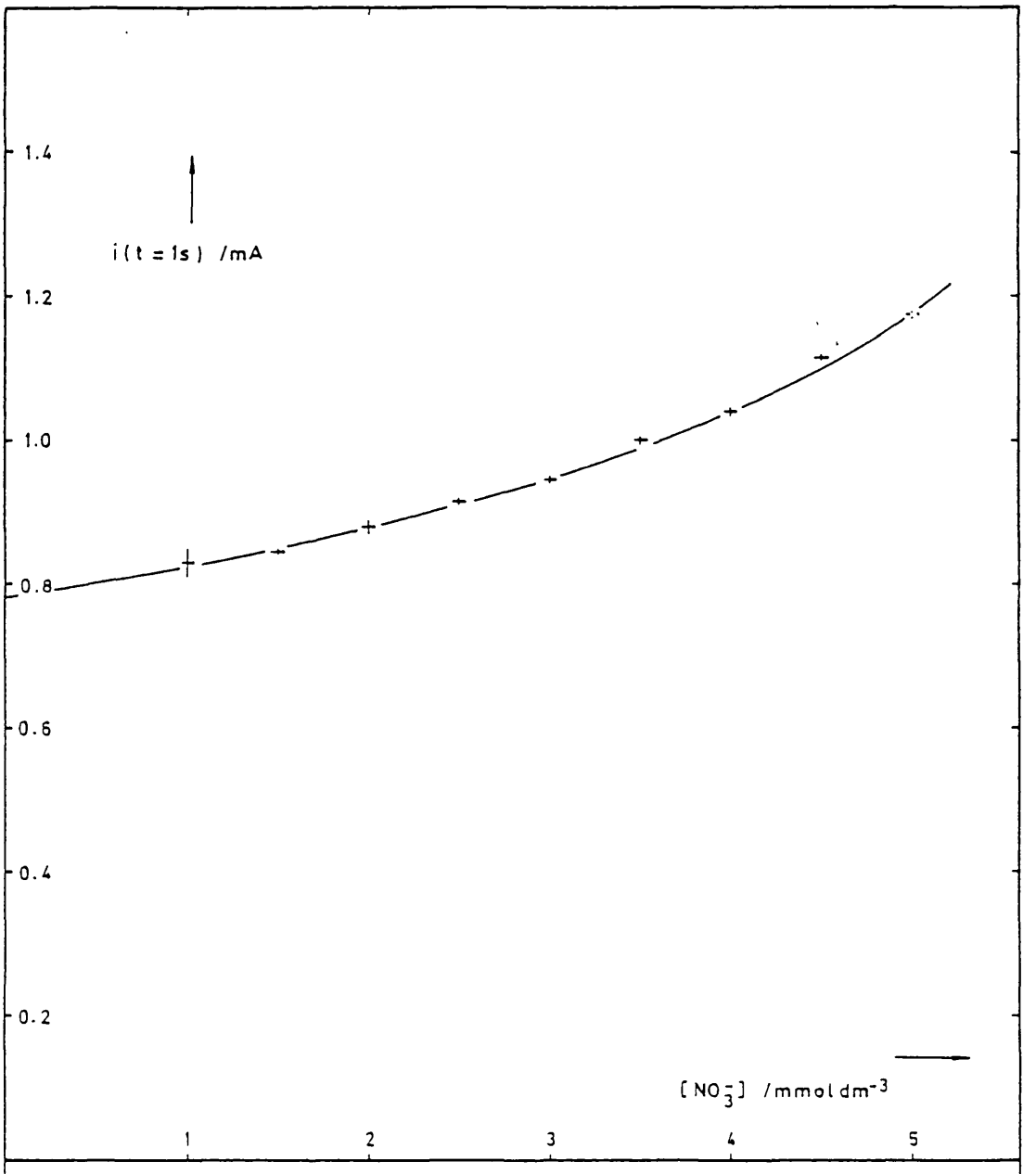

Fig.3.21. Sampled current response to $[NO_3^-]$ after four days of applying a potential pulse sequence to a copper rotating disc electrode.

Original $[NO_3^-] = 1\,mmol\,dm^{-3}$, $[HClO_4] = 0.1\,mol\,dm^{-3}$, $[NaNO_4] = 0.9\,mol\,dm^{-3}$,

$\omega = 9\,Hz$, $A = 0.3915\,cm^2$, $V = 100\,cm^2$.

Pulse sequence (E vs SCE): +0.1V (copper stripping, 8.8s) to -0.6V (nitrate reduction, 1.2s).

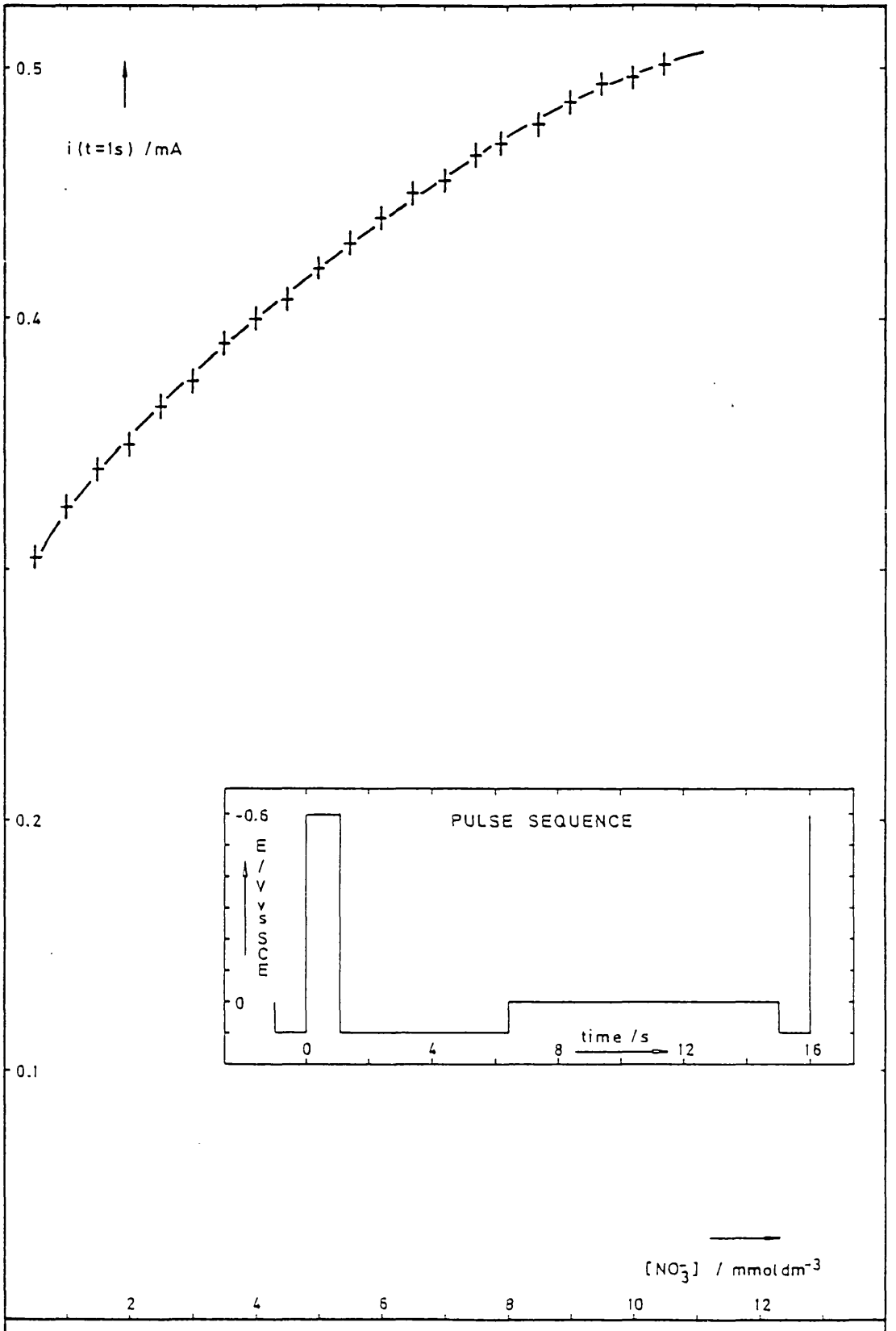

Fig.3.22. Sampled current response to nitrate concentration after 24hours of a double pulse sequence on a RCuDE.

Original [$NaNO_3$] = 1mmol dm^{-3}, [$HClO_4$] = 0.1mol dm^{-3}, [$NaClO_4$] = 0.9mol dm^{-3}

ω = 16Hz, A = 0.3915 cm^2.

(a) plating of copper ions just stripped from the electrode surface, and

(b) plating of copper ions which have accumulated in the bulk solution.

The latter is not a problem in a fresh solution and the former can be overcome by using a double pulse technique whereby the electrode is stepped to an intermediate potential where no reaction occurs, so as the copper ions just removed are given time to be swept away, before carrying out the nitrate reduction, Fig.3.23. The non-linear relationship between sampled current and nitrate concentration is maintained, however, Fig.3.24.

3.3.9 Rotation Speed Dependence of Potential Step Transients

The rotation speed dependence of the potential step transients is interesting, Fig.3.25. When the rotation speed is close to 1Hz then the cathodic step (-0.6V vs SCE) is sufficient to take the electrode into the nitrate reduction limiting current region, but when the rotation speed is much higher then the reaction is kinetically controlled, Fig.3.13.

At short times the current in the former case would be expected to be described by the Cottrell equation [85];

$$i = c_{\infty} nFA(D/\pi t)^{\frac{1}{2}} \qquad (3.88)$$

which indicates that $i \longrightarrow \infty$ as $t \longrightarrow 0$, while at long times the current would be expected to approach the steady-state value (Figs.3.13 and 3.17). To a first approximation this does appear to be the case, Fig.3.25.

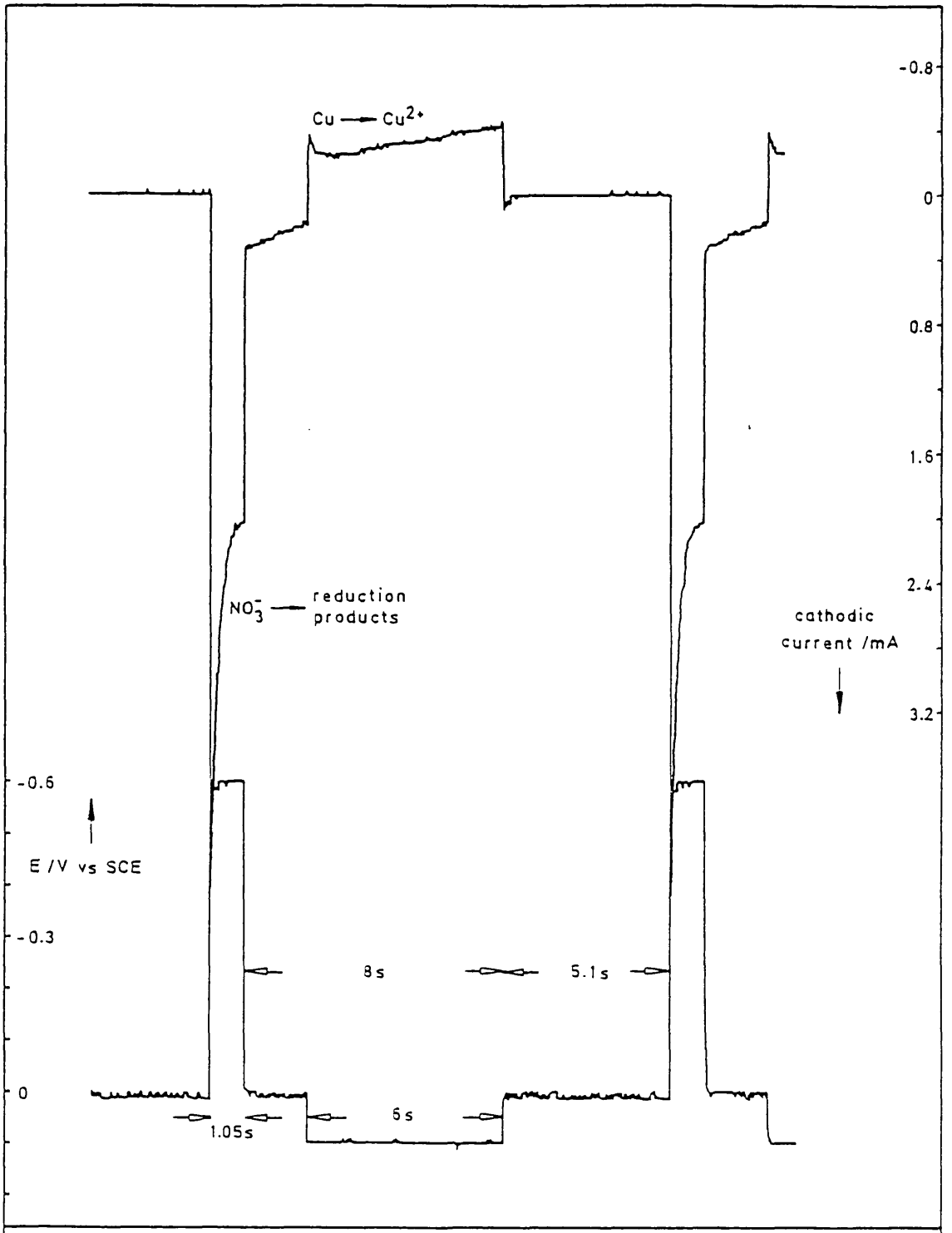

Fig.3.23. The double pulse sequence on a rotating copper disc electrode, showing the resulting current transients.

$[NaNO_3] = 1\,mmol\,dm^{-3}$, $[HClO_4] = 0{\cdot}1\,mol\,dm^{-3}$, $[NaClO_4] = 0{\cdot}9\,mol\,dm^{-3}$, $\omega = 4\,Hz$, $A = 0{\cdot}3915\,cm^2$.

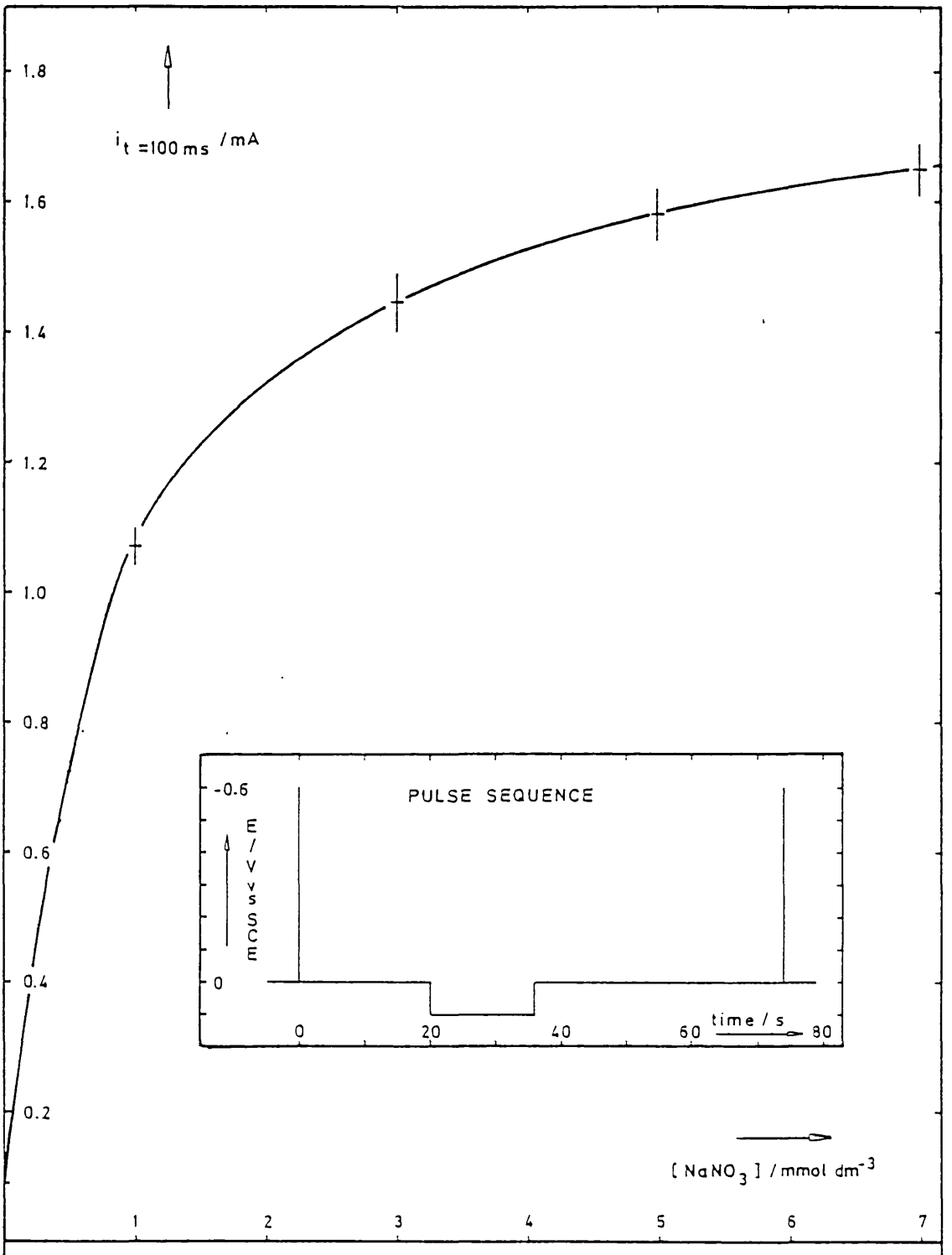

Fig.3.24. Sampled current response to nitrate on fresh double-pulsed RCuDE.

ω = 1Hz, $[HClO_4]$ = 0.1 mol dm^{-3}, $[NaClO_4]$ = 0.9 mol dm^{-3}, A = 0.3915 cm^2

Pulse sequence (E vs SCE): 0.0V (rest, 10s) to +0.1V (copper stripping, 8s) to 0.0V (rest, 20s) to -0.6V (nitrate reduction, 100ms).

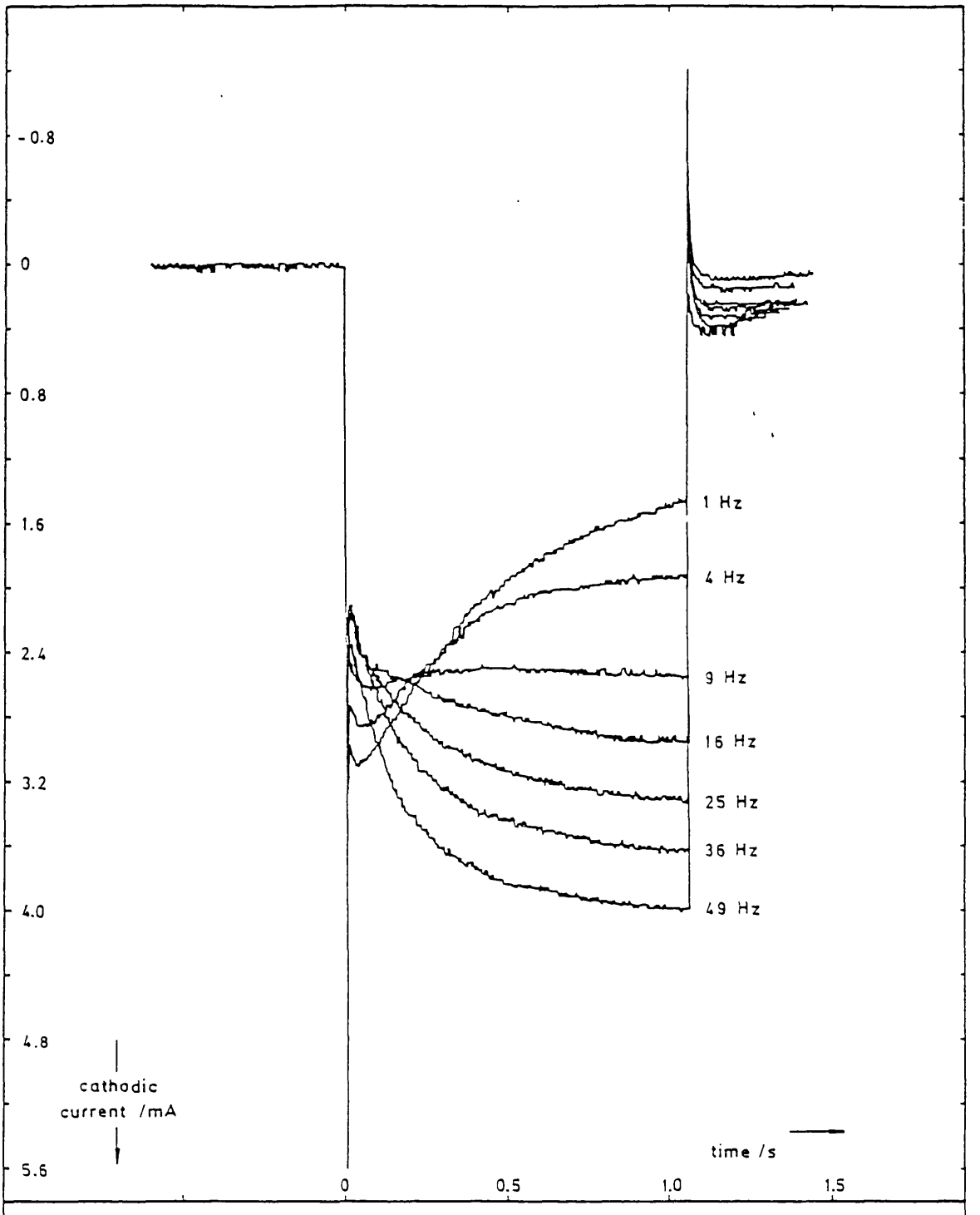

Fig.3.25. Detail from the double potential pulse sequence, on a copper disc electrode, showing the effect of rotation speed on the nitrate reduction current transient.

$[NaNO_3] = 1\,mmol\,dm^{-3}$, $[HClO_4] = 0{\cdot}1\,mol\,dm^{-3}$, $[NaClO_4] = 0{\cdot}9\,mol\,dm^{-3}$, $A = 0{\cdot}3915\,cm^2$.

For a potential step on a stationary electrode, the kinetically controlled current at short times is described by[86];

$$i = c_{\infty}nFAk'[1 - 2k'(t/\pi D)] \qquad (3.89)$$

which indicates that $i \longrightarrow c_{\infty}nFAk'$ as $t \longrightarrow 0$. For nitrate reduction on the rotating disc electrode the current does start at a finite value, as predicted, but this is less than the steady-state value (Figs.3.13 and 3.17). The reason for the very low initial value is unclear, but, consequently, the current increases with time rather than decreasing, as would be predicted.

3.3.10 Summary of Potential Step Analysis on the RCuDE

Stripping of copper ions from the electrode surface enhances its response to nitrate concentration even after extended periods of use, but potential step analysis on the RCuDE has been unsatisfactory since;

(a) the relationship between transient current and rotation speed is not understood,

(b) the relationship between sampled current and nitrate concentration is not linear, even on a fresh electrode, and

(c) the electrode surface is eroded so as the disc eventually becomes visibly recessed in its insulating sheath and this must have serious consequences for the solution hydrodynamics.

3.3.11 Copper Plating on an 'Inert' Substrate

Electrode degradation, due to copper stripping, can be circumvented by plating a thin layer of copper on to an otherwise inert substrate. The plated surface can be removed after each nitrate measurement with no erosion of the substrate. The concept has been successfully tested using a rotating platinim disc electrode, Fig.3.27.

3.4 Wall-Jet Electrodes (WJEs)

The rotating disc electrode is very useful for laboratory studies, but many analytical situations, such as hydroponics, require continuous measurements on a changing solution and the RDE is not very suitable for this purpose. Thus, a modified wall-jet electrode is being developed by other workers in Professor Albery's laboratories at Imperial College [87, 88].

The principle of the wall-jet electrode is to pump the test solution through a nozzle so as to produce a jet of liquid directed at a stationary disc electrode placed normal to the solution flow. This has several advantages over the RDE;

(a) the solution hydrodynamics can be controlled, but there are no moving parts in the electrochemical cell,

(b) small volumes of solution can be used (1-2 $cm^3 min^{-1}$) and the solution can be directed to waste after measurement at the disc.

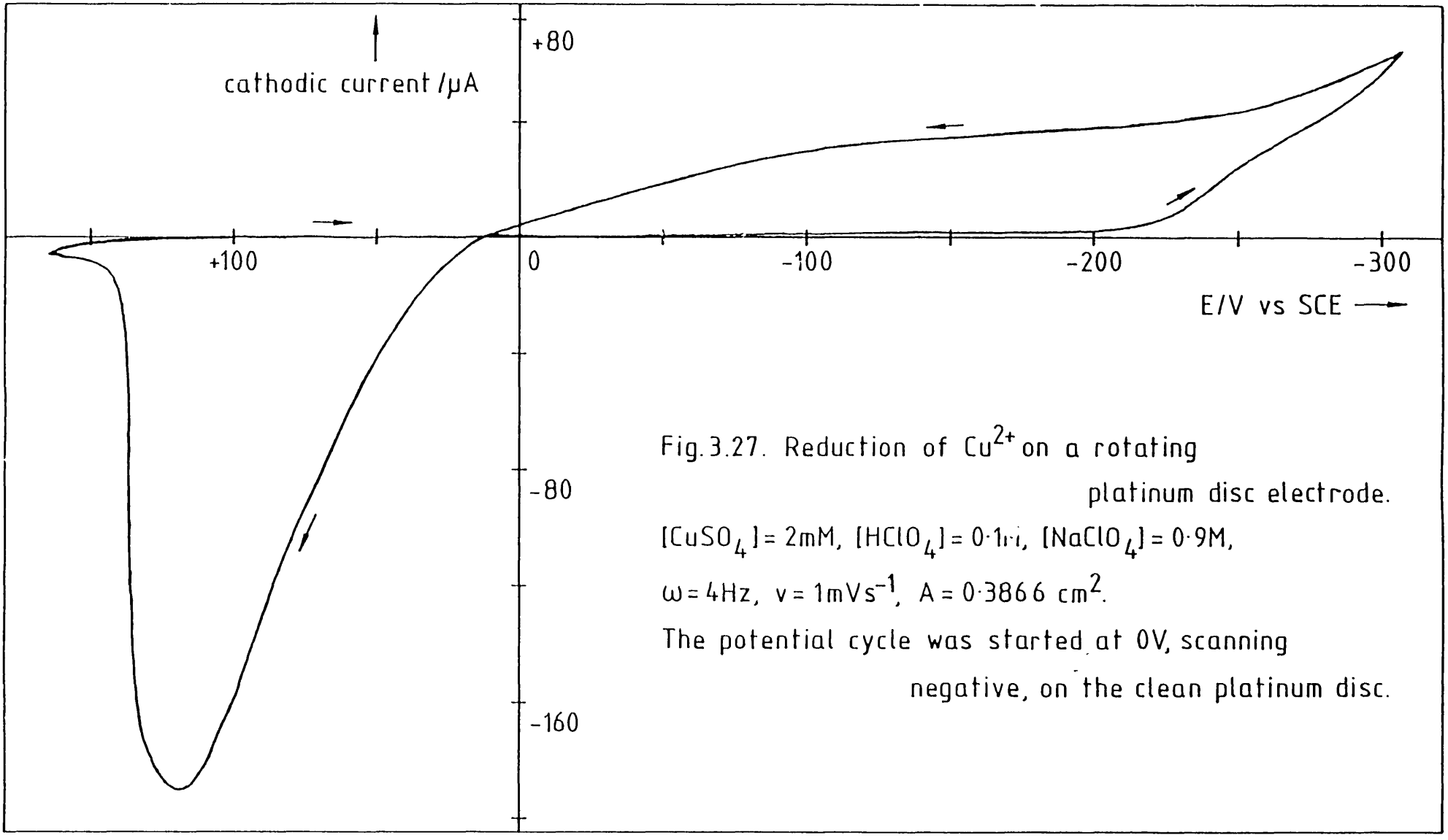

Fig. 3.27. Reduction of Cu^{2+} on a rotating platinum disc electrode.
$[CuSO_4] = 2mM$, $[HClO_4] = 0{\cdot}1M$, $[NaClO_4] = 0{\cdot}9M$,
$\omega = 4Hz$, $v = 1mVs^{-1}$, $A = 0{\cdot}3866\ cm^2$.
The potential cycle was started at 0V, scanning negative, on the clean platinum disc.

3.4.1 The Packed Bed Wall-Jet Electrode (PBWJE)

A PBWJE, Fig.3.28 is being developed for nitrate determinations[87, 88]. This is a conventional WJE with the incorporation of packed bed and counter electrodes upstream of the jet. The bed consists of copper chips contained within a copper tube. It can be galvanostatted so as to enable copper ions to be injected through the jet and, by application of a suitable potential, these ions can be plated on to the disc. The bed can be switched off when sufficient copper has been deposited and the cell is then ready to measure the nitrate concentration in the test solution. When this has been done then the copper surface can be removed from the disc and the cycle is ready to be repeated.

3.5 Summary

The reduction of nitrate at a copper cathode has been investigated, following the work of Pletcher et al. Reduction waves were obtained with a transfer number of about eight electrons, but good results were obtained only on a fresh electrode surface, which could be maintained for only three or four minutes, even under the best circumstances. After this period the limiting current decayed to a small fraction of its original value. This effect was not reported by Pletcher but has been observed by many other workers studying both electrochemical and non-electrochemical nitrate reduction on metal surfaces.

The current decay on copper can be accounted for by a first-order kinetics model which describes the deactivation of sites on the electrode surface. Detailed mechanistic studies

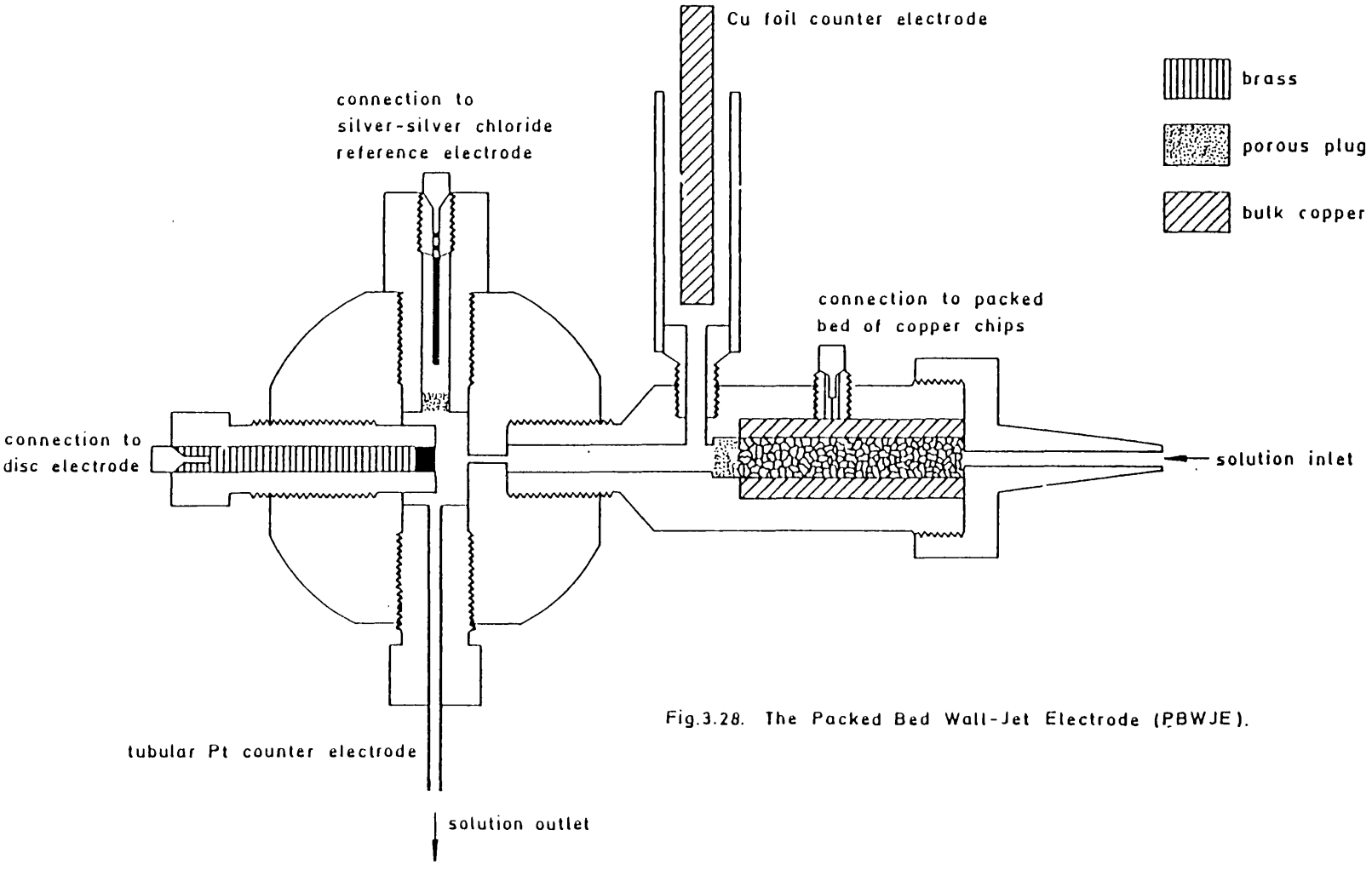

Fig.3.28. The Packed Bed Wall-Jet Electrode (PBWJE).

have not been carried out, but it is probable that Cu-O bonds are formed during the reduction process and these bonds are not subsequently broken. Consequently, the sites become deactivated.

The copper surface can be reactivated by holding the electrode surface in the hydrogen evolution region or by mechanical polishing or by stripping copper ions from the electrode surface.

A modified wall-jet electrode is being developed for the 'continuous' determination of nitrate concentration. It incorporates copper packed bed and counter electrodes upstream of the jet which allows copper ions to be injected through the jet and, by application of a suitable potential, these can be plated on to the otherwise inert disc electrode. This provides a fresh copper surface for the nitrate determination after which the used copper can be removed and the plating repeated.

CHAPTER 4

DEVELOPMENT OF A MEMBRANE-COVERED DISSOLVED OXYGEN SENSOR

4.0 Introduction

The primary intent of the work described in this chapter was to develop a method for using Clark-type electrodes to make membrane-independent measurements of dissolved oxygen concentration, but the work is applicable to other electroactive species and to certain electrochemical cells other than membrane-covered sensors.

Transient current measurements are examined and several models are developed to describe the processes occurring when a potential step is applied between working and reference electrodes.

4.0.1 Transient current measurements

It has long been recognised that a Clark-type electrode operated in a pulsed mode could be membrane independent. In this mode the working electrode would normally be switched 'off' - either by removing it from circuit, so as no current is passed, or by maintaining its potential in a region where no reaction occurs, Fig.4.1. Under these circumstances, the oxygen concentrations in the test fluid, membrane and electrolyte equiliberate so as the activity is uniform throughout. If the working electrode is subsequently allowed to pass the diffusion controlled current - either by switching the electrode into circuit or by stepping the electrode potential, then the initial current transient is independent of the membrane properties, fouling and test-fluid stirring. This

Fig.4.1. Simulated voltammogram

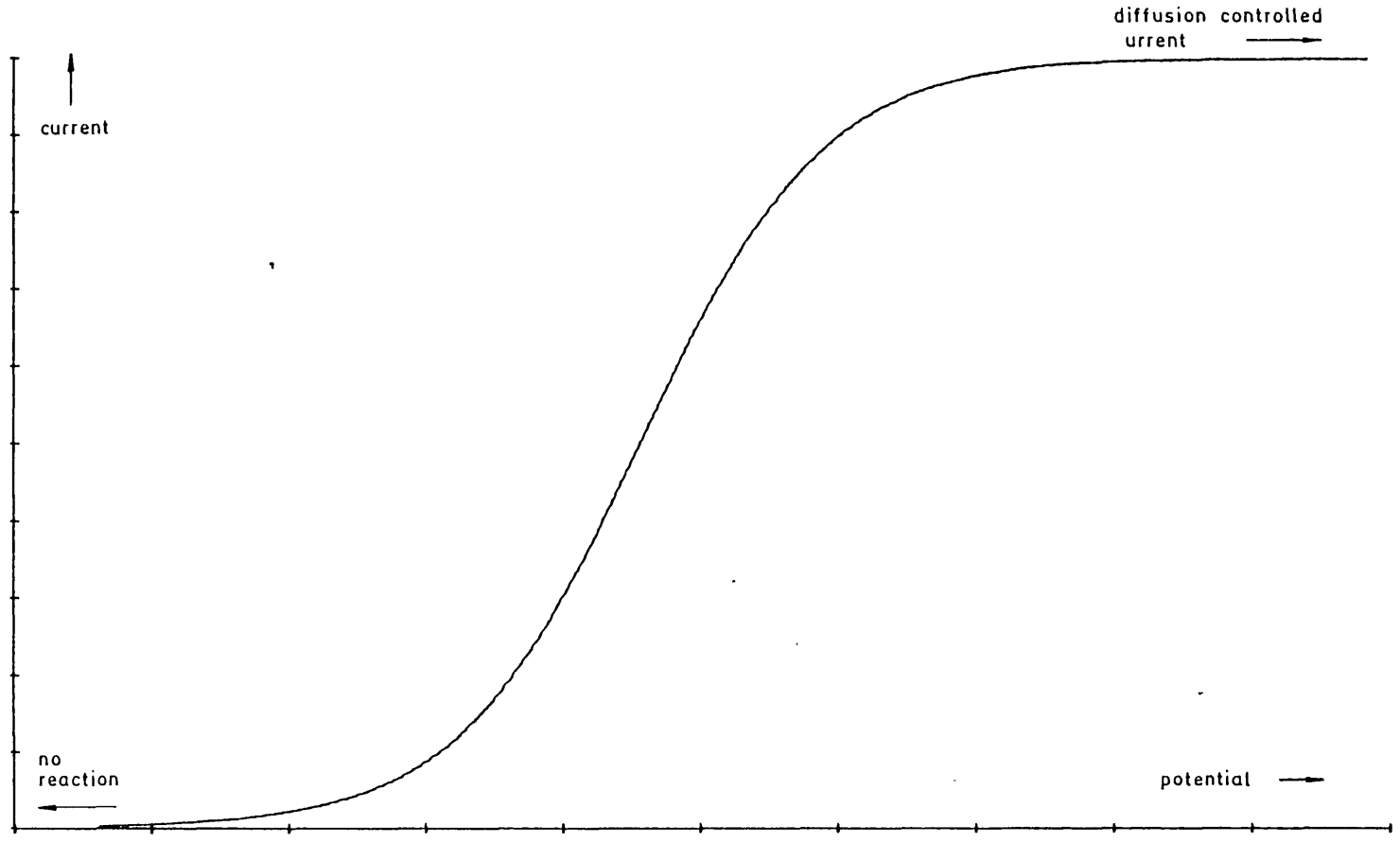

is because the depletion layer takes a finite time to cross the electrolyte layer, Fig.4.2.

Having sampled the current transient, the cycle is completed by switching the electrode 'off' and allowing the oxygen to re-equilibr The process can be repeated, as required.

4.1 Equilibrium oxygen concentration

Using the terminology of section 1.3, the equilibrium oxygen concentration, c_∞, in the electrolyte is related to the external oxygen concentration, c_s, by;

$$c_\infty = \alpha_e c_s / \alpha_s \quad \text{(liquid phase test fluid)} \qquad (4.1)$$

or $$c_\infty = \alpha_e p \quad \text{(gas phase test fluid)} \qquad (4.2)$$

Thus, there is a linear relationship between the equilibrium oxygen concentration in the electrolyte and the external oxygen concentration.

4.2 Diffusion layer thickness

The time available for sampling the membrane independent current is determined by the movement of the diffusion layer boundary across the electrolyte. When this boundary reaches the membrane then the observed current becomes a function of the membrane properties[52].

The 'random-walk' process can be used to derive[89a] an approximate relationship for the diffusion layer thickness, x_D;

$$x_D \simeq (2Dt)^{\frac{1}{2}} \qquad (4.3)$$

where D is the oxygen diffusion coefficient

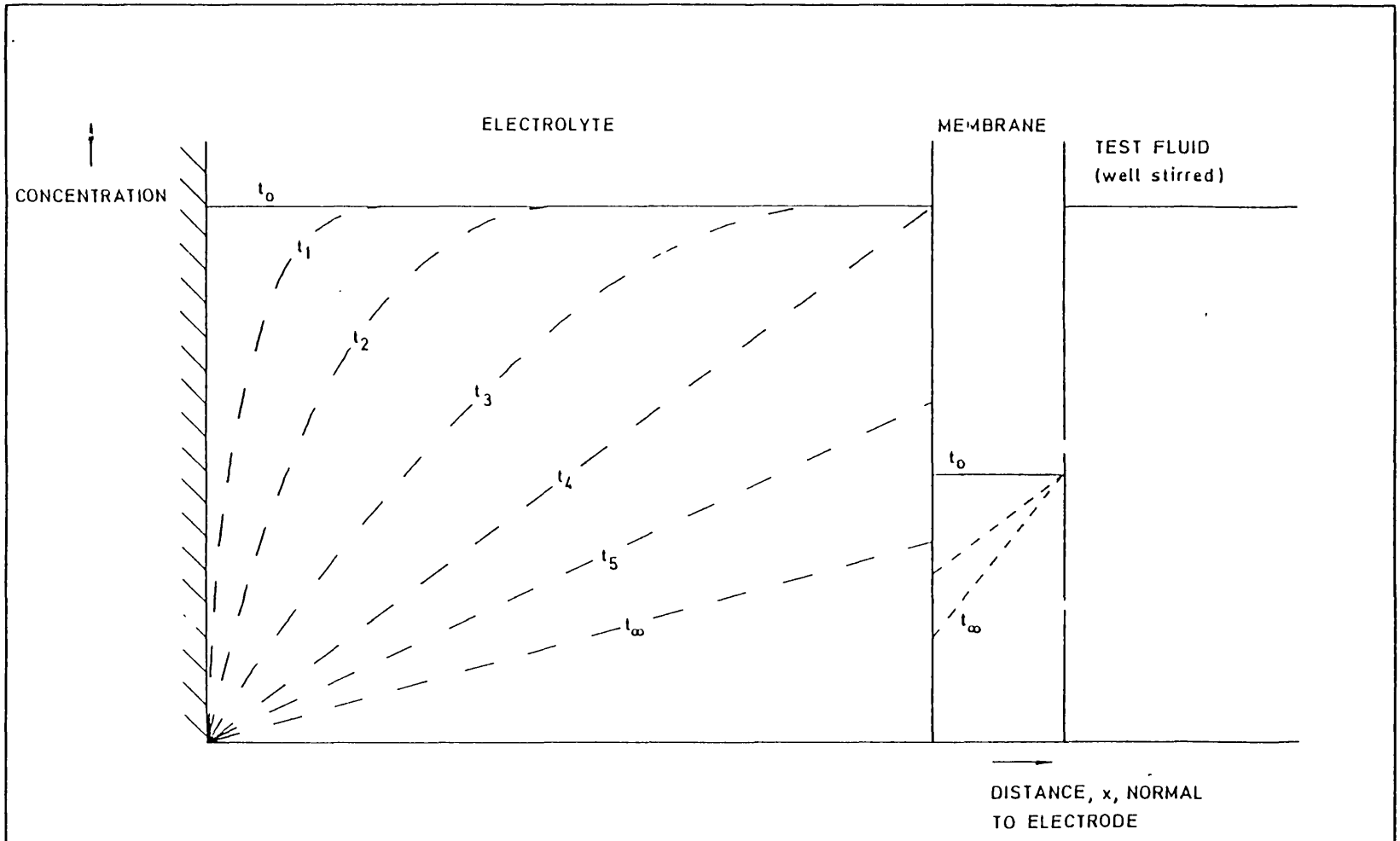

Fig.4.2. Changes in concentration profile: switch on (t_0) to steady state (t_∞).

t is the elapsed time since the electrode was switched 'on'.
The elecrolyte thickness can be substituted for x_D and the time available for sampling the membrane-independent current calculated by rearrangement of (4.3).

Alternatively, the concentration profile across the electrolyte layer can be calculated from the solution to Fick's second law;

$$dc(x,t)/dt = Dd^2c(x,t)/dx^2 \qquad (4.4)$$

under the boundary conditions;

$$c(x,t) = c_\infty \quad (\text{for } t<0) \qquad (4.5)$$

$$\lim_{x\to\infty} c(x,t) = c_\infty \quad (\text{for all } t) \qquad (4.6)$$

$$c(0,t) = 0 \quad (\text{for } t>0) \qquad (4.7)$$

where c_∞ is the equilibrium oxygen concentration in the electrolyte.

Appropriate Laplace transformation and inversion yields [89b];

$$c(x,t) = c_\infty \text{erf}[0.5x(Dt)^{-\frac{1}{2}}] \qquad (4.8)$$

The time taken for the concentration at the membrane boundary to fall to any given fraction of c_∞ can be calculated by setting x equal to the electrolyte layer thickness and rearranging (4.8) to give t.

The electrolyte thickness can be tailored to any required value, but the thicker the electrolyte the slower the response time of the sensor. Thus, the electrolyte thickness is normally a few microns or a few tens of microns. In this case

the transient current must certainly be sampled within ca.100ms if membrane independence is to be achieved.

4.3 Switch from open-circuit

Several workers[90, 91] have employed the technique of switching from open-circuit but relatively long sample delays were used. Hence, membrane independence was not achieved, however, there was increased sensitivity since the transient currents and much larger than the steady-state values.

An advantage of switching the working electrode from open-circuit is that the electrical double layer does not have to be fully charged each time the switch is made. On the other hand, there is some discharge of the double layer - even at open-circuit and the effective pulse length is partly determined by the dissolved oxygen concentration and this complicates the function of such a sensor[90, 92].

4.4 Potential step into the diffusion limited region

The transient current, i, upon stepping the electrode potential into the diffusion limited region is given by the relationship;

$$i = nFA(dc/dt)_o \qquad (4.9)$$

The partial differential can be obtained by solution of (4.4) with the associated boundary conditions (4.5-7). The final result produces the current-time response which is known as the Cottrell equation[85, 89c];

$$i = c_\infty nFA(D/\pi t)^{\frac{1}{2}} \qquad (4.10)$$

This indicates that the current sampled at a given time, t, is a linear function of the equilibrium oxygen concentration.

Wise, Smart and Mancy found that a potential step into the diffusion limited region gave rise to a current which varied little over a wide range of oxygen concentration[90]

In this laboratory, a linear relationship was found between sampled current and external oxygen concentration but there was a large residual current even in the absence of oxygen, Fig.4.3. The residual current was found to increase as the sample delay decreased.

4.4.1 Double layer charging

A prime candidate for the source of the residual current is charging of the electrical double layer at the working electrode-electrolyte interface.

In the absence of faradaic current the three electrode system has a simple electrical analogue, Fig.4.4.

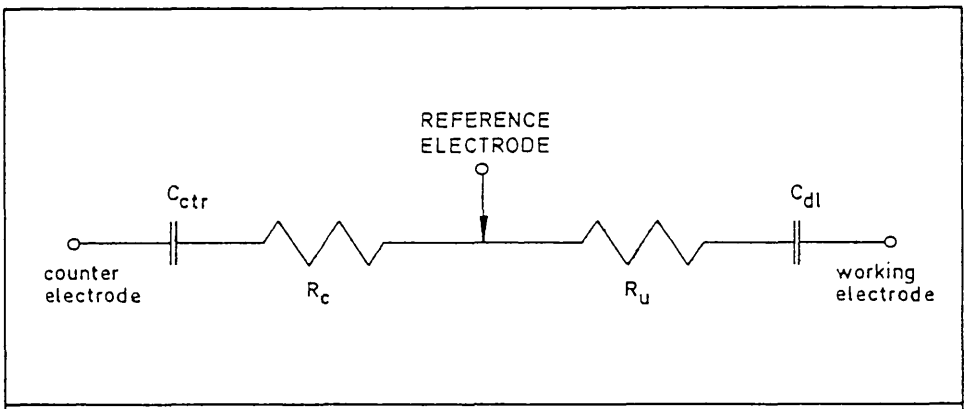

Fig.4.4. Resistor-capacitor analogue of a non-faradaic system.

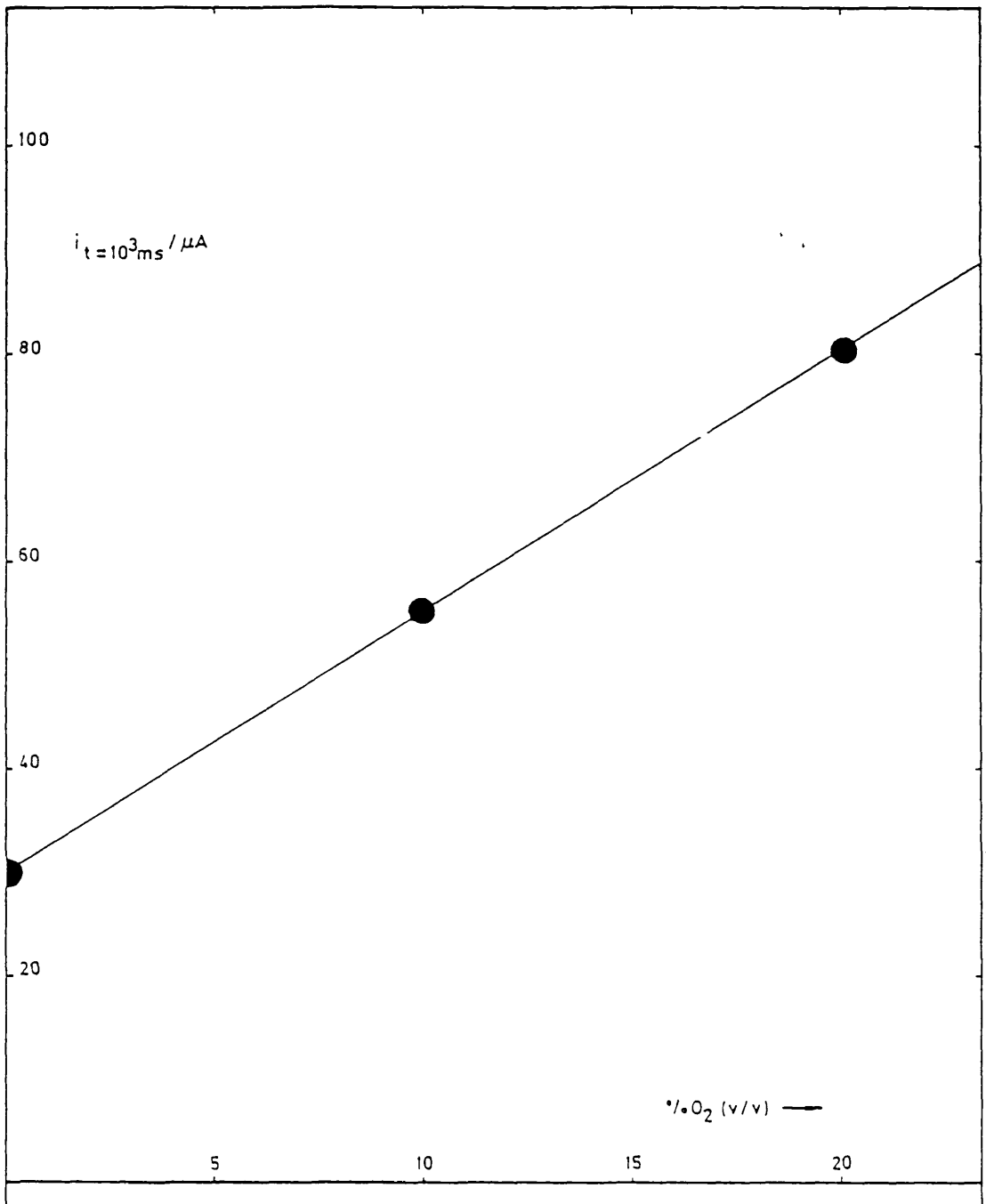

Fig.4.3. Single point sample response from a pulsed membrane-covered electrode

pH5 potassium hydrogen phthalate/NaOH buffer, 0.1 mol dm^{-3} sodium chloride,

gold electrode A = 0.071 cm^2, 12μ D602 teflon membrane with nylon spacer.

R_u is the uncompensated resistance, R_c is the compensated resistance, C_{dl} is the double layer capacitance at the working electrode-electrolyte interface and C_{ctr} is the capacitance of the counter electrode interface.

The total capacitance, C, of the system is given by;

$$1/C = 1/C_{dl} + 1/C_{ctr} \qquad (4.11)$$

Now, if the counter electrode is much larger than the working electrode then C_{ctr} will be very much larger than C_{dl} and the counter electrode capacitance may be ignored;

$$C = C_{dl} \qquad (4.12)$$

A potential step applied between the reference and working electrodes will give rise to a charging current, i_{dl}, given by;

$$i_{dl} = (\Delta V/R_u)\exp(-t/R_uC) \qquad (4.13)$$

where ΔV is the magnitute of the potential step

t is the time elapsed since the imposition of the step.

Thus, a finite current will be obtained even in the absence of oxygen.

4.4.2 Electrode Time Constant

The product of the electrode capacitance and the uncompensated resistance is a characteristic of the electrode, known as the time constant;

$$\text{time constant} = R_uC \qquad (4.14)$$

This value is particularly significant for a membrane covered electrode, for reasons which will become apparent.

4.4.3 Uncompensated Resistance

In bulk solution, the uncompensated resistance between the working and reference electrodes is determined by the electrolyte conductivity and the size of the working electrode. For a disc electrode, the ohmic drop, R_u, is given by[93];

$$R_u = (4Kr)^{-1} \qquad (4.15)$$

where K is the electrolyte conductivity

r is the electrode radius

A macro-size electrode in a reasonably concentrated electrolyte may have an uncompensated resistance of a few ohms.

Membrane covered electrodes, of the type used in this laboratory, have a resistance much larger than would be calculated from the Newman equation. This is because the resistance is primarily determined by the very thin electrolyte layer and in this case the ohmic drop will generally be at least 1kΩ and perhaps several tens of kΩ[90, 91]. Consequently the time constant of a membrane covered electrode is much greater than that of the uncovered electrode. It is this fact which seems to have deterred workers from using very short delays when sampling potential step current transients from membrane electrodes.

4.4.4 Membrane Electrode Simulation

Membrane covered sensors are differentiated from electrodes in bulk solution by the size of the uncompensated resistance. In many of the studies reported in this thesis it was convenient, however, to use disc electrodes, with separate reference and counter, rather than use membrane covered sensors. In these cases, it was a simple task to insert an external resistor, R_x, between the working electrode and the current-voltage convertor.

The results shown in Fig.4.5 were obtained using this technique. They show the effect of using different sample delays:

(i) the sampled current is linearly related to oxygen concentration but over an increasingly restricted range as the sample delay is decreased,

(ii) the residual current increases as the sample delay decreases.

Thus, the minimum sample delay is determined by the range over which it is desired to operate the sensor and by the amount of residual current which can be tolerated.

4.5 Background Current

A gold electrode, continually pulsed in background electrolyte, gives transient currents which decay over several hours until they approach some kind of 'steady-state' value, Fig.4.6. When using transient currents to measure conentration then best results could be obtained after this steady-state had been reached and theoretically the transients could have been corrected for the

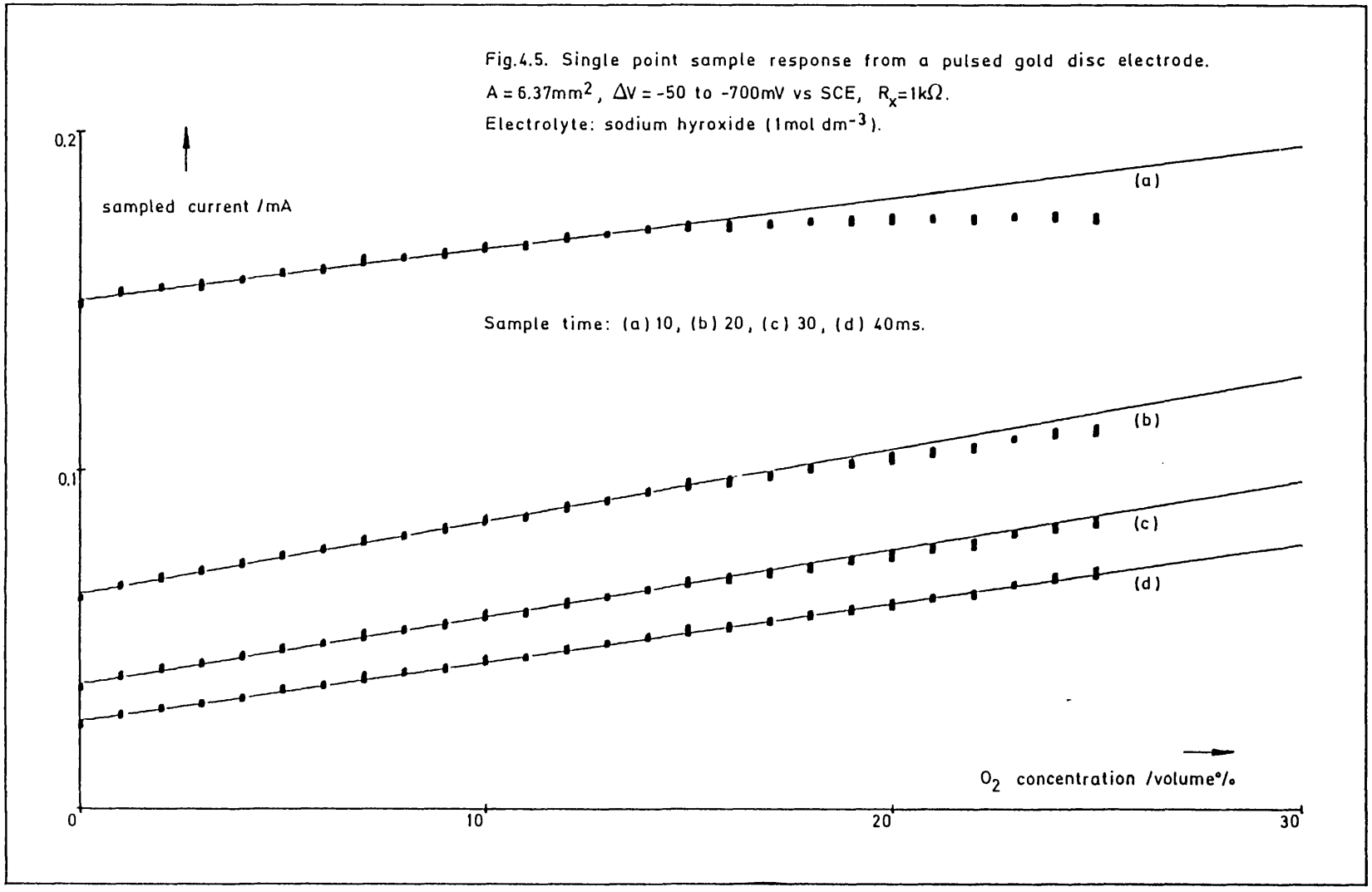

Fig.4.5. Single point sample response from a pulsed gold disc electrode.
$A = 6.37mm^2$, $\Delta V = -50$ to $-700mV$ vs SCE, $R_x = 1k\Omega$.
Electrolyte: sodium hyroxide ($1mol\ dm^{-3}$).

Fig.4.6. Time course of background transient currents on gold disc electrode No.6.

R_x=984Ω, ΔV = -100 to -700mV vs SCE. Electrolyte: deoxygenated NaOH (1mol dm^{-3}).

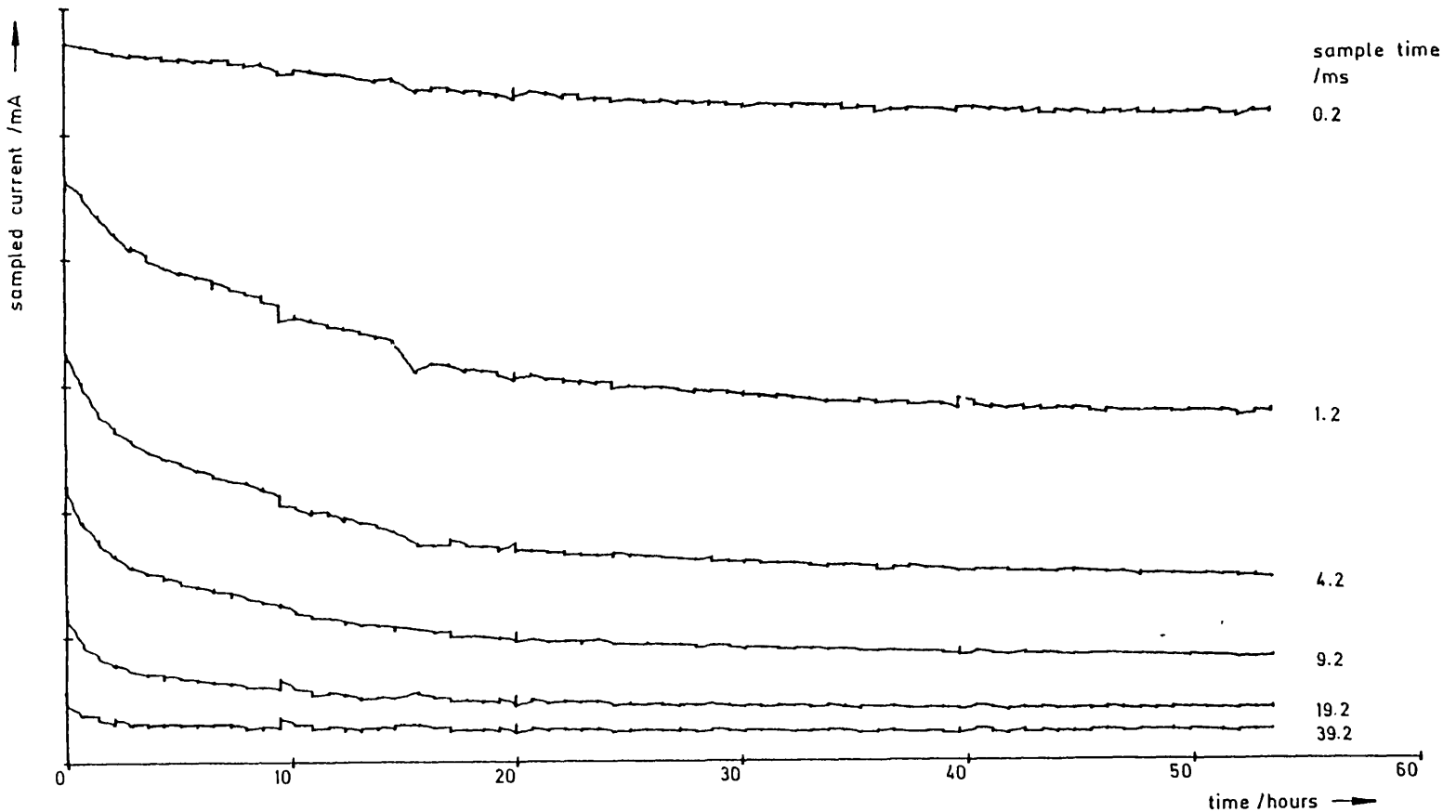

background component. Ultimately, however, the sensitivity of any such electrode would be determined by the contribution made by the residual currents. Thus, it would be beneficial to look for an electrode/electrolyte combination which gave the lowest possible background currents.

4.6 Linear Addition Model

A method of increasing the electrode sensitivity would be to separate the faradaic and capacitive components of the transient current. This could be done by using a microcomputer to analyse the complete transient rather than sampling the current at one point and throwing the rest of the information away.

If the faradaic and double layer charging currents are uncorrelated then the observed current is simply given by addition of the two;

$$i = i_f + i_{dl} \tag{4.16}$$

$$= c_\infty nFA(D/\pi t)^{\frac{1}{2}} + (\Delta V/R_u)\exp(-t/R_uC) \tag{4.17}$$

A transient which has been numerically simulated using this equation is shown in Fig.4.7.

Equation (4.17) can be manipulated to give the form;

$$it^{\frac{1}{2}} = c_\infty nFA(D/\pi)^{\frac{1}{2}} + t^{\frac{1}{2}}(\Delta V/R_u)\exp(-t/R_uC) \tag{4.18}$$

Thus, a plot of $it^{\frac{1}{2}}$ vs $t^{\frac{1}{2}}\exp(-t/R_uC)$ should be a straight line with

$$\text{slope} = \Delta V/R_u \tag{4.19}$$

$$\text{intercept} = c_\infty nFA(D/\pi)^{\frac{1}{2}} \tag{4.20}$$

Hence, the required concentration information could be extracted from the intercept of the $it^{\frac{1}{2}}$ plot.

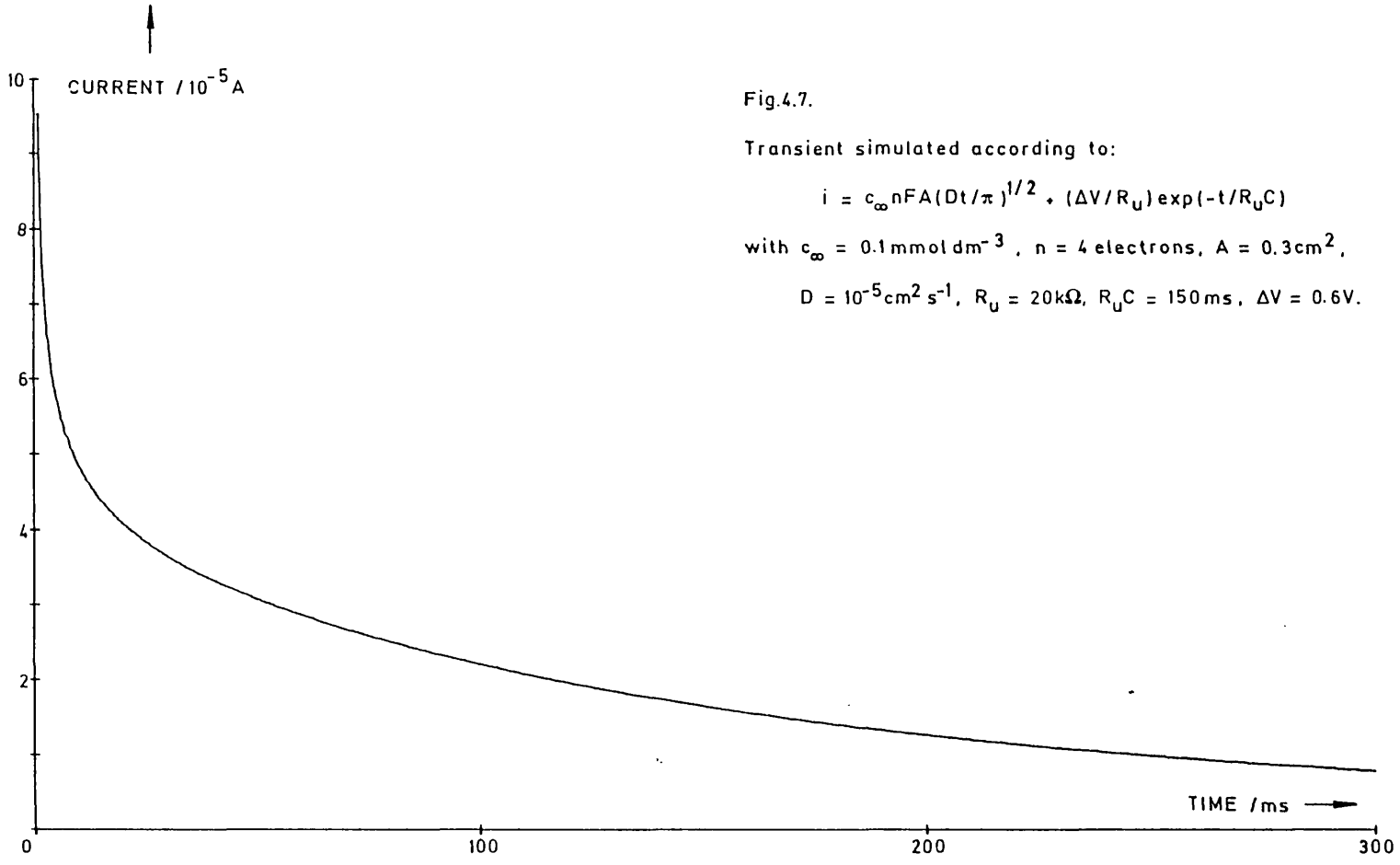

Fig.4.7.

Transient simulated according to:

$$i = c_\infty nFA(Dt/\pi)^{1/2} + (\Delta V/R_u)\exp(-t/R_uC)$$

with c_∞ = 0.1 mmol dm^{-3}, n = 4 electrons, A = 0.3 cm^2,

D = 10^{-5} cm^2 s^{-1}, R_u = 20 kΩ, R_uC = 150 ms, ΔV = 0.6 V.

4.6.1 Determination of the time constant

Time and current are easily measured quantities but it is also necessary to know the electrode time constant if the $it^{\frac{1}{2}}$ plot is to be used, as above. It is not possible to know the electrode time 'constant' a priori since it is liable to change.

Manipulation of (4.17) can yield many analytical solutions for the time constant in terms of the differential and/or integral currents. In practice, however, it is not possible to evaluate either the differentials or the integrals with sufficient accuracy. Thus, an alternative method for evaluating the time constant has to be found.

Fig.4.8 shows $it^{\frac{1}{2}}$ plots corresponding to the transient in Fig.4.7. In constructing the plots the time constant has been (a) underestimated, (b) made equal to the time constant used in simulating the original transient and (c) overestimated. Several points should be noted about these plots;

(i) as t increases, the points march out from the intercept, reach some point of maximum excursion then turn round and march back in again;

$$it^{\frac{1}{2}} \longrightarrow \text{intercept} \quad \text{as } t \longrightarrow 0, \qquad (4.21)$$

The intercept contains the desired concentration information, but neither of these two limits are liable to be useful in practice since at very short times the current information is unreliable - because of kinetic considerations - while at long times (4.17) no longer applies because diffusion in the membrane will have become important.

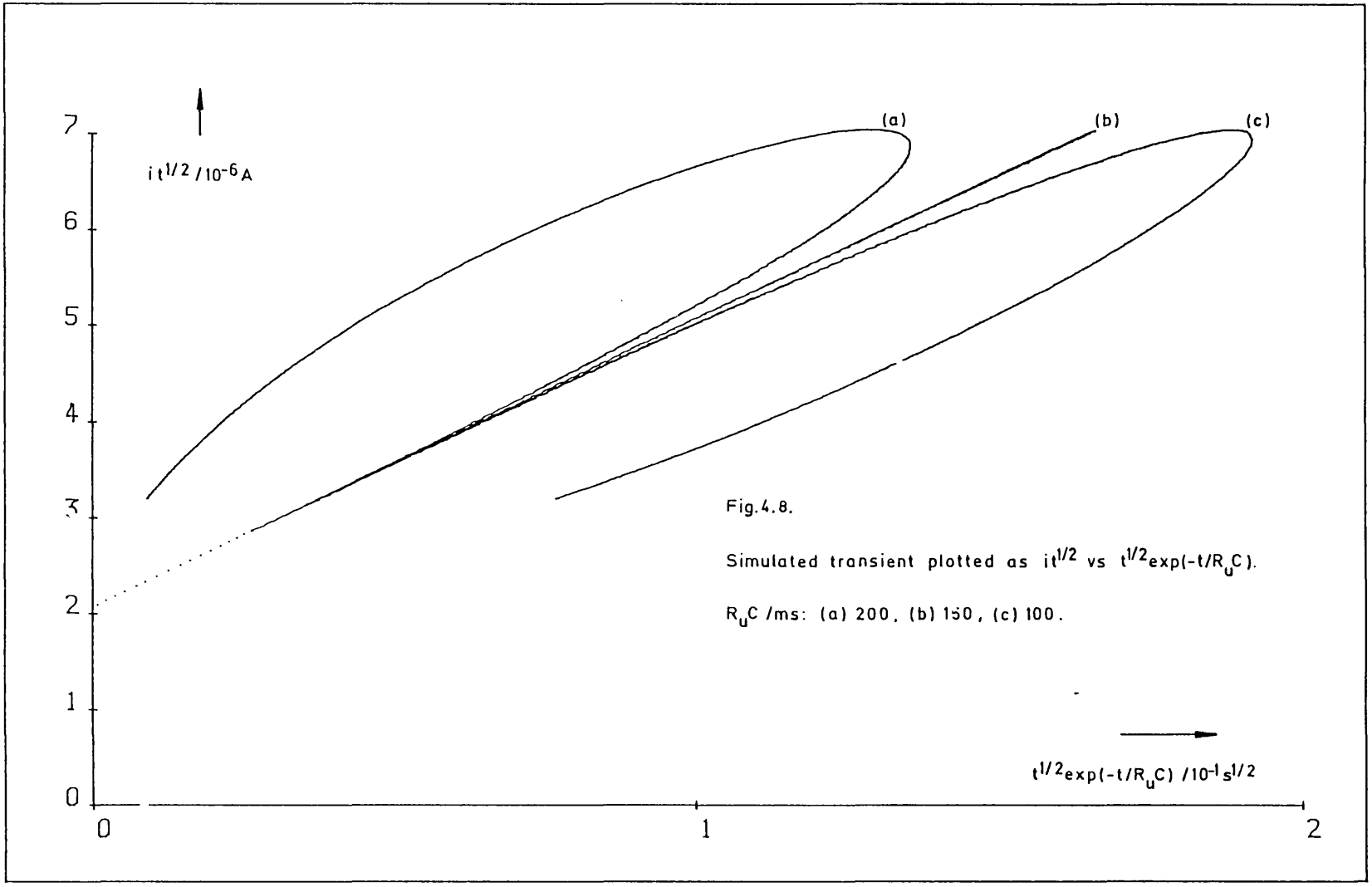

Fig.4.8.

Simulated transient plotted as $it^{1/2}$ vs $t^{1/2}exp(-t/R_uC)$.

R_uC /ms: (a) 200, (b) 150, (c) 100.

(ii) The shape of the $it^{\frac{1}{2}}$ plot is indicative of the proximity of the estimated time constant to the correct one. This feature can be used to determine an 'optimum' time constant for a real transient - a rough estimate can be used to initiate on iterative routine for locating the time constant which gives the best straight line.

4.6.2 Implementation of the $it^{\frac{1}{2}}$ analysis

A general purpose, membrane-covered sensor (Fig.2.2) was used to obtain the potential step transient shown in Fig.4.9. The corresponding $it^{\frac{1}{2}}$ plot is given in Fig.4.10. Linearity is good and least-mean-squares (LMS) analysis yields;

$$\text{slope} = (2.55 \pm 0.01)\times10^{-4}\ \text{A} \qquad (4.22)$$

$$\text{intercept} = (3.8 \pm 0.4)\times10^{-6}\ \text{As}^{\frac{1}{2}} \qquad (4.23)$$

The required concentration information lies in the intercept and the uncertainty in determining this value can be reduced by minimising the excursion of the experimental data from that point. In the absence of double-layer charging all of the points would lie at the intercept, but in a real system this is not the case. For the $it^{\frac{1}{2}}$ plot, the maximum excursion along the x-axis is when $t = R_uC/2$. Thus,

$$\text{max excursion on x-axis} = 0.428(R_uC)^{\frac{1}{2}} \qquad (4.24)$$

Knowing this and the slope of the line, then

$$\text{max excursion on y-axis} = 0.428\Delta V(C/R_u)^{\frac{1}{2}} \qquad (4.25)$$

Changing the uncompensated resistance has opposite effects on the two excursions. Thus, the precise effect on the determination of the intercept is

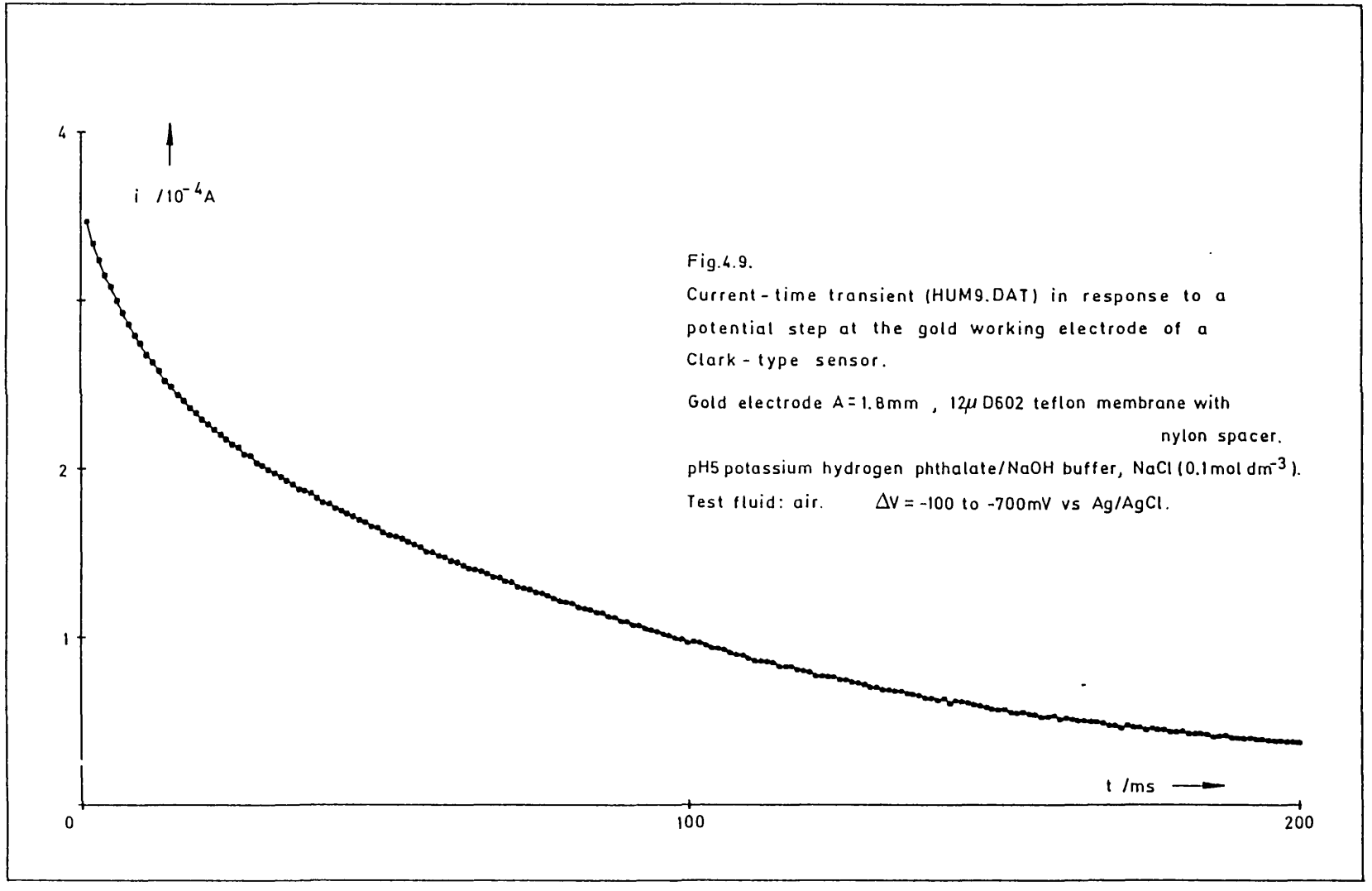

Fig.4.9.

Current-time transient (HUM9.DAT) in response to a potential step at the gold working electrode of a Clark-type sensor.

Gold electrode A = 1.8mm , 12μ D602 teflon membrane with nylon spacer.

pH5 potassium hydrogen phthalate/NaOH buffer, NaCl (0.1mol dm^{-3}).

Test fluid: air. ΔV = -100 to -700mV vs Ag/AgCl.

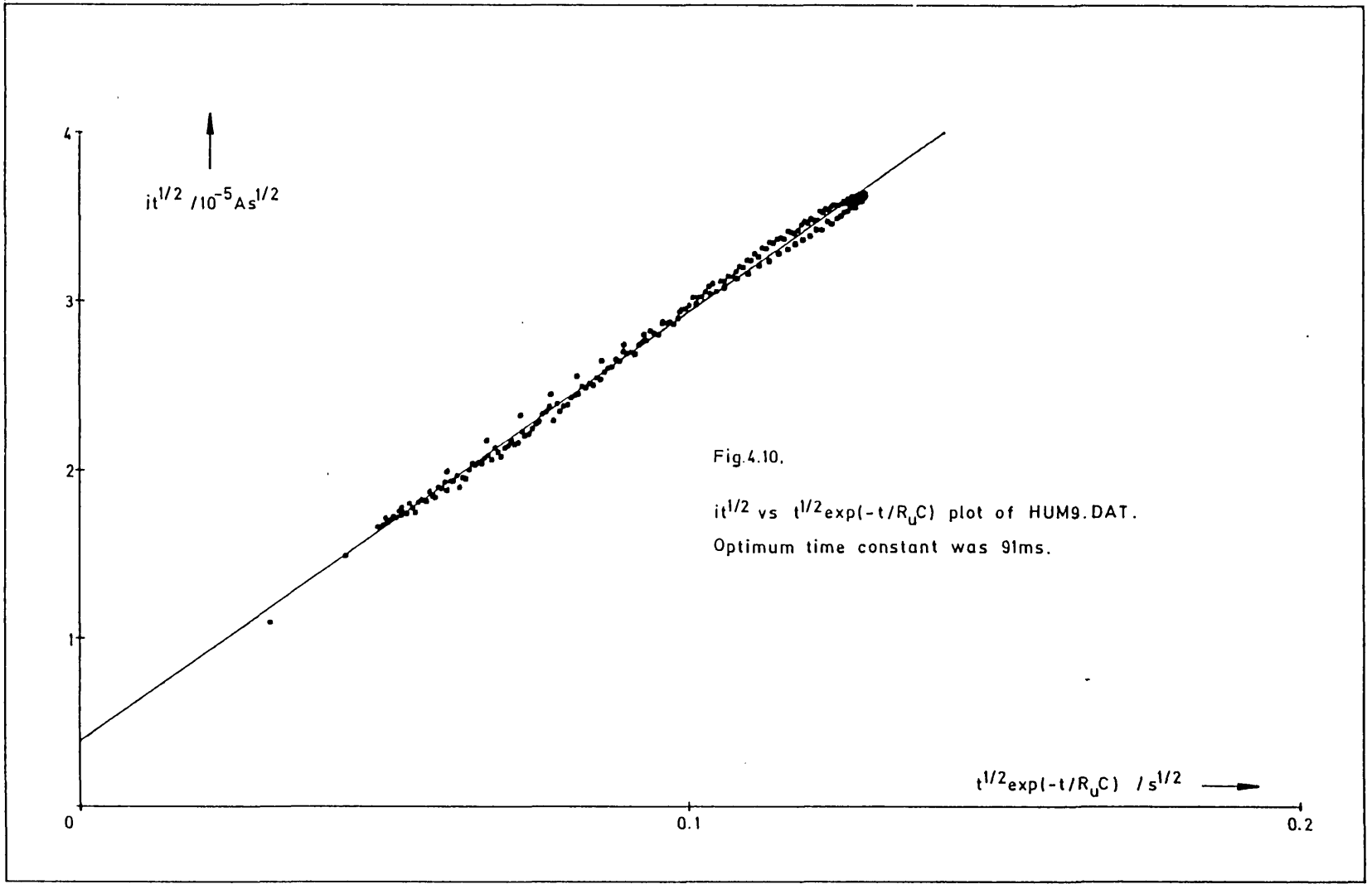

Fig.4.10.

$it^{1/2}$ vs $t^{1/2}exp(-t/R_uC)$ plot of HUM9.DAT.
Optimum time constant was 91ms.

unclear, but ultimately it must be a good idea to reduce the magnitude of R_u.

Minimising the electrode capacitance reduces the excursions along both axes. Now, C is proportional to the working electrode area. Thus, it would be beneficial to reduce the electrode radius. The Newman eqn.(4.15) says that this increases the uncompensated resistance, but in a membrane covered electrode this is not necessarily the case since the thin electrolyte layer normally determines R_u.

Two membrane-covered, microdisc electrodes were build to test the effect of electrode capacitance. The potential step transient in Fig.4.11 was obtained using the double-reference electrode, Fig.2.4. The corresponding $it^{\frac{1}{2}}$ plot is shown in Fig.4.12.

$$\text{slope} = (9.4 \pm 0.1)\times10^{-7}\ \text{A} \qquad (4.26)$$

$$\text{intercept} = (4.24 \pm 0.04)\times10^{-8}\ \text{As}^{\frac{1}{2}} \qquad (4.27)$$

Comparison with the previous results shows that the microdisc does have a beneficial effect on the uncertainty in determining the $it^{\frac{1}{2}}$ intercept and this, in turn, will have a beneficial effect on the sensitivity of such a sensor.

Microelectrodes, by their very nature, produce much smaller currents than their macro counterparts but this effect can be overcome, to some extent, by using arrays of microelectrodes[53,94,95].

A stationary disc electrode, with an external 1k resistor was used to measure the effect of oxygen concentration on the magnitude of the $it^{\frac{1}{2}}$

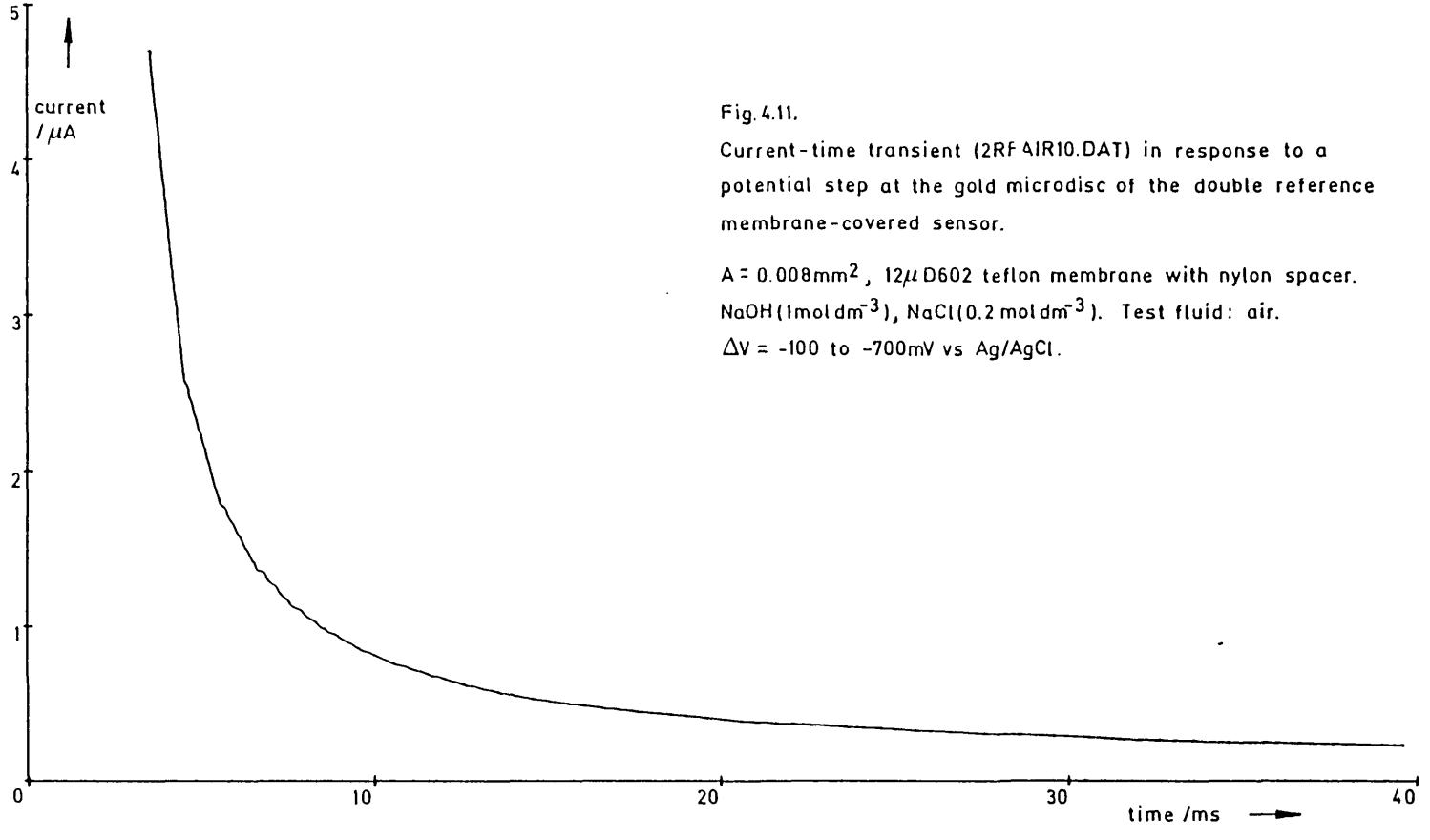

Fig. 4.11.

Current-time transient (2RFAIR10.DAT) in response to a potential step at the gold microdisc of the double reference membrane-covered sensor.

A = 0.008mm^2, 12μ D602 teflon membrane with nylon spacer. NaOH(1mol dm^{-3}), NaCl(0.2 mol dm^{-3}). Test fluid: air. ΔV = -100 to -700mV vs Ag/AgCl.

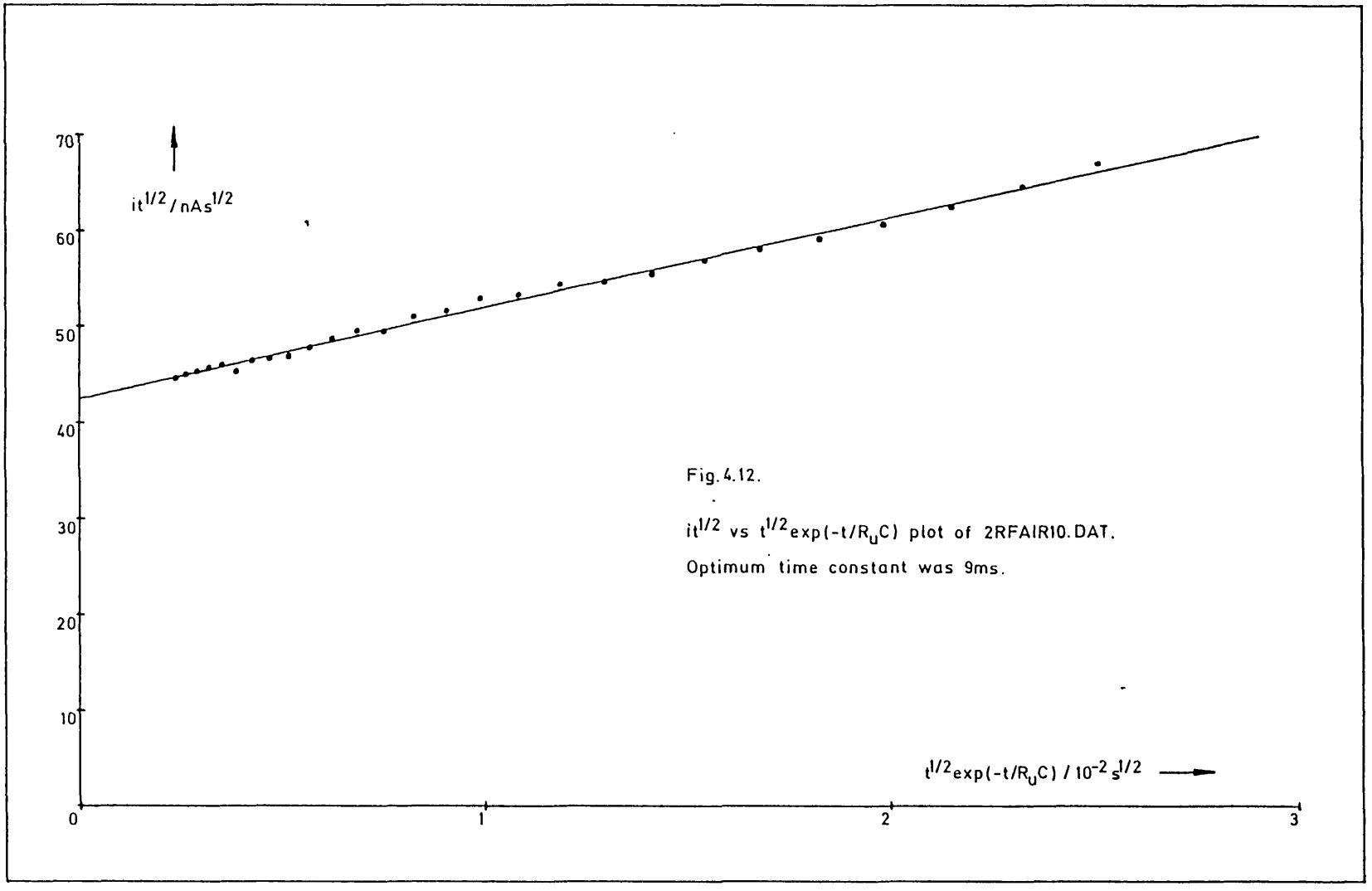

Fig. 4.12.

$it^{1/2}$ vs $t^{1/2}exp(-t/R_uC)$ plot of 2RFAIR10.DAT.

Optimum time constant was 9ms.

intercept. Fig.4.13 shows that there is a linear relationship with oxygen concentration, as would be expected from (4.21), but there is a significant intercept even in the absence of oxygen;

$$\text{slope} = (2.96 \pm 0.02)\times10^{-7}\ As^{\frac{1}{2}}(vol\%)^{-1} \qquad (4.28)$$

$$\text{intercept} = (4.8 \pm 0.2)\times10^{-6}\ As^{\frac{1}{2}} \qquad (4.29)$$

These results show that $it^{\frac{1}{2}}$ plots can be used to extract concentration information from fast potential step transients, but the electrode sensitivity is again limited by the magnitude of the transient currents in the absence of oxygen.

4.7 Induced Charging Model

The linear addition model assumed that there was no interaction between the faradaic and double layer charging currents. Examination of the effect of injecting current across the double layer, Fig.4.14, shows that this is not the case.

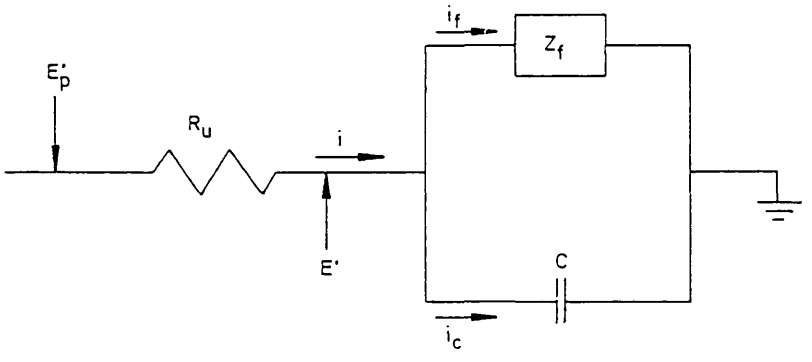

Fig.4.14. Resistor-capacitor analogue of a simple faradaic system.

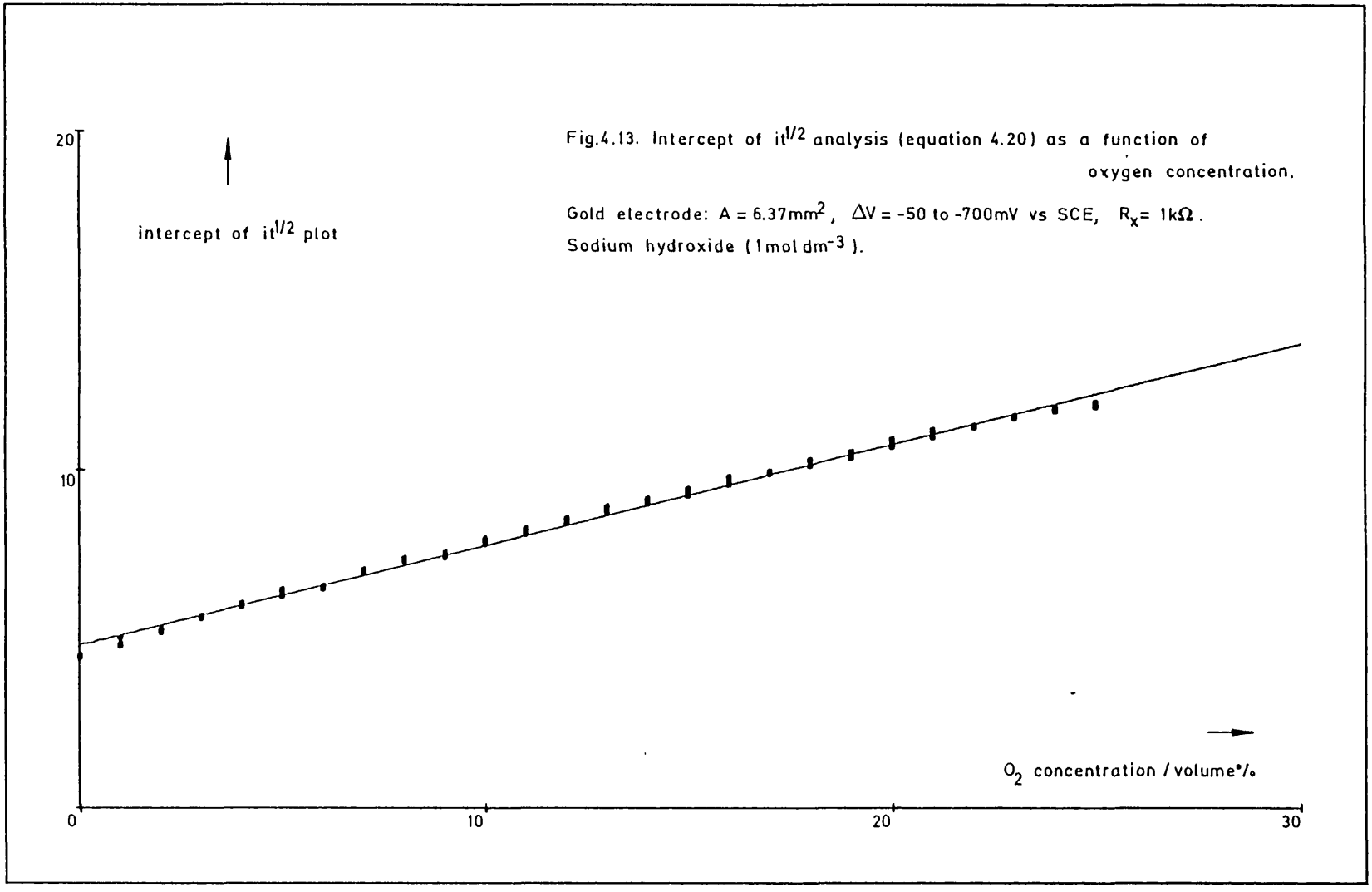

Fig.4.13. Intercept of $it^{1/2}$ analysis (equation 4.20) as a function of oxygen concentration.

Gold electrode: A = 6.37mm^2, ΔV = -50 to -700mV vs SCE, R_x = 1kΩ.
Sodium hydroxide (1mol dm^{-3}).

Z_f is the faradaic impedence, E_p' is the reference electrode potential, E' is the potential at the working electrode interface, i is the total current flowing, i_c is the charging current.

As before, the total current flowing in the electrolyte is given by the sum of the faradaic and charging currents.

$$i = i_f + i_c \qquad (4.30)$$

but the charging current is now given by

$$i_c = CdE/dt \qquad (4.31)$$

$$= -R_u C di/dt \qquad (4.32)$$

$$= -R_u C d(i_f + i_c)/dt \qquad (4.33)$$

Thus, the charging current is not independent of the faradaic reaction since it includes a component due to the changing faradaic current across the uncompensated resistance[96-98].

4.7.1 Faradaic current

Faradaic current, which contains conentration information, can be evaluated empirically;

$$i_f = i - i_c \qquad (4.34)$$

$$= i + R_u C di/dt \qquad (4.35)$$

Perone et al. have used this relationship to correct observed data for the effects of charging currents[97,98]. Time constants were evaluated using a potential step in background electrolyte while derivative currents were calculated using the Savitzky-Golay technique[99]. Data treated in

this manner was found to conform quite closely to Cottrell behaviour, but further improvement was made if a computer based iterative technique was used to calculate an 'effective' time constant[100].

Perone's work was primarily concerned with photoinitiated transients under potentiostatic conditions. However, similar techniques can be used to investigate the effects of induced charging currents on potential step transients for dissolved oxygen measurement. Treated data was plotted as $it^{\frac{1}{2}}$ vs t, Fig.4.15, and the intercepts of many such plots are collected together in Fig.4.16. Several points should be noted;

(i) the reasonably linear $it^{\frac{1}{2}}$ vs t fit shows that the faradaic current can be approximated to Cottrell behaviour. In this case the intercept of such a plot is given by;

$$\text{intercept} = c_{\infty} nFA(D/\pi)^{\frac{1}{2}} \qquad (4.36)$$

(ii) as expected from (4.36) there is a linear relationship between intercept and bulk oxygen concentration.

$$\text{slope} = (3.78 \pm 0.01)\times10^{-8}\ As^{\frac{1}{2}}(vol\%)^{-1} \qquad (4.37)$$

(iii) there is a significant amount of current even in the absence of oxygen;

$$\text{intercept} = (4.7 \pm 0.1)*10^{-7}\ As^{\frac{1}{2}} \qquad (4.38)$$

The magnitude of this intercept will limit the utility of this technique. For maximum sensitivity an electrode/elecrolyte combination, which gives rise to very small background currents, has to be found.

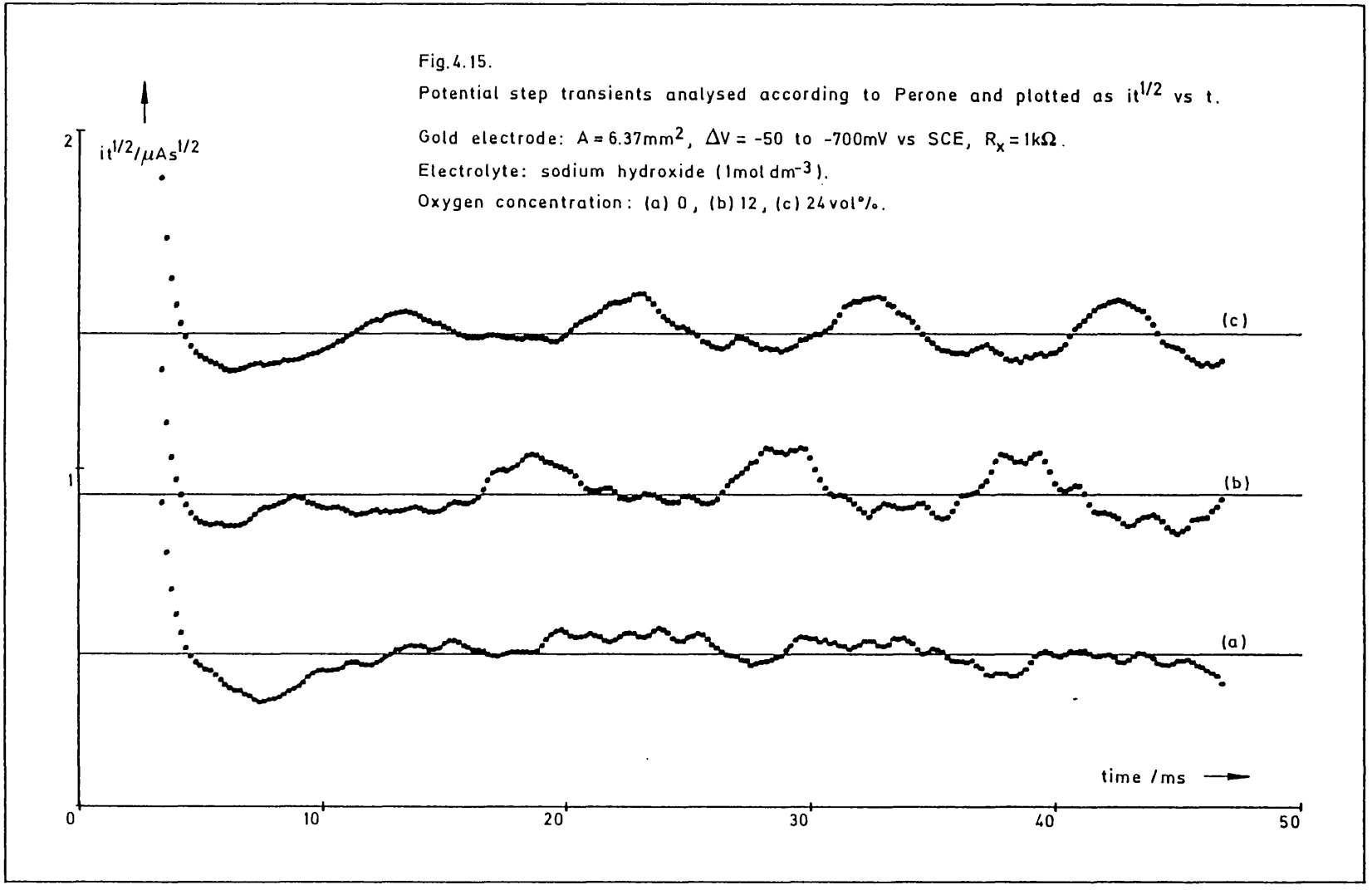

Fig. 4.15.

Potential step transients analysed according to Perone and plotted as $it^{1/2}$ vs t.

Gold electrode: $A = 6.37 mm^2$, $\Delta V = -50$ to $-700 mV$ vs SCE, $R_x = 1 k\Omega$.

Electrolyte: sodium hydroxide ($1 mol\, dm^{-3}$).

Oxygen concentration: (a) 0, (b) 12, (c) 24 vol%.

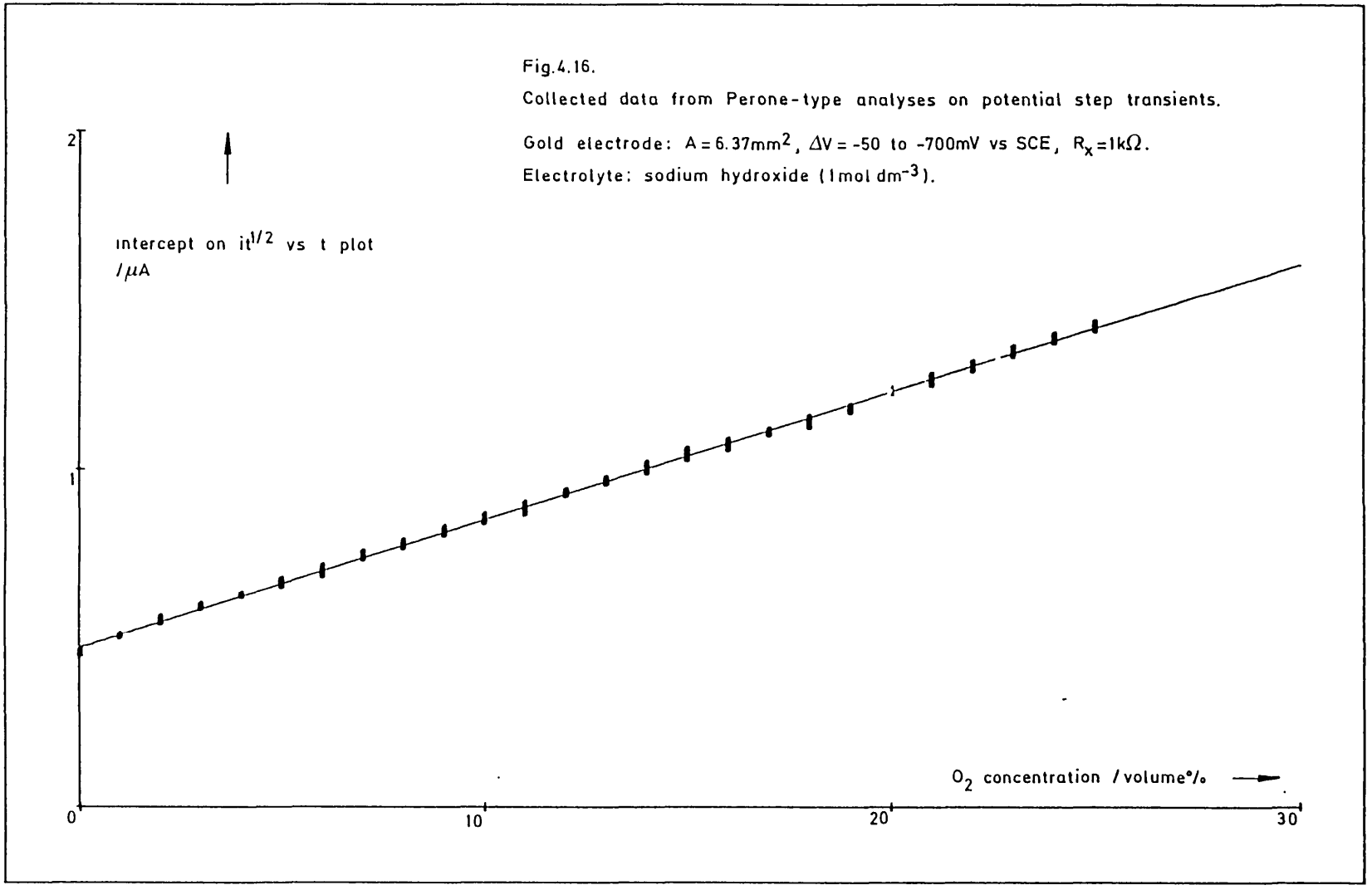

Fig.4.16.

Collected data from Perone-type analyses on potential step transients.

Gold electrode: $A = 6.37 mm^2$, $\Delta V = -50$ to $-700 mV$ vs SCE, $R_x = 1 k\Omega$.

Electrolyte: sodium hydroxide ($1 mol\ dm^{-3}$).

(iv) in the above results the faradaic current could be approximated to Cottrell behaviour, but in many cases this will not be possible, e.g. if the time constant is large then a potential step at the reference electrode will not appear as a potential step at the working electrode and on this time scale the faradaic current will not be described by the Cottrell equation. Membrane-covered electrodes can have very long time constants - thus, it is important to derive a more general relationship between observed current and bulk concentration.

4.7.2 Analysis of the induced charging model

Application of Kirchoff's law to the circuit in Fig.4.14 gives

$$E_p' - E' = (i_c + i_f)R_u \qquad (4.39)$$

The capacative current is given by (4.31) while the faradaic current is given by

$$i_f = c_o nFAk_o' \exp[\alpha(E'-E_o)F/RT] \qquad (4.40)$$

where c_o is the concentration of electroactive species at the electrode interface and E_o is a formal electrode potential.

From Fick's first law, the faradaic current must also be given by

$$i_f = nFAD(dc/dx)_o \qquad (4.41)$$

where x is the distance normal to the electrode interface.

Current can be normalised with respect to i_R where

$$i_R = E_p'/R_u \qquad (4.42)$$

and time can be normalised with respect to the electrode time constant. Hence,

$$T = t/R_u C \tag{4.43}$$

$$I_f' = i_f/i_R \tag{4.44}$$

and $$I_c' = i_c/i_R \tag{4.45}$$

In addition, a normalised potential is defined as

$$\theta' = E'/E_p' \tag{4.46}$$

Substituting these relationships into (4.39) yields

$$1 - \theta' = I_c' + I_f' \tag{4.47}$$

the capacitive current can be re-expressed as

$$I_c' = (CdE/dt)/(E_p'/R_u) \tag{4.48}$$

$$= d\theta'/dT \tag{4.49}$$

and this can be used in (4.47) to give

$$1 - \theta' = d\theta'/dT' - I_f' \tag{4.50}$$

and $$I_f' = (1 - \theta') + d(1 - \theta')/dT' \tag{4.51}$$

$$= \exp(-T').\ d[(1 - \theta')\exp(T')]/dT' \tag{4.52}$$

Rearrangement of this last equation gives

$$d[(1 - \theta')\exp(T')] = I_f'\exp(T')dT' \tag{4.53}$$

Integration yields

$$(1 - \theta')\exp(T') = 1 - \int_0^{T'} I_f\exp(T')dT' \tag{4.54}$$

Thus,

$$\theta' = 1 - \exp(-T') - \exp(-T')\int_0^{T'} I_f' \exp(T')\,dT' \tag{4.56}$$

Now, the current flowing will be mostly capacitive until the electrode interface is sufficiently charged to switch 'on' the faradaic current. Thus, at small T',

$$\theta' \simeq 1 - \exp(-T') \tag{4.57}$$

and $$I_c' \simeq \exp(-T') \tag{4.58}$$

This part of the transient is relatively boring and can be put to one side by shifting the theta and time axes closer to where the faradaic current switches on. Thus,

$$T = T' - T_* \tag{4.59}$$

and $$\theta = (E' - E_*)/(E_p' - E_*) \tag{4.60}$$

where T_* is the time and E_* the potential close to the switch. The currents can be renormalised on this theta scale. Thus,

$$E_p = E_p' - E_* \tag{4.61}$$

and $$I = I'E_p'/E_p \tag{4.62}$$

In addition, it can also be shown that

$$\theta' = (E_p\theta + E_*)/E_p' \tag{4.63}$$

$$d\theta' = (E_p/E_p')\,d\theta \tag{4.64}$$

$$dT' = dT \tag{4.65}$$

and $I'_f = (E_p/E'_p)I_f$ (4.66)

These relationships can be substituted into (4.47) to yield

$$1 - \theta = d\theta/dT + I_f \quad (4.67)$$

Thus, it can be seen that the shifting axes have no effect on the form of the relationship.

4.7.3 Faradaic current and concentration polarisation

Fick's second law may be written in terms of normalised time as

$$dc/dT = DR_uC.d^2c/dx^2 \quad (4.68)$$

Let the dimensionless parameters X and u be defined as

$$X = x(DR_uC)^{\frac{1}{2}} \quad (4.69)$$

$$u = (c_\infty - c)/c_\infty \quad (4.70)$$

Then,

$$du/dT = d^2u/dX^2 \quad (4.71)$$

while from (4.40) and (4.41);

$$I_f = nFAk'_oc_\infty(1 - u_o)\exp(\theta P)/i_R \quad (4.72)$$

$$= -nFA(D/R_uC)^{\frac{1}{2}}(c_\infty/i_R)(du/dx)_o \quad (4.73)$$

where

$$P = \alpha E_pF/RT \quad (4.74)$$

There are two factors which may be written as currents;

$$i_k = nFAk'_o c_\infty \tag{4.75}$$

and $$i_D = nFA(D/R_u C)^{\frac{1}{2}} c_\infty \tag{4.76}$$

Thus, the faradaic current may be written as;

$$I_f = (i_k/i_R)(1 - u_o)\exp(\theta P) \tag{4.77}$$

An expression for the surface concentration, u_o, can be found from (4.71). In Laplace space

$$s\bar{u} = d^2\bar{u}/dX^2 \tag{4.78}$$

A solution to this equation is

$$\bar{u} = \bar{u}_o \exp(-s^{\frac{1}{2}}X) \tag{4.79}$$

Differentiation and rearrangement yields;

$$\bar{u}_o = -s^{-\frac{1}{2}}(d\bar{u}/dX)_o \tag{4.80}$$

The convolution theorem gives the inverse transformation which describes the concentration polarisation;

$$u_o = \int_o^T - (du/dX)_o [\pi(T - T")]^{-\frac{1}{2}} dT" \tag{4.81}$$

The differential can be substituted using (4.73). Thus,

$$u_o = (i_R/i_D)\int_o^T I_f (T - T")^{-\frac{1}{2}} dT" . \pi^{-1/2} \tag{4.82}$$

Substituting this result into (4.77) yields

$$I_f(i_R/i_k)\exp(\theta P) + (i_R/i_D)\pi^{-\frac{1}{2}}\int_o^T I_f (T - T")^{-\frac{1}{2}} dT" = 1 \tag{4.83}$$

It is difficult to find a general solution to this equation, but there are two convenient cases which may be considered:

(i) $i_R < i_D$, in this case the current flowing in the cell is limited by the potential drop across the uncompensated resistance,

(ii) $i_R > i_D$, in this case the faradaic current is limited only by the diffusion controlled current.

4.8 Case 1. Bounded faradaic current

In this case the faradaic current is limited by the potential drop across the uncompensated resistance

$$i_k \longrightarrow i_R \tag{4.84}$$

and (4.83) may be written as

$$I_f \exp(-\theta P) + R_i \pi^{-\frac{1}{2}} \int_0^T I_f (T - T'')^{-1/2} dT'' = 1 \tag{4.85}$$

where

$$R_i = i_R / i_D < 1 \tag{4.86}$$

Rearrangement and integration by parts yields

$$I_f \exp(-\theta P) = 1 - 2R_i \pi^{-\frac{1}{2}} [I_f T^{-\frac{1}{2}} + \int_0^T (T-T'')^{1/2} (dI_f/dT'') dT''] \tag{4.87}$$

or

$$I_f = \frac{1 - 2R_i \pi^{-\frac{1}{2}} \int_0^T (T-T'')^{1/2} (dI_f/dT'') dT''}{\exp(-\theta P) + 2R_i (T/\pi)^{\frac{1}{2}}} \tag{4.88}$$

The integral can be solved numerically - if the interval between 0 and T is divided into n equal steps of width δT, and the faradaic current at step m is denoted by $(I_f)_m$, then,

(i) $n = 0$, integral $= 0$ (4.89)

(ii) $n = 1$,
integral $\simeq (\delta T)^{\frac{1}{2}}[(I_f)_1 - (I_f)_o]$ (4.90)

(iii) $n \geqslant 2$,
integral $\simeq (\delta T/4)^{\frac{1}{2}}\, n^{\frac{1}{2}}[(I_f)_1 - (I_f)_o] +$

$$(n-m)\sum_{m=1}^{m=n-1}[(I_f)_{m+1} - (I_f)_{m-1}] \qquad (4.91)$$

These are important relationships but first it is necessary to obtain an expression for $\delta\theta$ in terms of δT;

$$1 - \theta = d\theta/dT + I_f \qquad (4.92)$$

$$\delta\theta/\delta T \simeq d\theta/dT = 1 - \theta - I_f \qquad (4.93)$$

Thus,

$$\delta\theta \simeq \delta T\,[1 - \theta - I_f] \qquad (4.94)$$

and,

$$\theta_{T+\delta T} \simeq \theta_T + \delta T\,[1 - \theta_T - I_f] \qquad (4.95)$$

It is now possible to calculate the faradaic current as a function of time. Starting with a given value of δT and with $T = 0$, $\theta = 0$, $I_f = 1$, then (4.95) can be used to evaluate the next value of θ. This can then be inserted into (4.88) and the corresponding value of I_f calculated. This can be inserted back into (4.95) so as to repeat the process, as required. Care has to be taken to choose a sufficiently small δT otherwise the result oscillates wildly.

In addition, it is possible to shift the time-theta axes closer to the start of the potential jump. At short times

$$I_f \simeq [\exp(-\theta P) + 2R_i(T/\pi)^{\frac{1}{2}}]^{-1} \qquad (4.96)$$

and the origin may be chosen such that $0<I_{f,o}<1$ and

$$I_f = \frac{1 - 2R_i\pi^{-\frac{1}{2}}\int_o^T (T-T")^{+\frac{1}{2}} (dI_f/dT")dT"}{Q\exp(-\theta P) + 2R_i(T/\pi)^{\frac{1}{2}}} \qquad (4.97)$$

and Q is a number determined by the relationship

$$I_{f,o} = 1/Q \qquad (4.98)$$

A simulated transient is shown in Fig.4.17. The total current was calculated as $1 - \theta$ and the capacitive current was calculated as the difference between the total and faradaic currents. For comparison, an experimental transient is shown in Fig.4.18.

It can be seen that there has to be some charging of the double layer before the faradaic reaction switches on. Then the charging current switches off while the surface concentration, c_o, is titrated at essentially constant potential. When c_o reaches zero the faradaic current falls away and charging can resume.

4.8.1 Surface and bulk concentrations

The surface concentration of electroactive species can be calculated from the relationship

$$u_o = 1 - I_f Q\exp(-\theta P) \qquad (4.99)$$

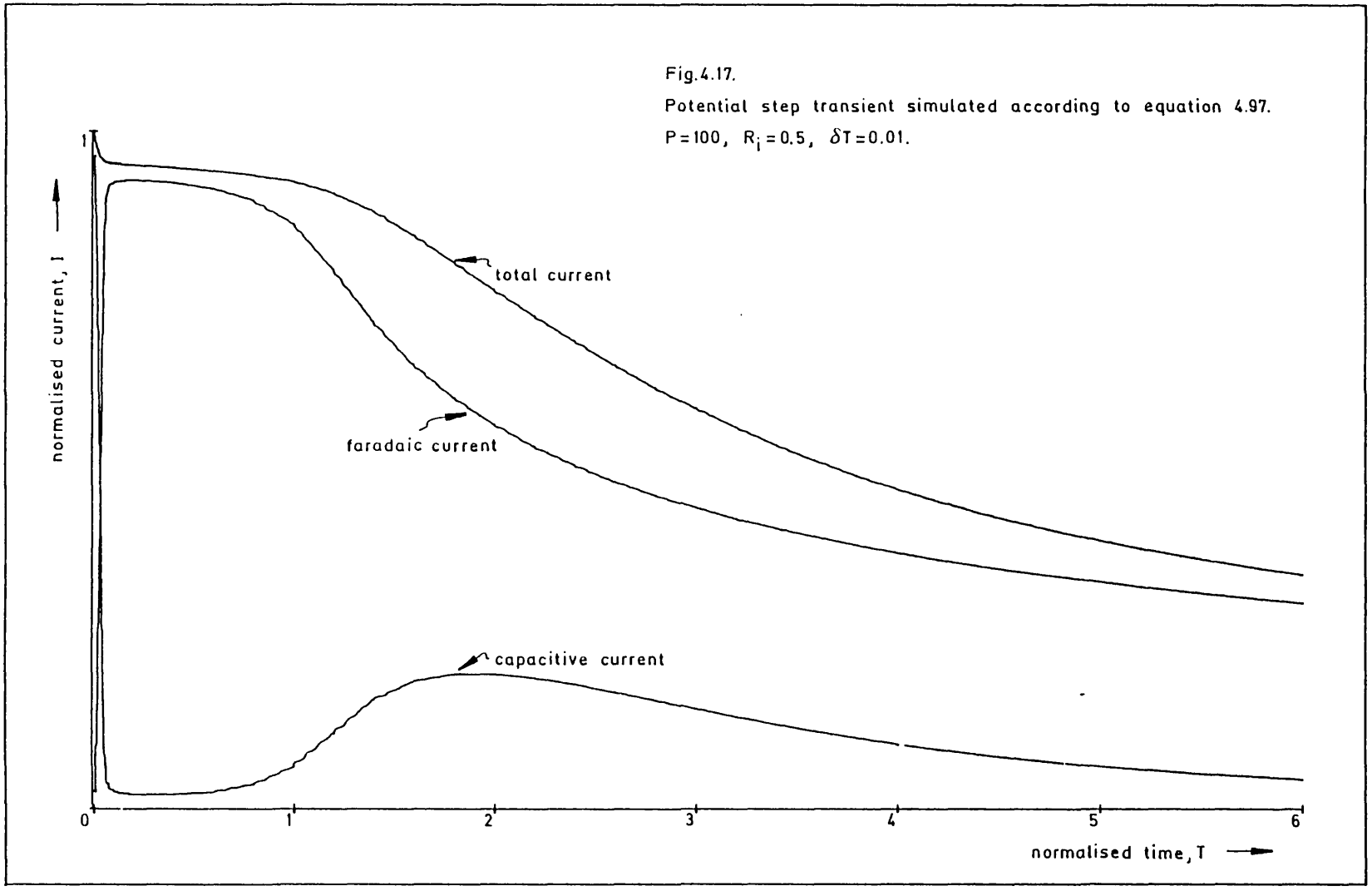

Fig.4.17.
Potential step transient simulated according to equation 4.97.
$P = 100$, $R_i = 0.5$, $\delta T = 0.01$.

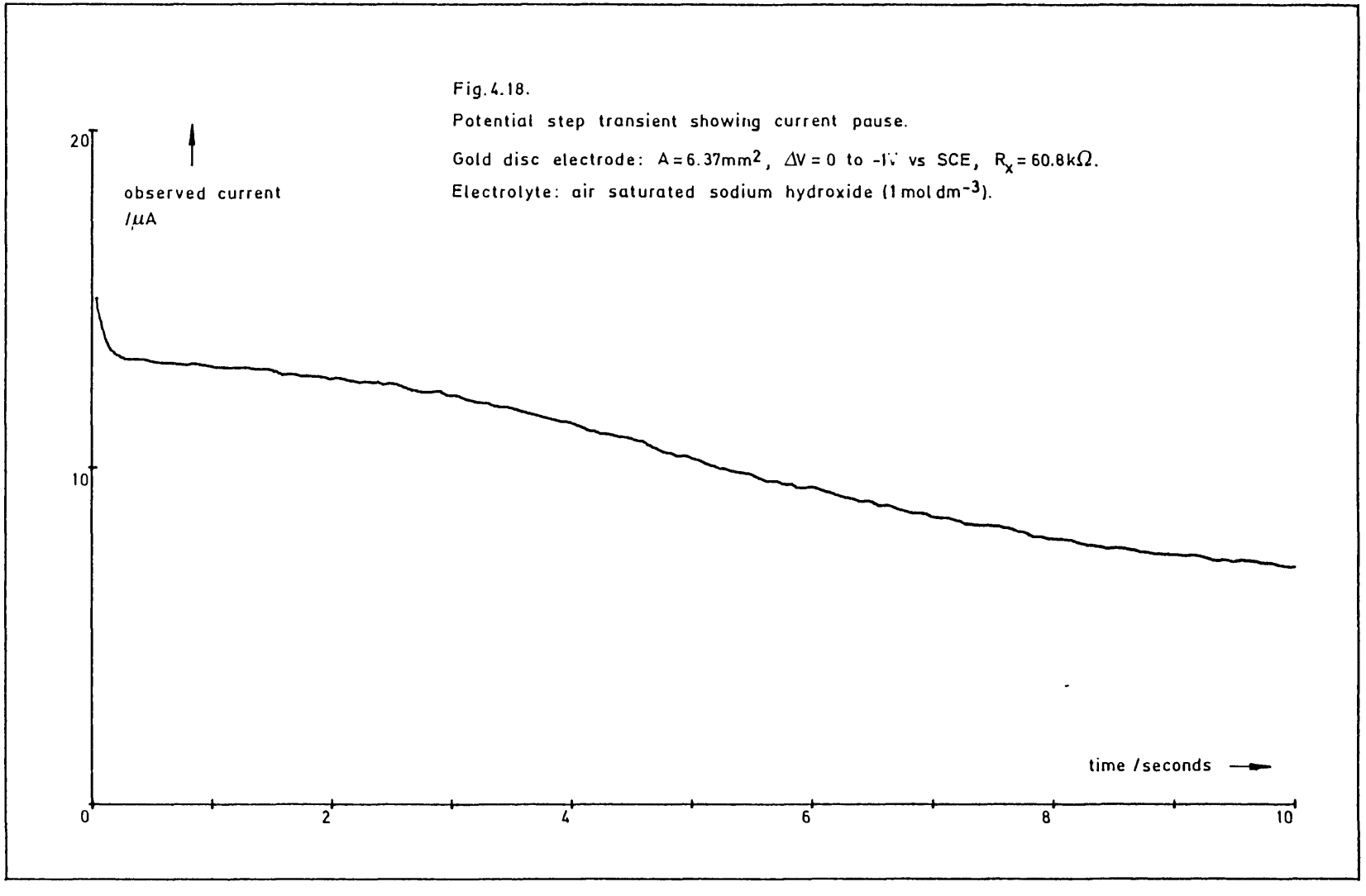

Fig. 4.18.

Potential step transient showing current pause.

Gold disc electrode: $A = 6.37 mm^2$, $\Delta V = 0$ to -1V vs SCE, $R_x = 60.8 k\Omega$.

Electrolyte: air saturated sodium hydroxide ($1 mol\ dm^{-3}$).

which is derived from (4.77) with appropriate modification.

The bulk concentration, c_∞, is inversely proportional to R_i. The effect of pushing up the concentration is shown in Fig.4.19. The duration of the current pause is increased and it is possible to show[101] that the transition time, t_2, is given by

$$t_2 = (D\pi/4)(c_\infty nFAR_u/E_p)^2 \qquad (4.100)$$

i.e. t_2 increases with the square of the concentration and also with the square of the uncompensated resistance, Fig.4.20. Thus, if the transition time could be determined it would provide a sensitive technique for measuring concentration.

4.8.2 Sand equation

Those familiar with controlled current techniques will recognise (4.100) as equivalent to the Sand equation[102];

$$it_2^{\frac{1}{2}} = 0.5c_\infty nFA(D\pi)^{\frac{1}{2}} \qquad (4.101)$$

This is not surprising since the latter describes a surface titration with controlled current, while, in the case of the membrane electrode, the faradaic switch fixes the potential across the uncompensated resistance and the faradaic current is effectively galvanostatted until the surface concentration is close to zero.

Controlled current electrolysis and bounded faradaic titration are both techniques whose analytical utility is limited by the accuracy with which the transition time can be determined. A collection of transients at different oxygen con-

Fig.4.19. Simulated effect of increasing concentration of electroactive species.

P = 100, R_i = (a) 1.0, (b) 0.9, (c) 0.8, (d) 0.7, (e) 0.6, (f) 0.5, (g) 0.4, (h) 0.3, (i) 0.2 .

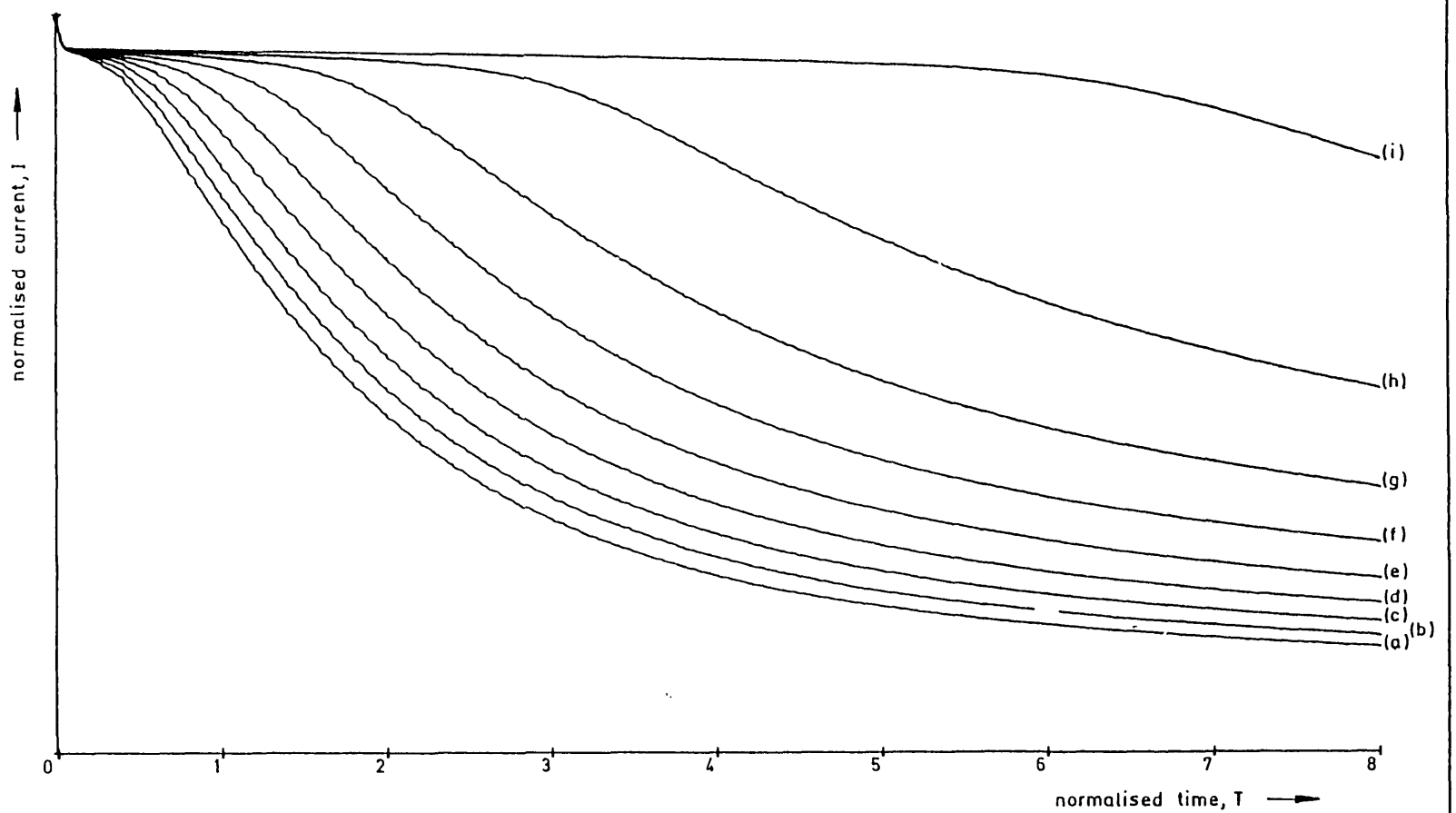

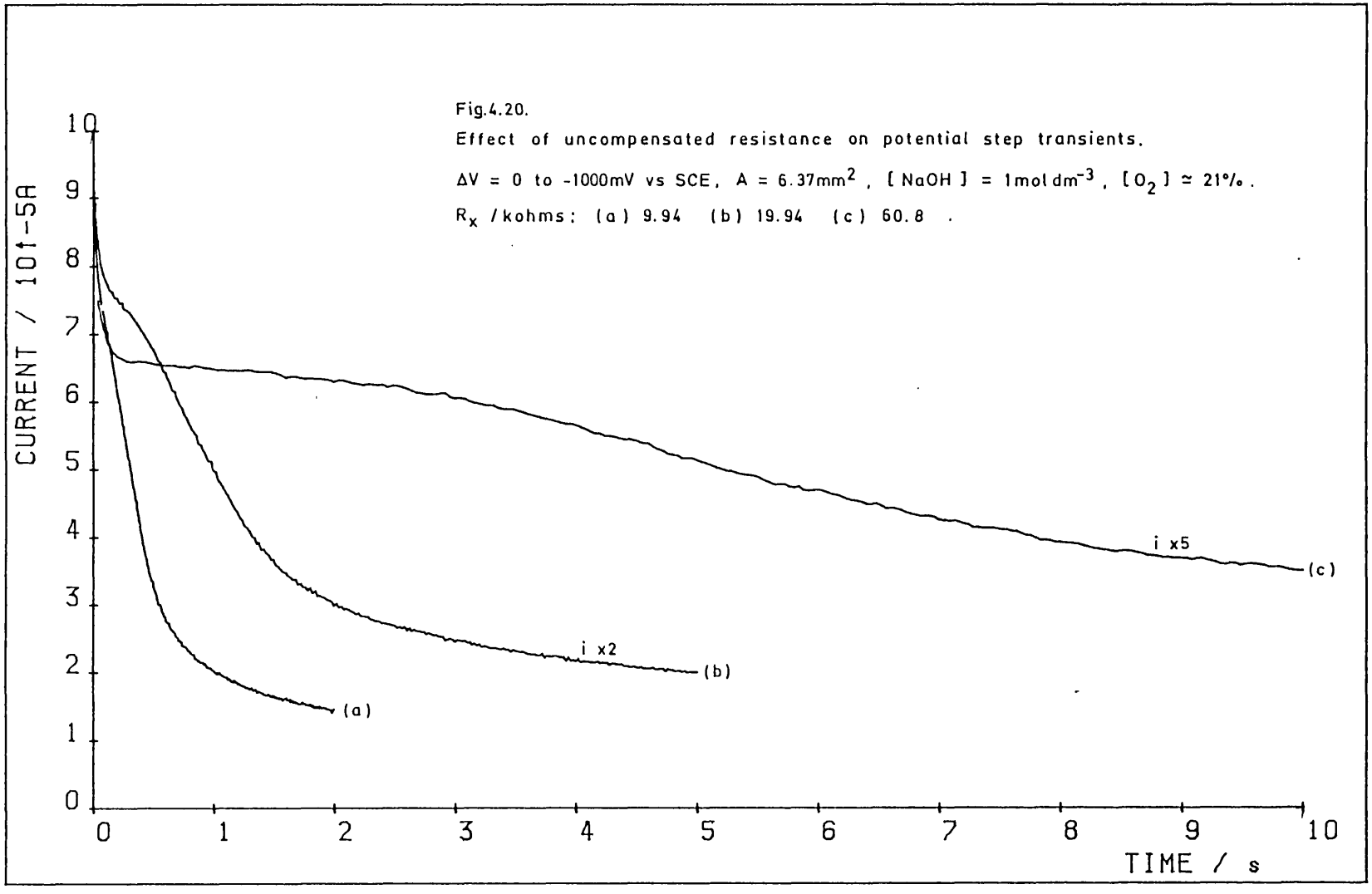

Fig.4.20.
Effect of uncompensated resistance on potential step transients.
ΔV = 0 to -1000mV vs SCE, A = 6.37mm^2, [NaOH] = 1mol dm^{-3}, [O_2] ≃ 21%.
R_x /kohms: (a) 9.94 (b) 19.94 (c) 60.8 .

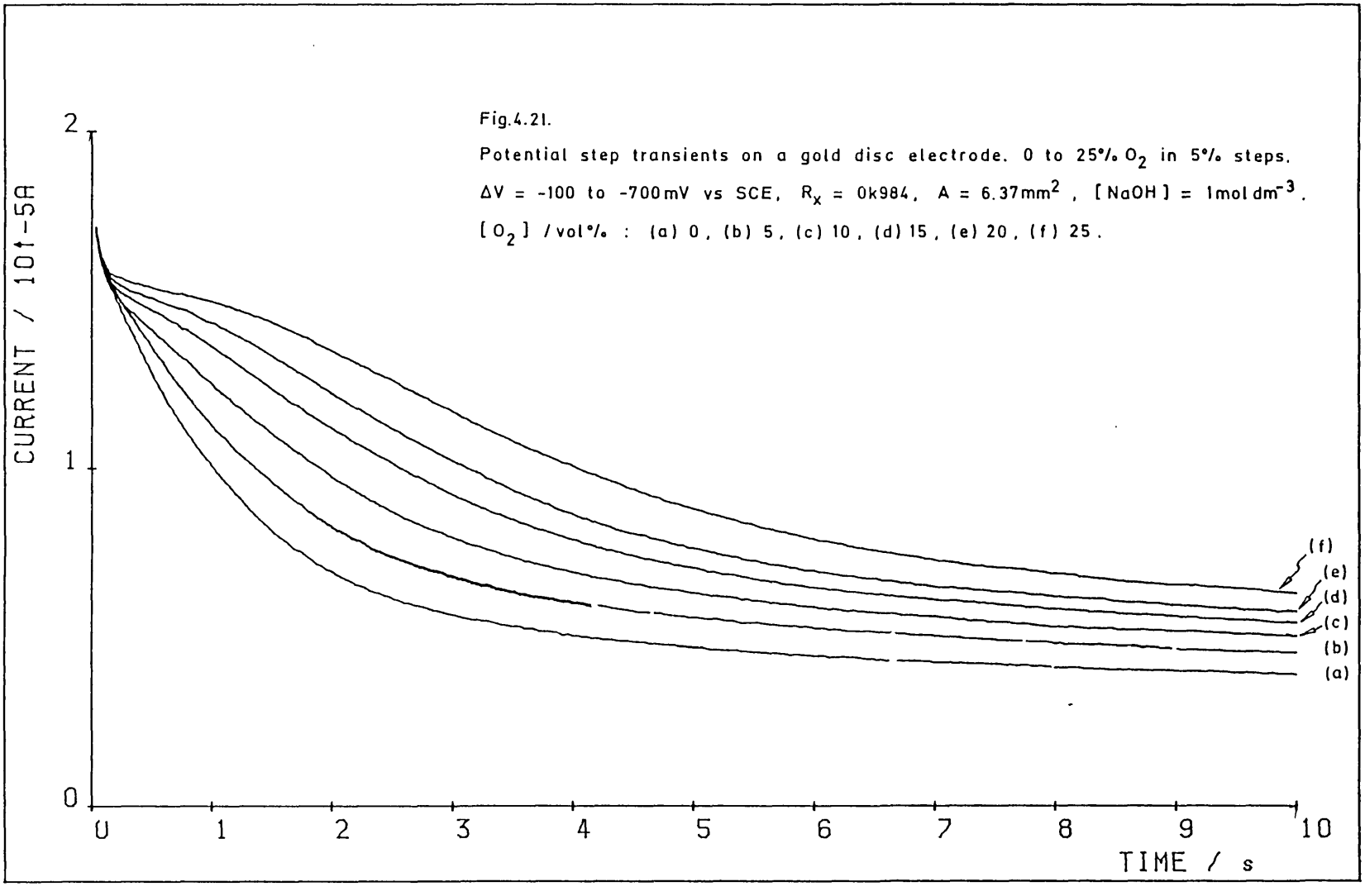

Fig.4.21.

Potential step transients on a gold disc electrode. 0 to 25% O_2 in 5% steps.

ΔV = -100 to -700 mV vs SCE, R_x = 0k984, A = 6.37 mm^2, [NaOH] = 1 mol dm^{-3}.

[O_2] / vol% : (a) 0, (b) 5, (c) 10, (d) 15, (e) 20, (f) 25.

centrations is shown in Fig.4.21. At low concentrations, the requirement $R_i>1$ is not satisfied and there is little or no current transition. However, even at the higher concentrations there is a major problem in determining where the transition period begins and ends - this is partly due to the nature of the oxygen reduction reaction (section 4.8.5). In addition, the shape of the transient in the background electrolyte shows that the current is not purely capacitive - there is a faradaic component which is due to surface reactions.

4.8.3 Surface reactions

Fig.4.22 shows a voltammogram on gold in deoxygenated sodium hydroxide (1 mol dm^{-3}). The peak at ca. +100mV is due to hydroxide desorption[103];

$$Au(OH)_{ads} \rightleftharpoons Au + OH^- \qquad (4.102)$$

A series of potential step transients across this peak were recorded, Fig.4.23. The shape of the current transients is that which would be expected from bounded faradaic titrations and the quantities of charge are considerable. Hydroxide desorption, however, is unlikely to be the particular process which gives rise to the background currents observed in the oxygen reduction transients, since the potentials of the two processes are far removed, but the transients do show how important surface reactions can be.

4.8.4 Silver migration

In membrane-covered electrodes the standard silver/silver chloride reference can give rise to acute problems when conducting transient measurements. Colloidal silver tends to migrate from the

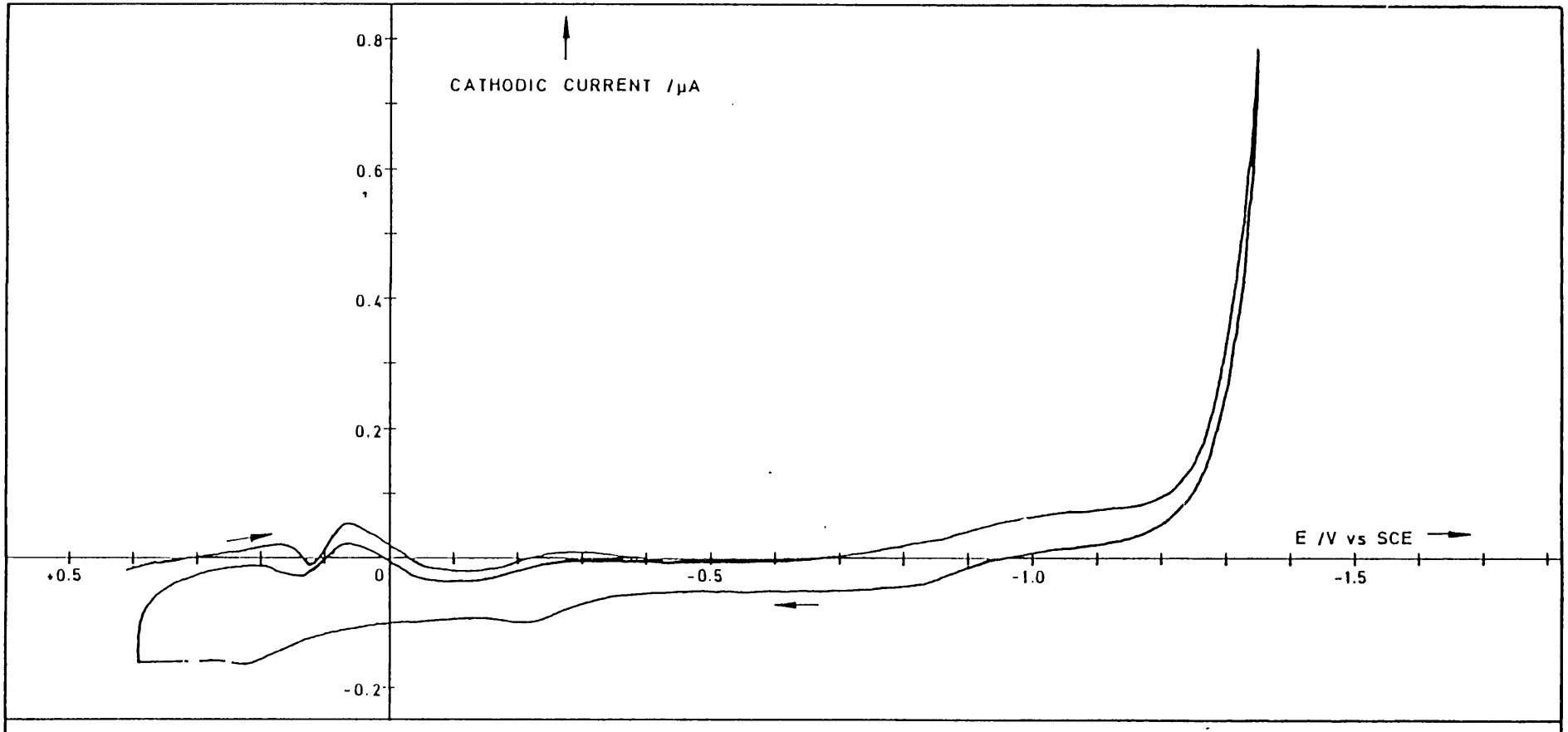

Fig.4.22. Background current in sodium hydroxide (1mol dm^{-3}) on AuDE No.18.

The cell was contained in an 'Atmos' bag and deoxygenated nitrogen was bubbled through the solution for ca.15 hours before recording the voltammogram. Counter electrode material was nickel; $v = 2 mVs^{-1}$.

Fig.4.23.

Effect of surface reactions on potential step transients.

R_x = 9k94, A = 6.37 mm^2, [NaOH] = 1 mol dm^{-3}, [O_2] = 0%.

ΔV /100mV vs SCE: 4.7 to (a) 4, (b) 3, (c) 2, (d) 1, (e) 0, (f) -1, (g) -2, (h) -3, (i) -4, (j) -5.

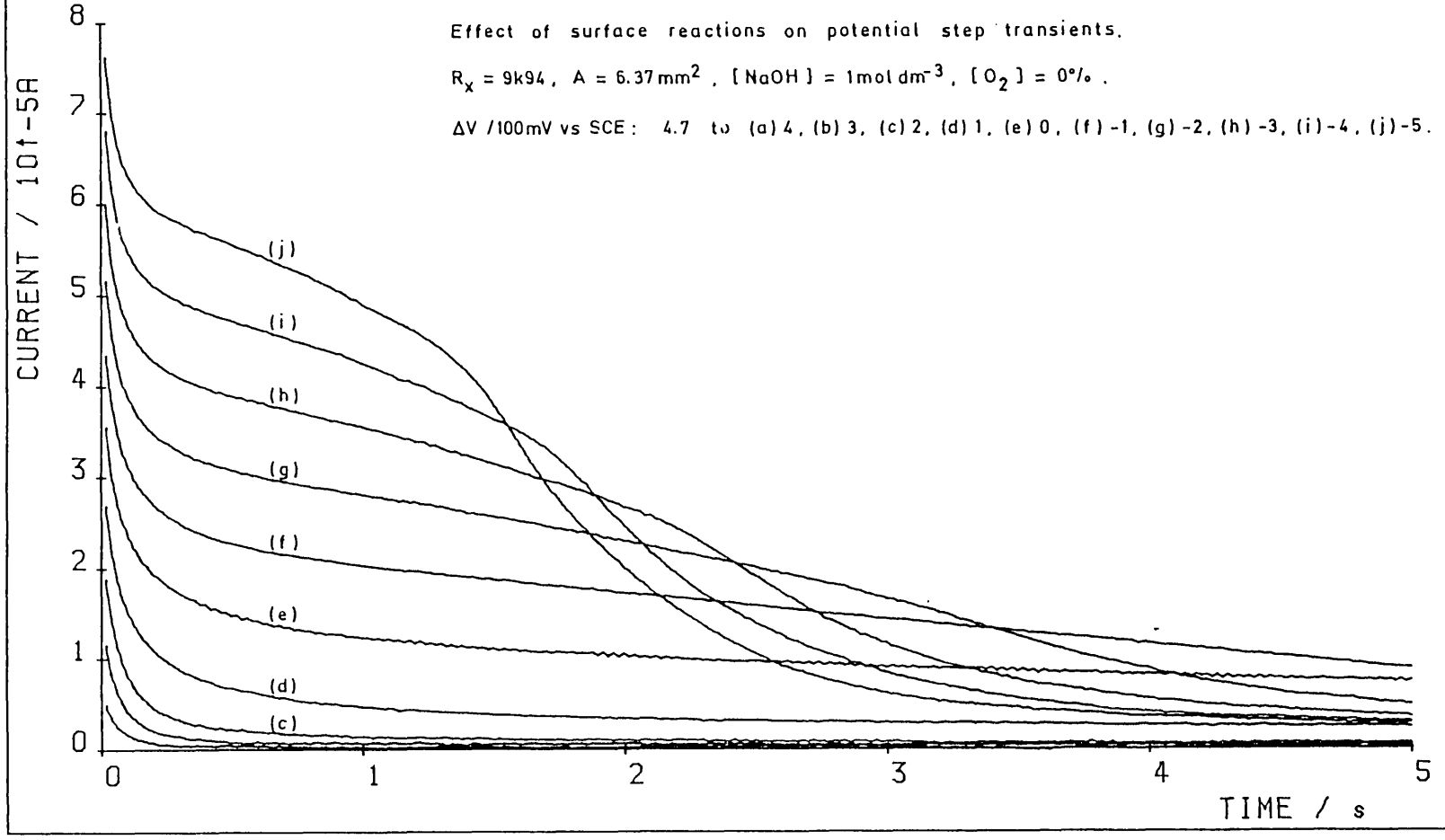

reference to the working electrode - the effect being particularly large in aqueous, concentrated base. The coverage at the working electrode can quickly become very significant, Fig.4.24.

In aqueous base, it may be advantageous to use the nickel hydroxide couple (qv) for both counter and reference electrodes in either two or three electrode cells, but this is feasible only at pH>11.

In aprotic solvents, such as dimethyl-sulphoxide (DMSO), silver migration is relatively small[64].

4.8.5 Step size and the electron transfer coefficient

Potential step size and the electron transfer coefficient are expressed in the parameter

$$P = \alpha E_p F/RT \qquad (4.74)$$

The effect of adjusting this parameter is illustrated in Fig.4.25. When P is large the transition period is relatively well-defined, but when P is small then the transition may not be observed at all.

Oxygen reduction in aqueous solution is not reversible. The transfer coefficient is low and, for a given step size, P is small. This accounts for the poorly defined transients observed for oxygen reduction. An idea of the effect of greater reversibility can be obtained from the hydroxide desorption transients, Fig.4.23.

It would be interesting to study oxygen reduction transients in DMSO since the reaction is essentially reversible and the step size could be

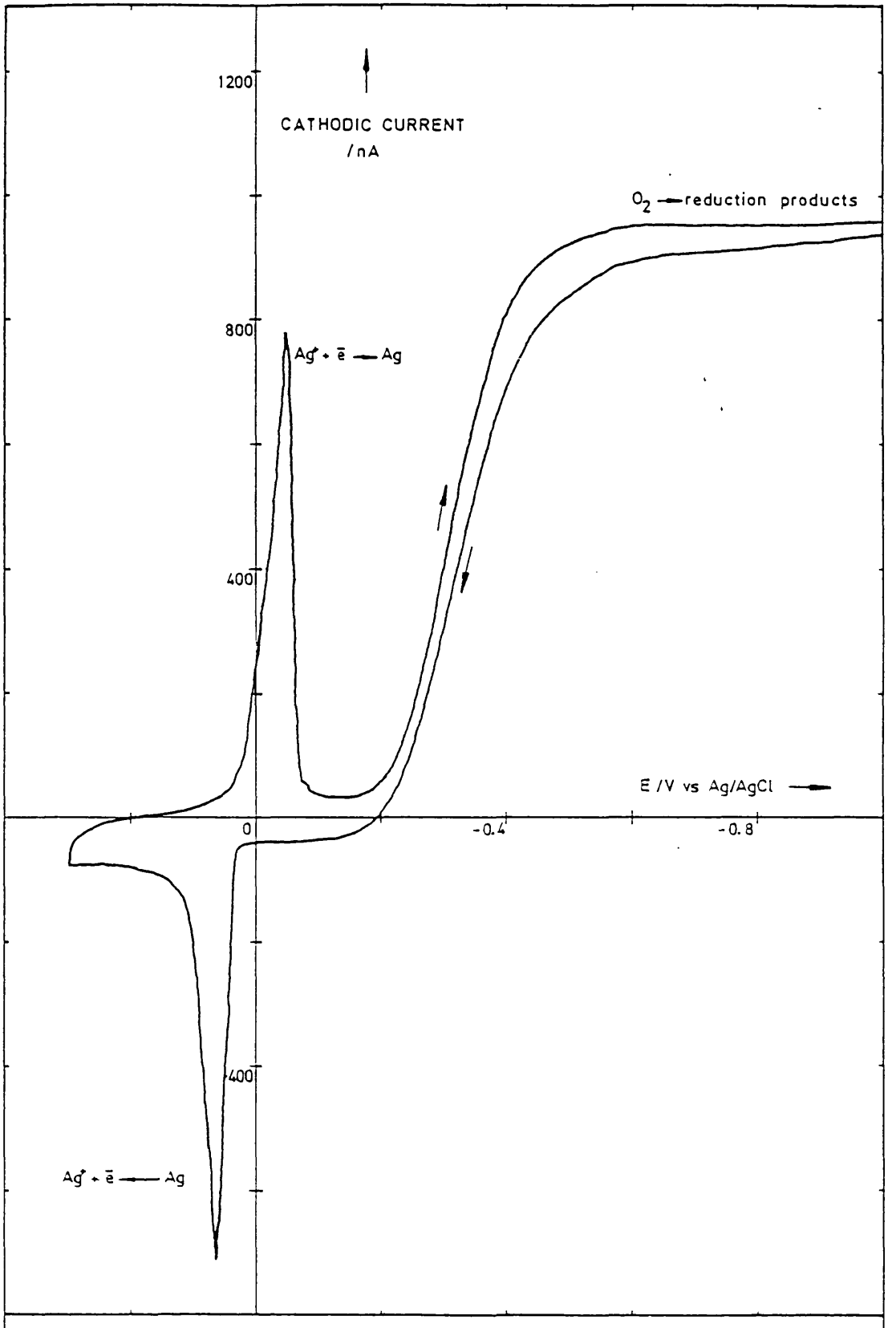

Fig. 4. 24. Voltammogram showing result of silver migration on to the working electrode of a membrane-covered sensor.

Gold electrode: A = 1.8mm^2, 12μ D602 teflon membrane + (50μ) nylon spacer, v = 5mV s^{-1}.
Electrolyte: oxygen saturated pH5 potassium hydrogen phthalate/NaOH buffer + KCl (0.1 mol dm^{-3}).

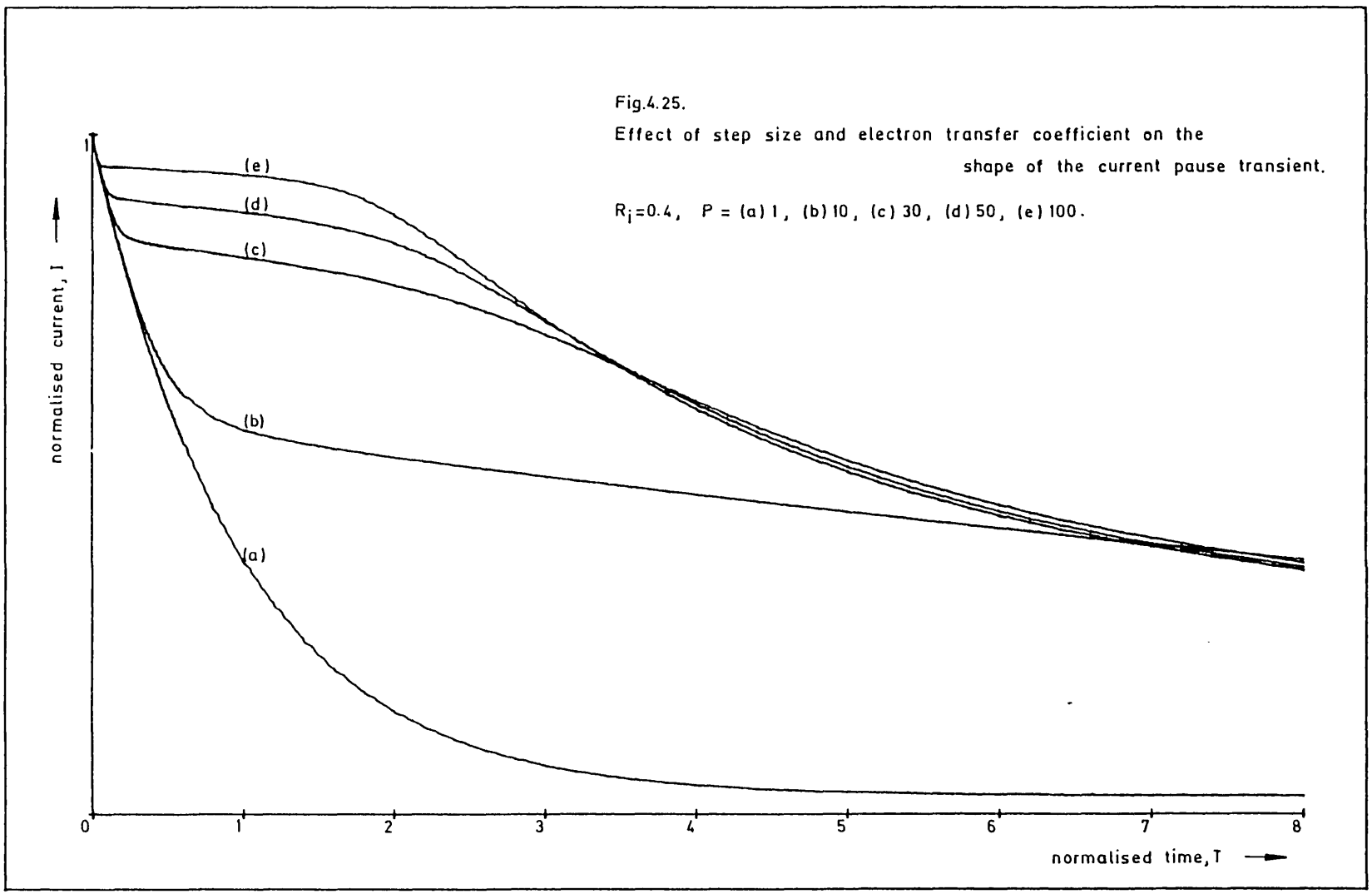

Fig.4.25.
Effect of step size and electron transfer coefficient on the shape of the current pause transient.

R_i=0.4, P = (a) 1, (b) 10, (c) 30, (d) 50, (e) 100.

made much larger because the solvent window is so much wider.

4.8.6 Summary

Theoretical and experimental results show that when faradaic current is bounded, as described above, then it can take several time constants before concencentration information can be extracted from potential step transients.

With a Clark-type electrode operating in this regime it would be impossible to make membrane independent measurements unless the electrode capacitance was small.

4.9 Case 2. Unbounded faradaic current

In this case the faradaic current is not bounded by the potential drop across the uncompensated resistance, i_F is limited only by the diffusion controlled current

$$i_k \longrightarrow i_D \tag{4.103}$$

With this restraint (4.83) may be rewritten as

$$I_f R_i \exp(-\theta P) + R_i \pi^{-\frac{1}{2}} \int_0^T I_f (T-T")^{-\frac{1}{2}} dT" = 1 \tag{4.104}$$

where

$$R_i = i_R / i_D > 1 \tag{4.105}$$

Rearrangement and integration by parts yields

$$I_f = \frac{R_i^{-1} - 2\pi^{-\frac{1}{2}} \int_0^T (T-T")^{1/2} (dI_f/dT") dT"}{\exp(-\theta P) + 2(T/\pi)^{\frac{1}{2}}} \tag{4.106}$$

This is similar to case 1, equation (4.88) and it can be solved in the same way.

A simulated transient is shown in Fig.4.26. In this case the charging current is continuous. There is a slight drop when the faradaic current switches on, but the two processes essentially occur simultaneously.

4.9.1 Concentration dependence

Concentration is inversely proportional to R_i. The effect of changing this parameter can be seen in Fig.4.27. When $R_i = \infty$ then the current is purely capacative and decays exponentially. Increasing the concentration increases the observed current and the shape of the transient changes until a hump appears as $R_i \longrightarrow 1$. At $R_i = 1$, equations (4.97) and (4.106) become identical. Any further increase in concentration results in a change of description of the transient, as given by (4.97).

4.9.2 Simplification of transient analysis

Two parameters, P and R_i are sufficient to simulate a complete set of transients, but when it is necessary to analyse experimental data then it can be particularly tedious if more than one parameter is involved.

For dissolved oxygen measurement it is necessary to analyse current transients in order to determine the bulk concentration, c_∞. This information is contained within the parameter R_i;

$$R_i = E_p C^{\frac{1}{2}} / (c_\infty nFADR_u^{\frac{1}{2}}) \qquad (4.107)$$

Now, if this ratio is sufficiently small, then the two parameter simulations can be dropped in favour

Fig.4.26.
Potential step transient simulated according to equation 4.106.
P=100, R_i=10, δT=0.01.

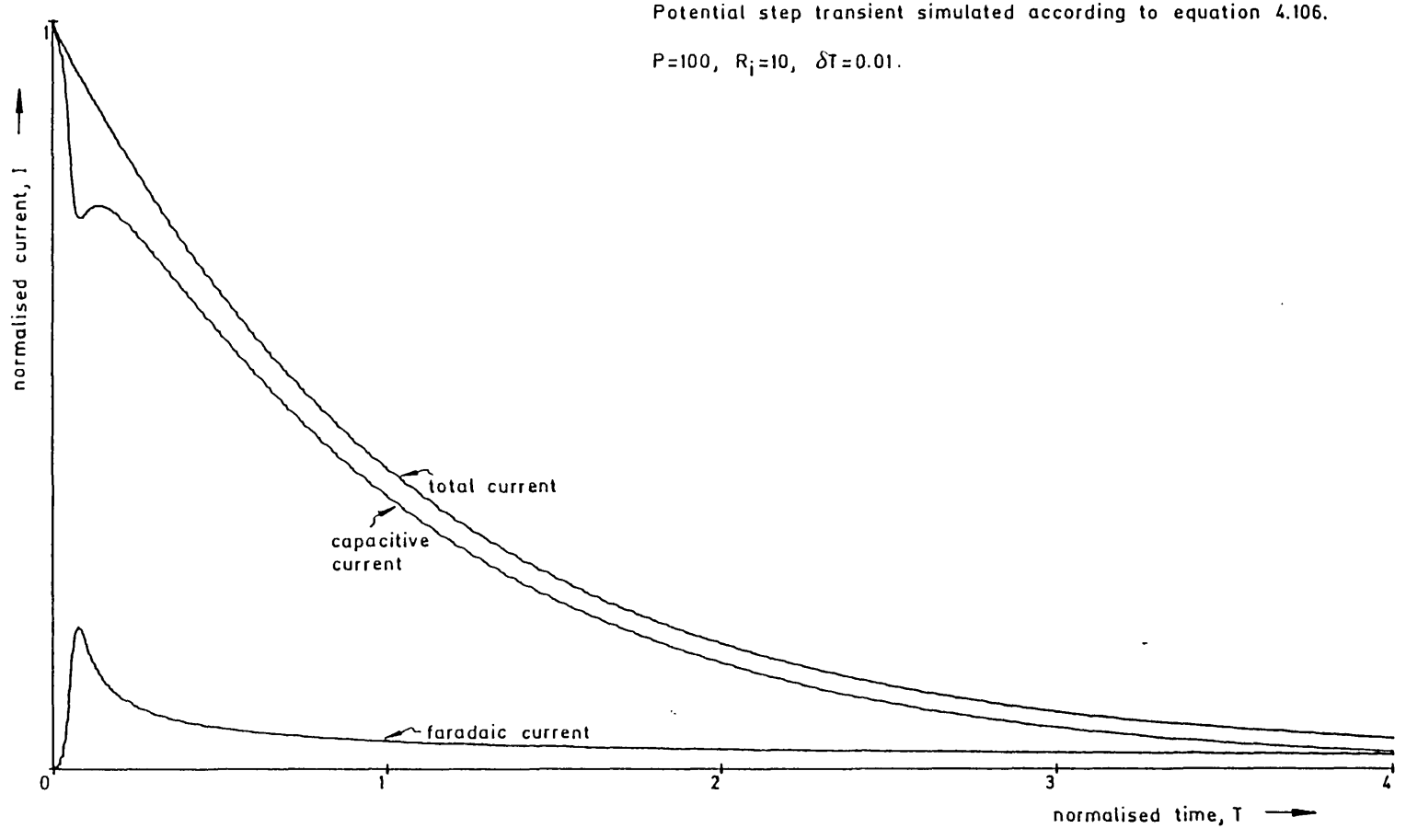

Fig.4.27.

Simulated effect of decreasing concentration of electroactive species.

P=100, R_j = (a) 1, (b) 2, (c) 5, (d) infinity.

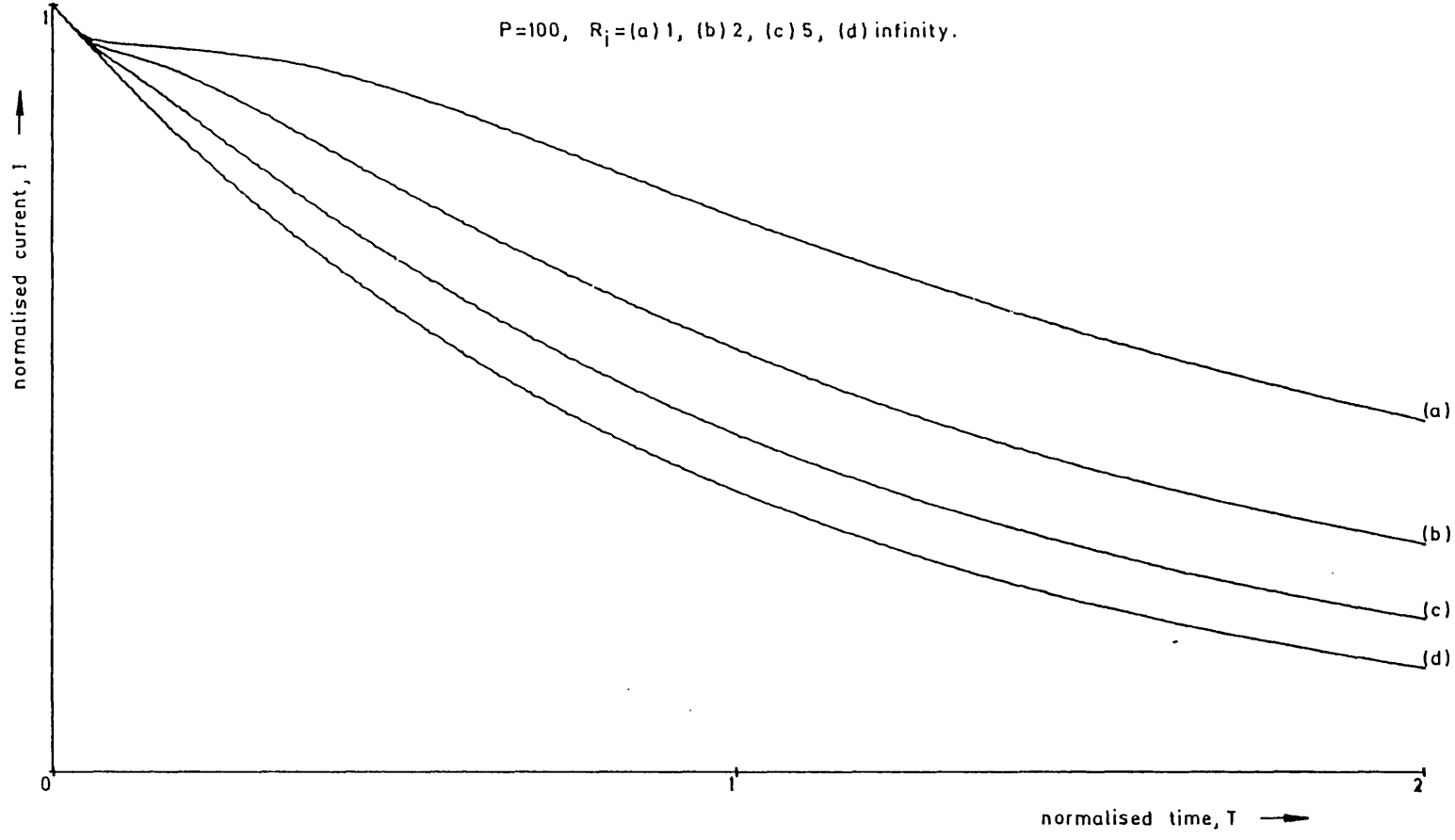

of the relatively simple linear addition model, section 4.6.

How small is "sufficiently small" can be determined by analysis of the simulated transients using the $it^{\frac{1}{2}}$ plot described in 4.6.1. Now, (4.18) can be written as

$$IT^{\frac{1}{2}} = T^{\frac{1}{2}}\exp(-T) + G \qquad (4.108)$$

where G is a constant.

Thus, a plot of $IT^{\frac{1}{2}}$ vs $T^{\frac{1}{2}}\exp(-T)$ should be a straight line with a slope of unity. Analysis of simulated transients shows that when P = 100 and R_i = 10 then the slope is determined to within 6% of unity and the effective time constant to within 12% of the actual time constant, Fig.4.28. When R_i = 100 then these percentages become 0.7 and 0.6 respectively.

Hence, "sufficiently small" depends on the required accuracy, but as a rule of thumb R_i^{-1} should be less than 0.1 otherwise significant errors will occur.

4.10 Summary

Significant advantages can be obtained by operating Clark-type sensors in a transient, rather than steady-state, mode. Several models, of varying complexity, have been developed to describe the transient current on application of a potential step at the working electrode. These models form a useful contribution to the understanding of the electrode processes and how to control them.

The complete range of current transients can be described by a two parameter solution, but, for

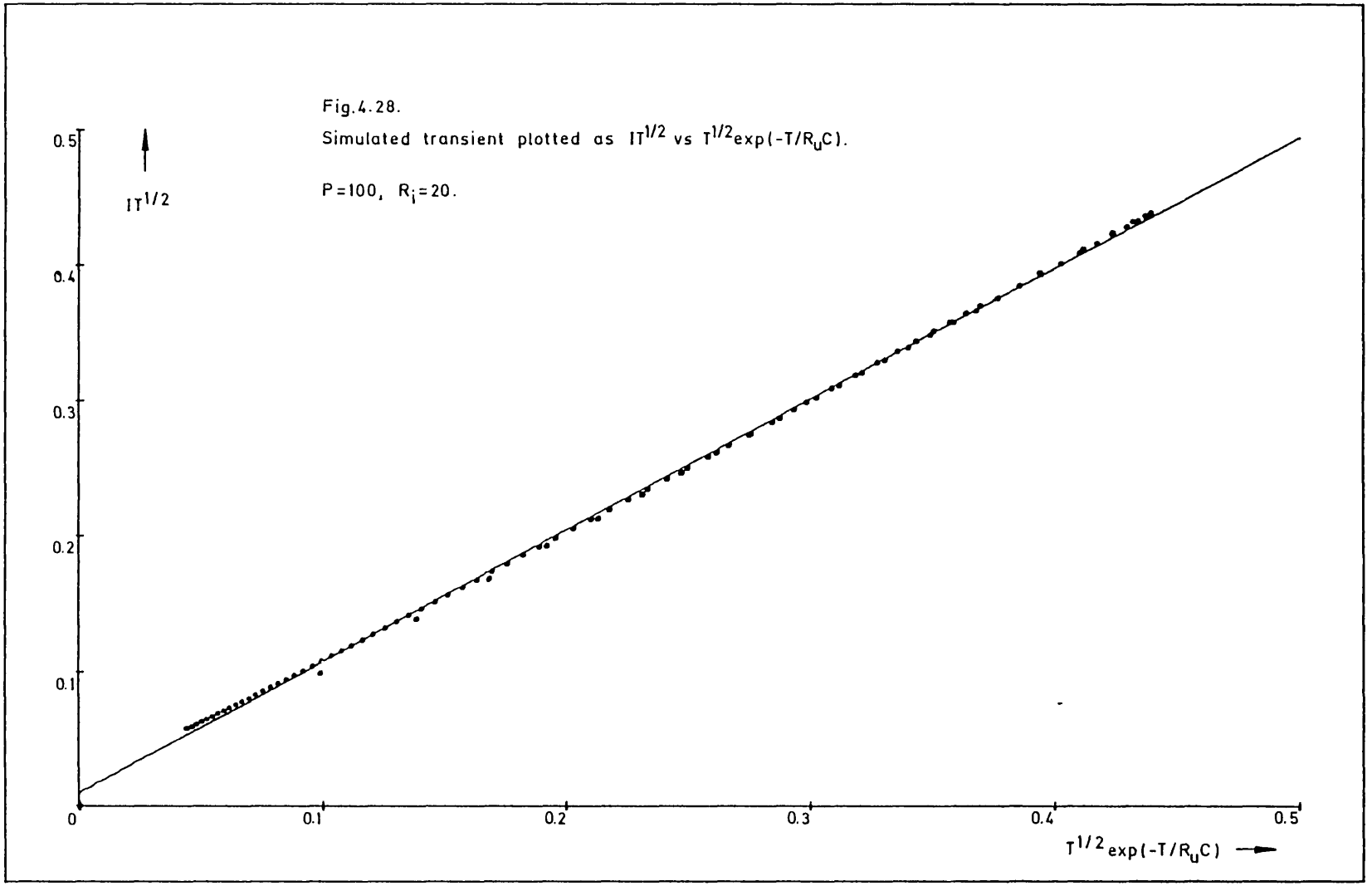
Fig.4.28.
Simulated transient plotted as $IT^{1/2}$ vs $T^{1/2}\exp(-T/R_uC)$.
P=100, R_i=20.
$IT^{1/2}$
0.5
0.4
0.3
0.2
0.1
0
0.1
0.2
0.3
0.4
0.5
$T^{1/2}\exp(-T/R_uC)$

practical purposes, it is useful to tailor the operating conditions so as to simplify the analysis.

It is found that surface reactions form an important contribution to transient currents. This can be corrected, but, ultimately, the sensitivity of any such electrode will be determined by the magnitude of the background currents.

REFERENCES

(1) (a) A.Cooper,"Nutrient film technique of growing crops".
Grower Books, London(1976)
(b) "Symposium on research on recirculating water culture".
Acta Horticulturae, No.98(March1980)

(2) D.Barnes,F.Wilson,"Chemistry and unit operations in sewage treatment".
Applied Science Publishers, London(1978)

(3) P.N.Hobson,A.M.Robertson,"Waste treatment in agriculture".
Applied Science Publishers, London(1977)

(4) A.G.Boon,"Oxygen transfer in the activated sludge
& process" and
(5) A.Ibrahim,"Denitrification of high nitrate wastes using an aerobic filter" in
G.Mattocks(Ed),"New processes of waste water treatment and recovery".
Ellis Horwood, Chichester(1978)

(6) H.Thompson,M.Riley,"On-line sensors in industrial water analysis".
Phil.Trans.R.Soc.Lond.A 302,327-338(1981).

(7) W.Luck,"New service instrument for monitoring the oxygen content of feed waters for boilers".
Siemens-Z.,41,527-533(1967)

(8) G.W.Winsor,"Nutrient film culture:an appraisal of its progress and prospects for crop protection under glass".
Glasshouse Crops Research Institute, Littlehampton, Annual Report(1977)

(9) P.Adams,"Nutrient-film culture".
Agricultural Water Management,4,471-478(1981)

(10) M.L.Hitchman,"Measurement of dissolved oxygen".
Wiley-Interscience, New York(1978)

(11) H.Degn,I.Balslev,R.Brooks(Eds),"Measurement of oxygen".
Elsevier, Amsterdam(1976)

(12) K.Grasshoff,"The electrochemical determination of oxygen" in
M.Whitfield,D.Jagner(Eds),"Marine Electrochemistry".
Wiley, New York(1981)

(13) P.L.Bailey,"Analysis with ion-selective electrodes".

Heyden, London(1976)

(14) L.W.Winkler,"The determination of dissolved oxygen in water".
Ber.Deut.Chem.Ges.,21,2843(1888)

(15) R.E.Meyer,F.A.Posey,P.M.Lantz,"An electrochemical method for monitoring the oxygen content of aqueous streams at the ppb level".
Desalination,11,329-340(1972)

(16) M.E.Bodini Cruz-Carrera,G.Copia Arancibia,"Influence of metallic cadmium on the electrochemical reduction of nitrate and nitrite ions".
Anales de Quimica,76,267-272(1979)

(17) (a) J.W.Collet,J.J.Lingane,"Polarography of nitrate ion".
J.Am.Chem.Soc.,76,4214-8(1954)

(b) G.L.Lundquist,G.Washinger,J.A.Cox,"Voltammetric determination of trace quantities of nitrate in an anion exchange membrane isolated cell".
Anal.Chem.,47,319-322(1975)

(c) J.A.Cox,A.Brajter,"Mechanisms of zirconium(IV) and lanthanum(III) catalysis of the reduction of nitrate at mercury".
Electrochimica Acta,24,517-20(1979)

(18) (a) M.G.Johnson,R.J.Robinson,"Analytical applications of the polarography of molybdenum".
Anal.Chem.,24,366-98(1952)

(b) G.P.Haight,"Mechanism of the molbdate catalyzed reductions of perchlorate and nitrate ions at the dropping mercury electrode".
Acta Chemica Scandinavia,15,2012-20(1961)

(c) I.M.Kolthoff,I.Hodara,"Polarographic study of the molybdate catalyzed reduction of chlorate, perchlorate and nitrate".
J.Electroanal.Chem.,5,2-16(1963)

(19) N.Kato,K.Yoshikiyo,K.Nakano,K.Tanaka,"Polarographic determination of nitrate and nitrite ions by catalytic wave of vanadium(IV)-cyclohexane diaminetetraa etato complex".
Bunseki Kagaku (E),32,139-42(1983)

(20) (a) S.W.Boese,V.S.Archer,J.W.O'Laughlin,"Differential pulse polarographic determination of nitrate and nitrate".
Anal.Chem.,49,479-84(1977)

(b) S.W.Boese,V.S.Archer,"Electrochemical reduction of nitrate ion in the presence of ytterbium(III)". J.Electroanal.Chem.,138,273-94(1982)

(c) W.Erkang,L.Xiangqin,"Differential pulse polarographic behaviour of nitrate,nitrite and hydroxylamine". J.Electroanal.Chem.,136,311-21(1982)

(21) (a) M.C.Rand,H.Heukelekian,"Polarographic detemination of nitrates in sanitary analysis". Anal.Chem.,25,878-81(1953)

(b) PH.Meckelynck,C.Mechelynck-David,"Etude du comportement polarographique du zirconium en milieu acide et en presence d'ions nitrate". Anal.Chim.Acta,21,432-9(1959)

(c) H.W.Wharton,"Polarographic reduction of nitrate ions in the presence of zirconium salts". J.Electroanal.Chem.,9,134-9(1965)

See also (17).

(22) M.E.Bodini,D.T.Şawyer,"Voltammetric determination of nitrate at parts-per-billion levels". Anal.Chem.,49,485-9(1977)

(23) (a) R.E.Hamm,C.D.Withrow,"Polarographic nitrate determination". Anal.Chem.,27,1913-5(1955)

(b) D.N.Willett,H.P.Peterson,R.J.Moubry,"A polarographic determination of nitrates in silage". J.Ass.Offic.Anal.Chem.,51,658-61(1968)

(24) R.J.Davenport,D.C.Johnson,"Voltammetric determination of nitrate and nitrite ions using a rotating cadmium disc electrode". Anal.Chem.,45,1979-80(1973)

(25) R.J.Davenport,D.C.Johnson,"Determination of nitrate by forced-flow liquid chromatography with electrochemical detection". Anal.Chem.,46,1971-8(1974)

(26) D.Pletcher,Z.Poorabedi,"The reduction of nitrate at a copper cathode in aqueous solution". Electrochimica Acta,24,1253-6(1979)

(27) R.K.Kvaratskheliya,"Mechanism of the electrochemical reduction of a nitrate ion on a copper electrode". Soobshch.Akad.Nauk.Gruz.SSR,50,631-6(1968)

(28) B.N.Kabanov,N.N.Tomashova,I.G.Kiseleva,"Reduction of

nitrate on the lead electrode".
Soviet Electrochemistry,6,598-600(1970)

(29) R.K.Kvaratskheliya,"Joint reduction of nitrate ion and hydroxylamine on the lead cathode".
Sobshch.Akad.Nauk.Gruz.SSR,62,325-8(1968)

(30) W.H.Edwards,N.A.Hampson,"The formation of Plante cells using a nitrate process".
J.Appl.Electrochem.,9,381-7(1979)

(31) H.J.T.Ellingham,"Alternative electrode reactions.Part I.Reactions at a platinum cathode in nitric acid solutions".
J.Chem.Soc.Transactions,1565-79(1932).

(32) K.J.Vetter,"Electrchemical kinetics",pp490-3.
Academic Press, New York(1967)

(33) R.I.Agladze,D.E.Karchava,R.I.Kvaratskheliya, "Electrochemical reduction of nitric acid in an acetic acid medium".
Soobshch.Akad.Nauk.Gruz.SSR,52,75-80(1968)

(34) R.K.Kvaratskheliya, R.I.Agladze,"Regular features of the kinetics of the reduction of potassium nitrate at a copper cathode with time".
Soviet Electrochemistry,5,851-5(1969)

(35) A.Damjanovic,"Mechanistic analysis of oxygen electrode reactions" in
J.O'M.Bockris,B.E.Conway(Eds),"Modern aspects of electrochemistry No.5".
Plenum Press, New York(1969)

(36) R.W.Zurilla,R.K.Sen,E.Yeager,"The kinetics of the oxygen reduction reaction on gold in alkaline solution".
J.Electrochem.Soc.,125,1103-9(1978)

(37) (a) M.A.Genshaw,A.Damjanovic,J.O'M.Bockris,"Hydrogen peroxide formation in oxygen reduction at gold electrodes. I.Acid solution".
J.Electroanal.Chem.,15,163-172(1967)

(b) A.Damjanovic,M.A.Genshaw,J.O'M.Bockris,"Hydrogen peroxide formation in oxygen reduction at gold electrodes. II.Alkaline solution".
J.Electroanal.Chem.,15,173-180(1967)

(38) R.J.Taylor,A.A.Humffray,"Electrochemical studies on glassy carbon electrodes.II.Oxygen reduction in solutions of high pH (pH>10)".
J.Electroanal.Chem.,64,63-84(1975)

(39) B.Lovrecek,M.Batinic,J.Caja,"The electrochemical oxygen reduction on the graphite electrode". Electrochimica Acta,28,685-90(1983)

(40) K.Shigehara,F.C.Anson,"Catalysis of the reduction of dioxygen to water at graphite electrodes coated with two transition metal catalysts acting in series". J.Electroanal.Chem.,132,107-118(1982)

(41) R.R.Durand,F.C.Anson,"Catalysis of dioxygen reduction at graphite electrodes by an adsorbed cobalt(II) porphyrin". J.Electroanal.Chem.,134,273-289(1982)

(42) (a) I M.Kolthoff,C.S.Miller,"The reduction of oxygen at the dropping mercury electrode". J.Am.Chem.Soc.,63,1013-1017(1941)

(b) D.M.H.Kern,"The polarography and standard potential of the oxygen-hydrogen peroxide couple". J.Am.Chem.Soc.,76,4208-14(1954)

(43) (a) C.J.VanVelzen et al."The electrochemical reduction of oxygen to hydrogen peroxide at the dropping mercury electrode.Part I.Its kinetics at 6.5<pH<12.5". J.Electroanal.Chem.,134,87-100(1982)

(b) C.J.VanVelzen et al.,"The electrochemical reduction of oxygen to hydrogen peroxide at the dropping mercury electrode.Part II.Its kinetics at 0.4<pH<5.9". J.Electroanal.Chem.,142,229-242(1982)

(44) D.Sepa,M.Vojnovic,A.Damjanovic,"Oxygen reduction at silver electrodes in alkaline solutions". Electrochimica Acta,15,1355-66(1970)

(45) (a) J.J.Lingane,"Chronopotentiometric study of oxygen production at a platinum wire cathode". J.Electroanal.Chem.,2,296-309(1961)

(b) A.Damjanovic,M.A.Genshaw,J.O'M.Bockris,"Mechanism of oxygen reduction at platinum in alkaline solutions with special reference to hydrogen peroxide". J.Electrochem.Soc.114,1107-12(1967)

(c) D.B.Sepa,M.V.Vojnovic,A.Damjanovic,"Reaction intermediates as a controlling factor in the kinetics and mechanism of oxygen reduction at platinum electrodes". Electrochimica Acta,26,781-93(1981)

(46) K-L.Hsueh,E.R.Gonzalez,S.Srinivasan,"Electrolyte effects on oxygen reduction kinetics at platinum: a

rotating ring-disc electrode analysis".
Electrochimica Acta,28,691-697(1983)

(47) L.C.Clark et al.,"Continuous recording of blood oxygen tensions by polarography".
J.Appl.Physiol.,6,189(1953)

(48) L.C.Clark,"Monitor and control of blood and tissue oxygen tensions".
Trans.Am.Soc.Artificial Internal Organs,2,41,(1956)

(49) L.C.Clark,"Electrochemical device for chemical analysis".
US Patent 2,913,386 Nov.17,1959

(50) F.J.H.Mackereth,"An improved galvanic cell for determination of oxygen concentration in fluids".
J.Sci.Instrum.,41,38-41(1964)

(51) V.Stannett,"Simple gases" in
J.Crank,G.S.Park,"Diffusion in Polymers".
Academic Press, London(1968)

(52) K.H.Mancy,D.A.Okun,C.N.Reilley,"A galvanic cell oxygen analyser".
J.Electroanal.Chem.,4,65-92(1962)

(53) W.Siu,R.S.C.Cobbold,"Characteristics of a multicathode polarographic oxygen electrode".
Med.Biol.Eng.,14,109-120(1976)

(54) R.Briggs,M.Viney,"The design and performance of temperature compensated electrodes for oxygen measurements".
J.Sci.Instrum.,41,78-83(1964)

(55) S.Ben-Yaakov,E.Ruth,"A method for reducing the flow sensitivity of a polarographic dissolved-oxygen sensor".
Talanta,27,391-395(1980)

(56) O.J.Jensen,T.Jacobsen,K.Thomsen,"Membrane-covered oxygen electrodes.I.Electrode dimensions and electrode sensitivity".
J.Electroanal.Chem.,87,203-11(1978)

(57) R.A.Butler,J.F.Nunn,S.Askill,"Coiled cathode oxygen polarograph".
Nature,126,781(1962)

(58) I.Fatt,R.St.Helen,"A multicathode polarographic oxygen sensor and its performances".
J.Appl.Physiol.,27,435-7(1969)

(59) Ross,"Method and apparatus for electrolytically

determining a species in a fluid".
US Patent 3,260,656 July 1966

(60) J.G.Connery,E.C.Muly,R.M.Taylor,"Apparatus for electroltically determining a species in a fluid and method of use".
US Patent 4,076,596 28 February 1978

(61) D.M.Phelan,R.M.Taylor,S.Fricke,"A maintenance-free dissolved oxygen monitor".
Am.Lab.(Fairfield,Conn.),14(7),65-72(1982)

(62) C.C.Herrmann,G.G.Perrault,A.A.Pilla,"Dual reference electrode for electrochemical pulse studies".
Anal.Chem.,40,1173-4(1968)

(63) D.Midgley,K.Torrence,"Potentiometric water analysis",p341.
Wiley, Chichester(1978)

(64) D.Clark,H.J.J.Drummond. Personal communication(1984)

(65) G.W.D.Briggs,W.F.K.Wynne-Jones,"The nickel hydroxide electrode; the effects of ageing-I.X-ray diffraction study of the electrode process".
Electrochimica Acta,7,241-8(1962)

(66) G.W.D.Briggs,G.W.Stott,W.F.K.Wynne-Jones,"The nickel hydroxide electrode; the effect of ageing-II.Changes in electrochemical behaviour".
Electrochimica Acta,7,249-56(1962)

(67) T.Yoshimura,T.Fujinaga,"Voltammetric behaviour of nickel electrode in an alkaline solution".
Nippon Kagaku Kaishi,614-9(1982)

(68) T.L.Markin,R.M.Dell,"Recent developments in nickel oxide-hydrogen batteries"
J.Electroanal.Chem.,118,217-28(1981)

(69) R.Barnard,C.F.Randell,F.L.Tye,"Studies concerning charged nickel hydroxide electrodes.Part III.Reversible potentials at low states of charge".
J.Electroanal.Chem.,119,17-24(1981)

(70) L.D.Burke,T.A.M.Twomey,"Influence of pH on the redox behaviour of hydrous nickel oxide".
J.Electroanal.Chem.,134,353-62(1982)

(71) A.Levy,"The accuracy of the bubble meter method for gas flow measurements".
J.Sci.Instrum.,41,449-53(1964)

(72) I.Sinko,J.Dolezal,"Effect of the cathodic current of oxygen on oxidation current-potential curves in anodic

stripping voltammetry".
J.Electroanal.Chem.,25,53-60(1970)

(73) R.Kalvoda,"Operational amplifiers in chemical instrumentation".
Ellis Horwood, Chichester(1975)

(74) G.Pu,"The study of the reduction of nitrate ion at a copper disc electrode".
Unpublished report, Imperial College, London(1981)

(75) P.Delahay,"Theory of irreversible waves in oscillographic polarography".
J.Am.Chem.Soc.,75,1190-6(1953)

(76) R.S.Nicholson,I.Shain,"Theory of stationary electrode polarography".
Anal.Chem.,36,706-723(1964)

(77) N.S.Bayliss,D.W.Watts,"The decomposition of sodium nitrite solutions in aqueous sulphuric and perchloric acids".
Aust.J.Chem.,16,927-32(1963)

(78) N.S.Bayliss,R.Dingle,D.W.Watts,R.J.Wilkie,"The spectrophotometry of sodium nitrite solutions in aqueous sulphuric and perchloric acids and the equilibrium between nitrosonium ion and nitrous acid".
Aust.J.Chem.,16,933-42(1963)

(79) V.G.Levich,"Physicochemical hydrodynamics".
Prentice-Hall, Englewood Cliffs, NJ(1962)

(80) P.C.Andricacos,H.Y.Cheh,"The application of linear sweep voltammetry to a rotating disc electrode for the reversible deposition of an insoluble species".
J.Electrochem.Soc.,127,2153-7(1980)

(81) P.C.Andricacos,H.Y.Cheh,"The application of linear sweep voltammetry to a rotating disc electrode for a reversible reaction with a soluble product".
J.Electrochem.Soc.,127,2385-8(1980)

(82) J.Koutecky, B.G.Levich,"The application of the rotating disc electrode to studies of kinetic and catalytic processes">
Zh.Fiz.Khim.,32,1565-75(1958)

(83) A.R.Hillman,"The mechanisms of some electrochemical reactions".
D.Phil.thesis, University College, Oxford(1979)

(84) W.N.Brooks,"Electroanalytical techniques for anaesthetic gases".
D.Phil.thesis, University College, Oxford(1980)

(85) F.G.Cottrell, Z.Physik.Chem.,42,385(1902)

(86) D.D.Macdonald,"Transient techniques in electrochemistry".
Plenum Press, New York(1977)

(87) C.P.Jones,"A novel packed bed wall-jet disc electrode for on-line detection of nitrate".
Unpublished report, Imperial College, London(1983)

(88) W.J.Albery,B.G.D.Haggett,C.P.Jones,L.R.Svanberg, "Packed bed wall-jet electrode and the determination of nitrate".
To be published (J.Electroanal.Chem.)

(89) A.J.Bard,L.R.Faulkner,"Electrochemical methods". Wiley, New York(1980)
(a) p129, (b) p144, (c) p143, (d) p223.

(90) K.D.Wise,R.B.Smart,K.H.Mancy,"A transient monitoring and electrde characterising system for a pulsed oxygen electrode".
Anal.Chim.Acta,116,297-305(1980)

(91) J.M.Hale,M.L.Hitchman,"Some considerations of the steady-state and transient behaviour of membrane-covered dissolved oxygen detectors".
J.Electroanal.Chem.,107,281-94(1980)

(92) J.L.Morris,L.R.Faulkner,"Normal pulse voltammetry in electrochemically poised systems".
Anal.Chem.,49,489-94(1977)

(93) J.J.Newman,"Resistance for flow of current to a disc"
J.Electrochem.Soc.,113,501(1966)

(94) H.Reller,E.Kirowa-Eisner,E.Gileadi,"Ensembles of microelectrodes. A digital simulation".
J.Electroanal.Chem.,138,65-77(1982)

(95) K.Aoki,J.Osteryoung,"Diffusion controlled current at a stationary finite disc electrode".
J.Electroanal.Chem.,125,315-20(1981)

(96) S.S.Fratoni,S.P.Perone,"Studies in photoelectrochemistry.III.Theory for induced charging currents in potentiostatic chronoamperometry involving competing chemical reactions".
J.Electrochem.Soc.,123,1672-6(1976)

(97) K.F.Dahnke,S.P.Perone,"Studies in photoelectrochemistry.IV.Flash photolysis studies of pH dependence of benzophenone photodimerization".
J.Electrochem.Soc.,123,1677-83(1976)

(98) L-H.L.Miaw,S.P.Perone,"Theoretical and experimental studies of the effects of charging currents in potential-step voltammetry".
Anal.Chem.,51,1645-50(1979)

(99) A.Savitzky,M.J.EGolay,"Smoothing and differentiation of data by simplified least squares procedures".
Anal.Chem.,36,1627-39(1964)

(100) K.F.Dahnke,S.S.Fratoni,S.P.Perone,"Studies in photoelectrochemistry:extraction of faradaic signals from flash photocurrent measurements-bezophenone photolysis".
Anal.Chem.,48,296-303(1976)

(101) W.J.Albery,B.G.D.Haggett
Unpublished work, Imperial College, London(1983)

(102) H.J.S.Sand. Phil.Mag.,1,45(1901)

(103) D.W.Kirk,F.R.Foulkes,W.F.Graydon,"The electrochemical formation of Au(I) hydroxide on gold in aqueous potassium hydroxide".
J.Electrochem.Soc.,127,1069-76(1980)

(104) S.Bruckenstein,S.Prager,"Current transients at a rotating disc electrode produced by a potential step".
Analyt.Chem.,39,1161-3(1967)

(105) V.Y.Filinovskii,E.M.Podgaetskii,"Establishment of a stationary current on a rotating disc electrode in the case of an irreversible electrochemical reaction".
Soviet Electrochemistry,4,596-9(1968)

(106) K.Viswanathan,H.Y.Cheh,"The application of pulsed potential and pulsed current to a rotating disc electrode system".
J.Applied Electrochem.,9,537-43(1979)

(107) R.R.Adzic,N.M.Markovic,V.B.Vesovic,"Structural effects in electrocatalysis. Oxygen reduction on the gold(100) single crystal electrode".
J.Electroanal.Chem.,165,105-20(1984)

(108) N.M.Markovic,R.R.Adzic,V.B.Vesovic,"Structural effects in electrocatalysis. Oxygen reduction on the gold single crystal electrodes with (110) and (111) orientations".
J.Electroanal.Chem.,165,121-33(1984)